NMRF/VR/04/2023

NCUM Global Model Verification:

Monsoon (JJAS) 2023

K. NIRANJAN KUMAR, SUKHWINDER KAUR, MOHANA S. THOTA, M. VENKATARAMI REDDY, SUSHANT KUMAR, HARVIR SINGH, ANUMEHA DUBE, SUMIT KUMAR, AND RAGHAVENDRA ASHRIT

Dec 2023

National Centre for Medium Range Weather Forecasting
Ministry of Earth Sciences, Government of India
A-50, Sector-62, NOIDA-201 309, INDIA

NCUM Global Model Verification: Monsoon (JJAS) 2023

K. NIRANJAN KUMAR, SUKHWINDER KAUR, MOHANA S. THOTA, M. VENKATARAMI REDDY, SUSHANT KUMAR, HARVIR SINGH, ANUMEHA DUBE, SUMIT KUMAR, AND RAGHAVENDRA ASHRIT

NMRF/VR/04/2023

Data Control Sheet

1	Name of the Institute	National Center for Medium range Weather Forecasting
2	Document Number	NMRF/VR/04/2023
3	Date of Publication	December 2023
4	Title of the document	NCUM Global Model Verification: Monsoon (JJAS) 2023
5	Type of the document	Verification Report
6	Number of pages, figures, and Tables	65 pages, 44 figures, 7 Tables (including Appendix Figures and Tables)
7	Authors	K. Niranjan Kumar, Sukhwinder Kaur, Mohana S. Thota, M. Venkatarami Reddy, Sushant Kumar, Harvir Singh, Anumeha Dube, Sumit Kumar, and Raghavendra Ashrit
8	Originating Unit	National Centre for Medium Range Weather Forecasting (NCMRWF), A-50, Sector-62, NOIDA201 309, India.
9	Abstract	This comprehensive report assesses the performance of the National Centre for Medium-Range Weather Forecasting (NCMRWF) model forecasts during the 2023 monsoon season (June-September, JJAS). The focus is on real-time medium-range forecasts generated by the Global NCMRWF Unified Model (NCUM-G). The forecast verification is conducted by comparing the model's predictions to model analysis and observations. The results are summarized to provide insights into the average biases and forecast performances throughout the monsoon season. This report is tailored to both forecasters and model developers.
10	References	30
11	Security classification	Unrestricted
12	Distribution	General

Table of Contents

NCUM Global Model Verification:
Monsoon (JJAS) 2023

K. Niranjan Kumar, Sukhwinder Kaur, Mohana S. Thota, M. Venkatarami Reddy, Sushant Kumar, Harvir Singh, Anumeha Dube, Sumit Kumar, and Raghavendra Ashrit

सारांश

यह व्यापक रिपोर्ट 2023 मानसून सीज़न (जून-सितंबर, जे.जे.ए.एस.) के दौरान नेशनल सेंटर फॉर मीडियम-रेंज वेदर फोरकास्टिंग (रा.म.अ.मौ.पू.कें.) मॉडल पूर्वानुमानों के प्रदर्शन का आकलन करती है। वैश्विक रा.म.अ.मौ.पू.कें. यूनिफाइड मॉडल (एन.सी.यू.एम.-जी) द्वारा उत्पन्न वास्तविक समय के मध्यम-श्रेणी के पूर्वानुमानों पर ध्यान केंद्रित किया गया है। पूर्वानुमान सत्यापन मॉडल के पूर्वानुमानों की मॉडल विश्लेषण और टिप्पणियों से तुलना करके किया जाता है। पूरे मानसून सीज़न में औसत पूर्वाग्रहों और पूर्वानुमानित प्रदर्शनों की जानकारी प्रदान करने के लिए परिणामों को संक्षेप में प्रस्तुत किया गया है। यह रिपोर्ट पूर्वानुमानकर्ताओं और मॉडल डेवलपर्स दोनों के लिए तैयार की गई है।

Abstract

This comprehensive report assesses the performance of the National Centre for Medium-Range Weather Forecasting (NCMRWF) model forecasts during the 2023 monsoon season (June-September, JJAS). The focus is on real-time medium-range forecasts generated by the Global NCMRWF Unified Model (NCUM-G). The forecast verification is conducted by comparing the model's predictions to model analysis and observations. The results are summarized to provide insights into the average biases and forecast performances throughout the monsoon season. This report is tailored to both forecasters and model developers.

1. Introduction

This report assesses the performance of the National Centre for Medium-Range Weather Forecasting (NCMRWF) model forecasts during the monsoon season (June-September, JJAS) of 2023. The focus is on real-time medium-range forecasts generated by the Global NCMRWF Unified Model (NCUM-G). Forecast verification is conducted against model analysis and observational data. The results are summarized to gain insights into average biases and forecast performances during the monsoon season. This report is designed for both forecasters and model developers. Section 2 provides a detailed overview of recent advancements in the NCUM-G model and data assimilation system at NCMRWF. It also briefly presents the verification of the NCMRWF Ensemble Prediction System (NEPS-G). Additionally, the NCUM-G modeling system and observational datasets used are briefly discussed in Section 2. Sections 3 conducts a detailed analysis of the seasonal mean and corresponding anomalies, providing a comprehensive overview of the model's performance throughout the monsoon season. Following this, Section 4 of the report delves into systematic biases in the model forecasts of large-scale upper air fields such as wind, temperature, humidity, rainfall, etc. This information is expected to be valuable for forecasters in effectively utilizing model forecast products. Section 5 then thoroughly validates the forecasts with meticulous attention to detail. Sections 6-7 of the report present diagnostic analysis and focus on verification of intra-seasonal features such as active/break spells, monsoon onset, and synoptic scale variability. Additionally, investigations into some of the model biases are conducted, which may aid modelers in addressing these issues. Section 8 presents the verification of ensemble forecasts from NEPS-G. Section 9 provides a summary of the key findings.

The NCMRWF model forecasts during the monsoon season (JJAS) of 2023 demonstrate overall satisfactory performance. However, there are areas for improvement, particularly in reducing systematic biases and enhancing intra-seasonal forecast accuracy. The insights provided in this report can guide forecasters in effectively utilizing model forecasts and inform model developers in their efforts to improve model performance.

2. NCMRWF Unified Modelling System & Verification datasets

2.1. *Model Description*

The first Global NCMRWF Unified model (NCUM-G) for numerical weather prediction (NWP) was made operational in 2012 (Figure 1) with a grid resolution of 25km (NCUM-G:V1) which was upgraded to 17km (NCUM-G:V3) in 2015, 12km (NCUM-G:V5) in 2018, 12 km resolution with improved model physics in

2020 (NCUM-G:V6). The present version (NCUM-G:V7) of NCUM-G has a horizontal grid resolution of ~12 km with 70 vertical levels in the atmosphere reaching 80 km height above earth surface. It uses an "ENDGame" dynamical core, which provides improved accuracy of the solution of primitive model equations and reduced damping. This helps in producing finer details in the simulations of synoptic features such as cyclones, fronts, troughs, and jet stream winds. The "ENDGame" also increases variability in the tropics, which leads to an improved representation of tropical cyclones and other tropical phenomena. The NCUM-G:V7 features the Global Atmosphere 7.2 configuration (GA7.2) of the Met Office Unified Model and the Global Land 8.1 configuration (GL8.1) of the Joint UK Land Environment Simulator (JULES) land surface model (Walters et al., 2017, 2019). Walters et al (2019) give a detailed account of the model upgrade, of which a brief summary is presented here. GA7.2 included atmospheric parametrization schemes developed over several years that improve the fidelity and internal consistency of the model. These include an (i) improved treatment of gaseous absorption in the radiation scheme, (ii) improvements to the treatment of warm rain and ice clouds, and (iii) an improvement to the numerics in the model's convection scheme and microphysics. These have resulted in large reductions in our four critical model errors, namely (i) rainfall deficits over India during the South Asian monsoon, (ii) temperature and humidity biases in the tropical tropopause layer (TTL), (iii) deficiencies in the model's numerical conservation, and (iv) surface flux biases over the Southern Ocean (Walters et al., 2019). An advanced data assimilation method of Hybrid 4-dimensional Variational (4D-Var) is used for the creation of NCUM global analysis. The advantage of the "Hybrid 4D-Var" is that it uses a blend of "climatological" background error, and day-to-day varying flow dependent background error (derived from the 22–members ensemble forecasts). The hybrid approach elegantly combines the benefits of ensemble data assimilation (which provides the flow-dependent co-variances) with the known benefits of 4D-Var within a single data assimilation system (Barker, 2011). A brief description of the NCUM Hybrid 4D-Var global data assimilation system is given in Kumar et al. (2021, 2020, 2019). More details about the DA system are presented in section 2.2.

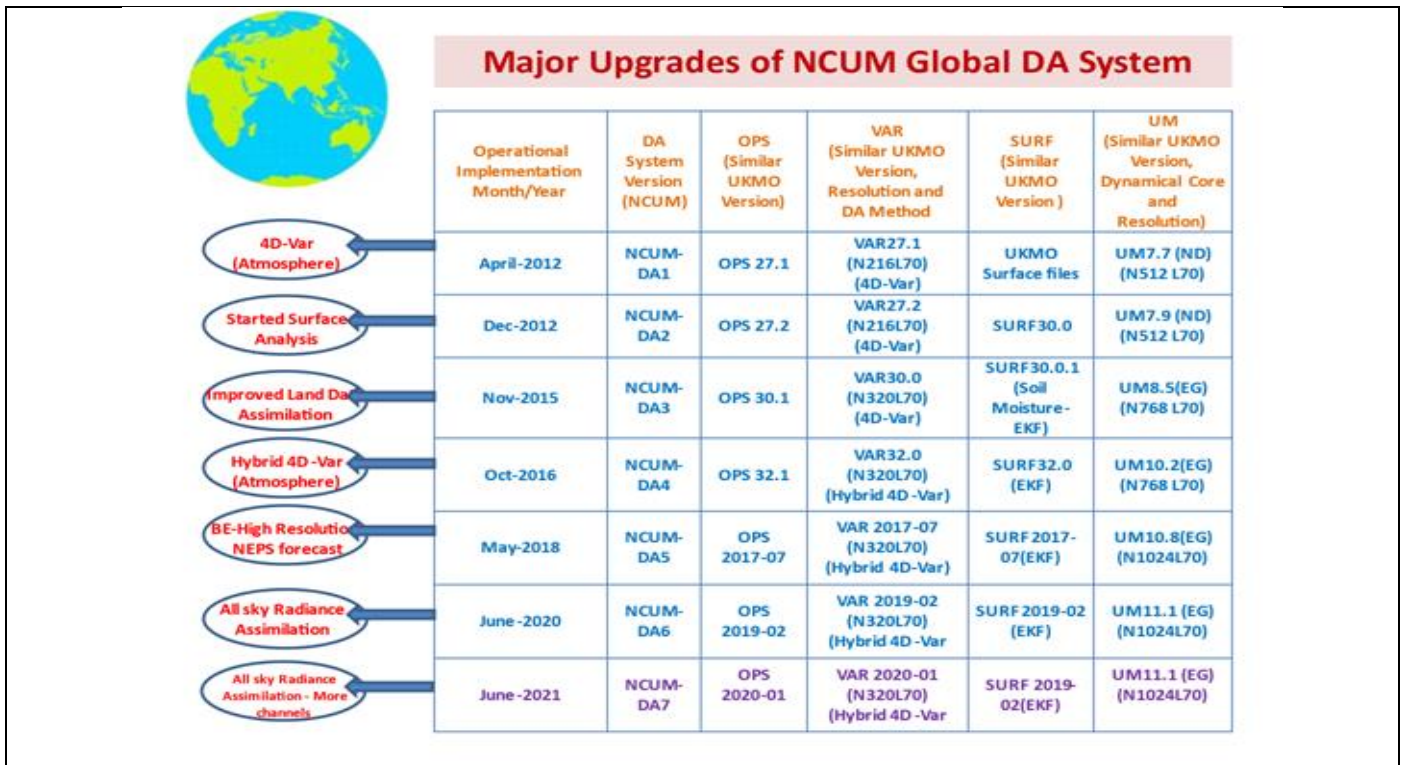**Figure 1. Recent developments and upgrades in the NCUM-G Modelling and Data Assimilation system at NCMRWF.**
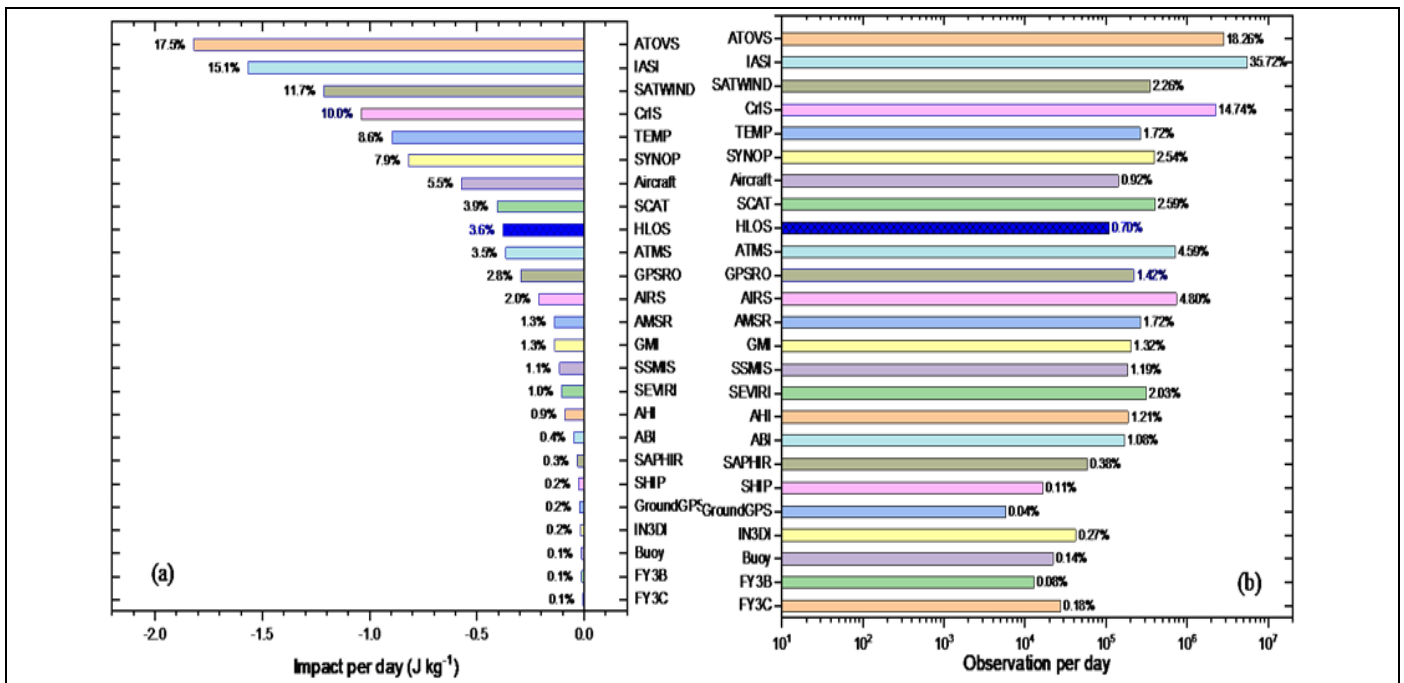

Figure 2. The global mean impact per day (a) of various observations and the count of observations per day, (b) for a one-month period starting from 21st May 2020 on a pre-operational experimental assimilation of the new Aeolus HLOS wind observations along with all other operationally used data.

2.2. *Data Assimilation*

The Data Assimilation (DA) system prepares the initial condition for the model forecast. The data assimilation technique adopted in the NCUM-G is based on the 4D-Var data assimilation method (Rawlins et al., 2007) for the generation of 6 hourly atmospheric analyses since its operational implementation at NCMRWF in 2012. The 4D-Var method allows more effective use of observations through the consistent use of observation operators in the model equations (Rabier et al., 1998, 2007). The NCUM-G DA has undergone many modifications during the last one decade. Many newer observational datasets are included in the data assimilation system. Resolution of the data assimilation system has been increased. One of the major weaknesses of the 4D-Var method is the use of the "climatological" model of the error covariance, which does not represent the flow dependent "error of the day" (Lorenc 2003). To address this, the NCUM-G "4D-Var" data assimilation system has been upgraded to "Hybrid 4D-Var" method following Clayton et al. (2013). The term "Hybrid" in the "Hybrid 4D-Var" method refers to the use of information from other DA systems; here the use of covariances calculated from an ensemble of forecasts (in combination with climatological error covariance), which are designed to sample the current uncertainty. NCMRWF runs a global ensemble prediction system based on NCUM-G, name as the NCMRWF Ensemble Prediction System, NEPS (Sarkar et al., 2016, Mamgain et al., 2018). The NCUM-G Hybrid 4D-Var assimilation system combines the flow dependent errors calculated from the Ensemble Transform Kalman Filter (ETKF) based NEPS forecasts with the "climatological" background errors.

Various in-situ and remotely sensed observations are used in the data assimilation system. Satellite remote sensing offers indirect measurement of atmospheric temperature and humidity in terms of radiances. Before assimilating the radiances (as brightness temperatures) in the NWP models, satellite-measured radiances have to be bias-corrected. The bias correction method can be static or adaptive irrespective of the data assimilation system. A static bias correction scheme based on Harris and Kelly (2001) was used in the NCUM-G assimilation system till October 2016, using 1000 to 300 hPa thickness, 200 to 50 hPa thickness, and total column water vapor as predictors. Since October 2016, the bias correction scheme has been changed from static to adaptive. The adaptive bias correction, commonly known as Variational bias correction (VarBC) is based on Cameron and Bell (2018) and closely follows the incremental formulation based on Auligne et al., (2007), while keeping the same set of predictors as that used in the static method. In VarBC, the bias correction is applied through the bias control variable in the variational analysis equation.

In addition to the above changes in the data assimilation method and bias correction, several observations were also introduced in the operational NCUM-G data assimilation system in recent periods. They include, the radiances and atmospheric motion vectors from Spinning Enhanced Visible and InfraRed Imager (SEVIRI) onboard Meteosat-8 relocated to the Indian Ocean Data Coverage (IODC) in February 2017,

scatterometer sea surface winds from Scatsat-1 operated by Indian Space Research Organization (ISRO) since November 2017, Advanced Himawari Imager (AHI) radiances from Himawari-8 satellite, and sea surface winds from Windsat since May 2018, Global Precipitation Mission (GPM) Microwave Imager (GMI) radiances and INSAT-3D imager radiances (Rani et al., 2019) since August 2018. *The currently used DA system, operational since June 2022 has the capability to assimilate many all-sky satellite observations, especially the cloud-affected microwave humidity sounder observations from MHS of ATOVS. This improved operational DA system has the capability to assimilates novel observations such as Horizontal Line Of Sight (HLOS) observation from Aeolus satellite.* The impact of assimilating HLOS observations is quantified using the Forecast Sensitivity to Observations (FSO) in Figures 2 a, b. A detailed list of observations assimilated in the current operational NCUM DA system is given in Table-1. For the accurate prediction of the location and track of the tropical cyclones, the location and the magnitude of the low pressure in the model analysis should be as realistic as possible. In the NCUM-G, the location and the estimated minimum low-pressure value associated with the tropical cyclone are assimilated from the Tropical Cyclone Vital (TC Vital) reports since October 2018.

Table 1. *List of Satellite based observation types and variables assimilated in the NCUM-G data assimilation system.*

Observation Type	Observation Description	Assimilated Variables
Surface	Surface observations over Land and Ocean (TAC & BUFR), TC bogus *(*Surface Pressure)	Wind, Temperature, Humidity, Surface Pressure
Sonde	Radiosonde (TAC & BUFR), Pilot balloons, Wind profiles, & Radar VAD winds	Wind, Temperature, Humidity
Aircraft	Upper-air wind and temperature from aircraft (AMDAR & AIREP)	Wind, Temperature
Ground GPS	Ground based GPS observations	Zenith Total Delay
Satellite: GPSRO	Global Positioning System Radio Occultation observations from various satellites (Terra-Sar X, COSMIC (E1 to E6), FY3D, KOMPSAT, MetOp (A, B, & C))	Bending Angle
Satellite: Satwind	Atmospheric Motion Vectors from geostationary and polar orbiting satellites (MSG, JMA, GOES, MetOp, INSAT-3D, & INSAT-3DR, MODIS, NOAA)	Wind
Satellite: Scatwind	Advanced Scatterometer in MetOp-A & B, ScatSat-1, WindSat	Wind
Satellite: MicroWave Sounder/Imager	Microwave sounders / imagers ATMS, AMSU, GMI, MWHS, AMSR2, SAPHIR, SSMIS	*Brightness Temperature*
Satellite: Hyperspectral IR	Hyperspectral infrared sounders IASI, CrIS, AIRS	*Brightness Temperature*
Satellite: Geostationary Sounder/Imager	Sounder/Imagers from MSG, GOES, Himawari, INSAT	*Brightness Temperature*
Satellite: HLOS Wind	Mie-scattering and Rayleigh-scattering Horizontal Line-Of-Sight (HLOS) winds from AEOLUS satellite	HLOS wind

2.3. Observed/analysis Data used for the Verification

The seasonal mean analysis and anomalies are studied against the fifth-generation European Centre for Medium-Range Weather Forecasts (ECMWF) reanalysis product (ERA-5) (Hershbach et al., 2020) climatology (1979-2018). The high-resolution (12km) NCUM-G analysis data is interpolated to ERA-5 grid resolution (0.25^0 x 0.25^0) for the verification studies. For verification of the forecasts, the NCUM-G model analysis is also used. All systematic errors are computed at a native grid resolution of 12km.

Detailed quantitative rainfall forecast verification is carried out against the India Meteorological Department (IMD)-NCMRWF daily high resolution (0.25^0) rainfall analysis (Mitra et al. 2009, 2013). The rainfall analysis objectively analyses IMD daily rain gauge observations onto a 0.25^0 grid using a successive corrections technique, with the GPM Satellite rainfall providing the first guess estimates. The model forecasts are gridded to the 0.25^0 observed rainfall grids over Indian land regions for 122 days from 1st June to 30th September 2023. As noted by Mitra et al. (2009), the merged analysis at 0.25^0 grid resolution is appropriate for capturing the large-scale rain features associated with the monsoon. The merging of the IMD gauge data into GPM estimates not only corrects the mean biases in the satellite estimates but also improves the large-scale spatial patterns in the satellite field, which is affected by temporal sampling errors (Mitra et al. 2009).

3. NCUM-G Analysis Mean and Anomalies during JJAS 2023

The NCUM-G mean analysis fields and anomalies relative to climatology are assessed in this section during JJAS 2023. The discussion is presented for Winds, Temperature, and Relative Humidity for four standard levels of 850, 700, 500, and 200 hPa. The anomalies are computed against the ERA5 climatology (1979-2018).

The mean winds and anomalies at 850 & 700 hPa levels from NCUM-G analysis are shown in Figure 3. The following features can be seen at the 850 hPa level figure (a) cross-equatorial flow, (b) strong south-westerlies over the Arabian Sea (AS) with core winds exceeding 18 m/s, (c) south-westerlies over Bay of Bengal (BoB), (d) westerlies/south-westerlies over peninsular India, central India, and (e) south-westerlies and southerlies widespread over the Southeast (SE) Asia (Figure 3a). The anomaly winds in Figure 3c show (a) weak cross-equatorial flow and (b) south-easterly anomaly winds over the Arabian Sea. Over the Arabian Sea the negative anomaly indicated in red shade also suggests (c) weaker south-westerlies, (d) weaker westerlies/south-westerlies over north-eastern Indian region and head Bay of Bengal. At 700 hPa level (Figure 3b) the mean winds show most of the features very similar to flow at 850 hPa. In addition, Northeasterly flow is prominent over the horn of Africa and adjoining Arabian Sea which was not seen at 850 hPa. Another feature to be noted at 700 hPa level is the strong cross equatorial and south westerly winds. The wind anomalies at 700 hPa show

an anomalous cyclonic circulation over the AS indicating a stronger monsoon current over the AS (Figure 3d). Over the equatorial Indian Ocean, specifically in southern latitudes, the SW winds are weaker in NCUM-G analysis resulting in strong anomalous easterlies/south-easterlies. Similarly, over the Indian land region, the easterly anomalies over north-eastern India indicate weak westerly winds relative to ERA-5 climatology.

A similar analysis is presented for 500 and 200 hPa in Figure 4. At 500 hPa, the SW flow over the Arabian Sea, Bay of Bengal, & peninsula India is seen however, w.r.t ERA5 climatology the anomalies are relatively weak (Figures 4a, c). Weaker south-westerlies indicated by negative anomalies over the Bay of Bengal. In contrast, positive anomalies are observed over across the western parts of India and extending into adjoining Arabian Sea (Figure 4c). At 200 hPa (Figure 4b), the mean circulation prominently features the (a) strong westerlies over the north of India, (b) Tibetan anticyclone, and (c) widespread easterlies/northeasterly over the peninsula and the Indian Ocean. The anomalous winds (Figure 4d) indicate weaker than normal easterlies/northeasterly over the AS, southern Bay of Bengal, peninsular India, and parts of SE Asia, as indicated by a negative anomaly in red shade. Over the north of India between 40-95^{0}E the analysis features stronger westerlies (a positive anomaly in the blue shade).
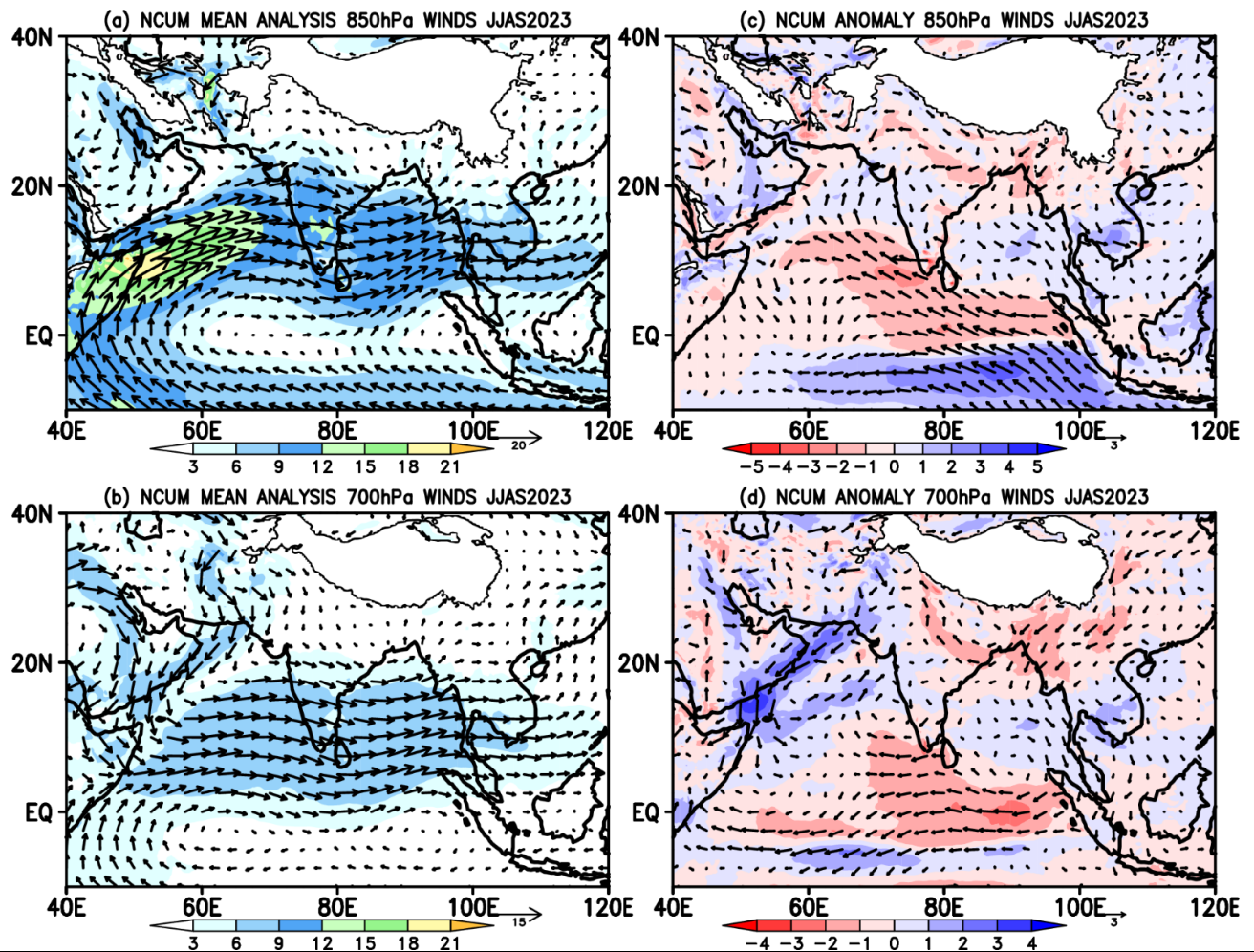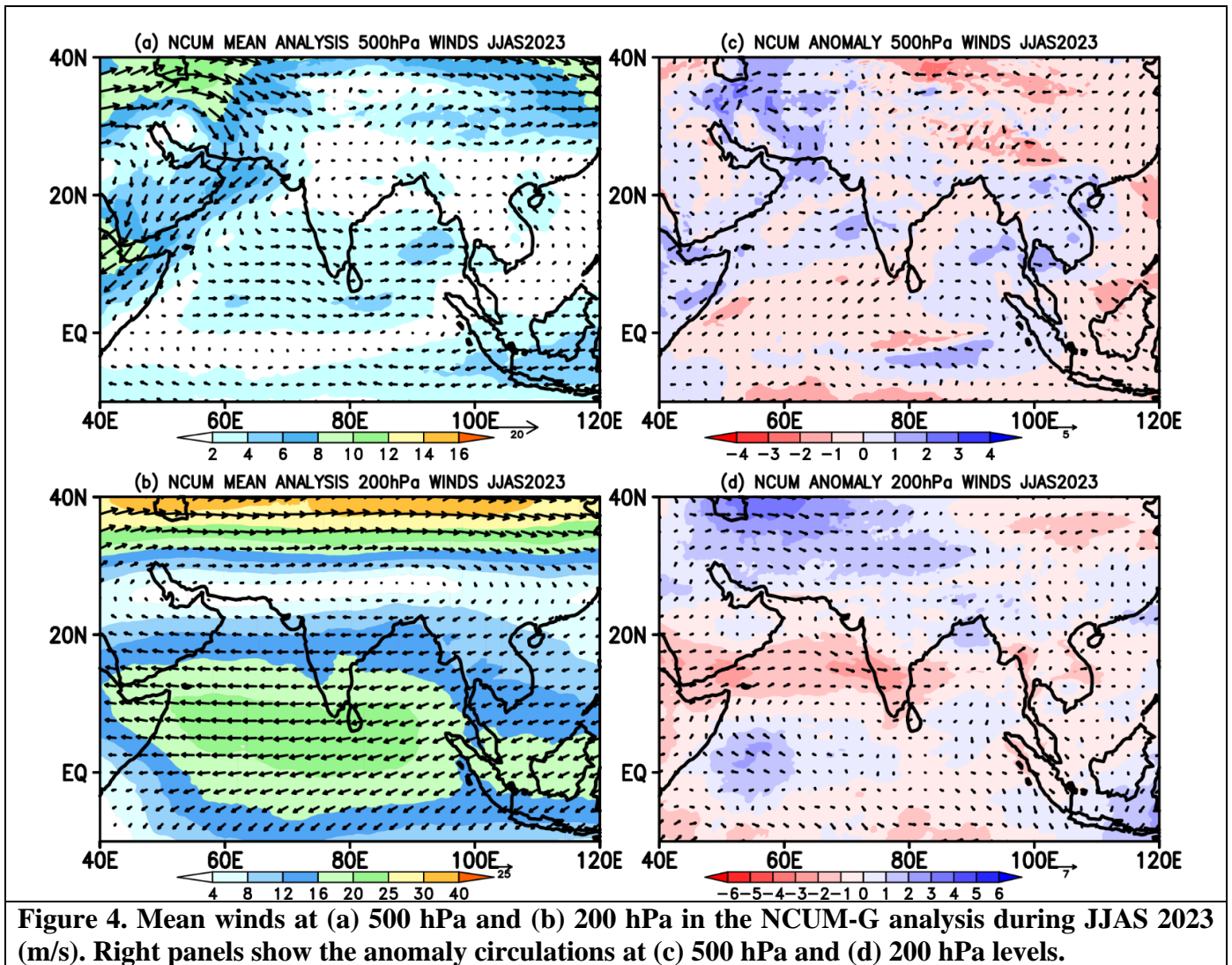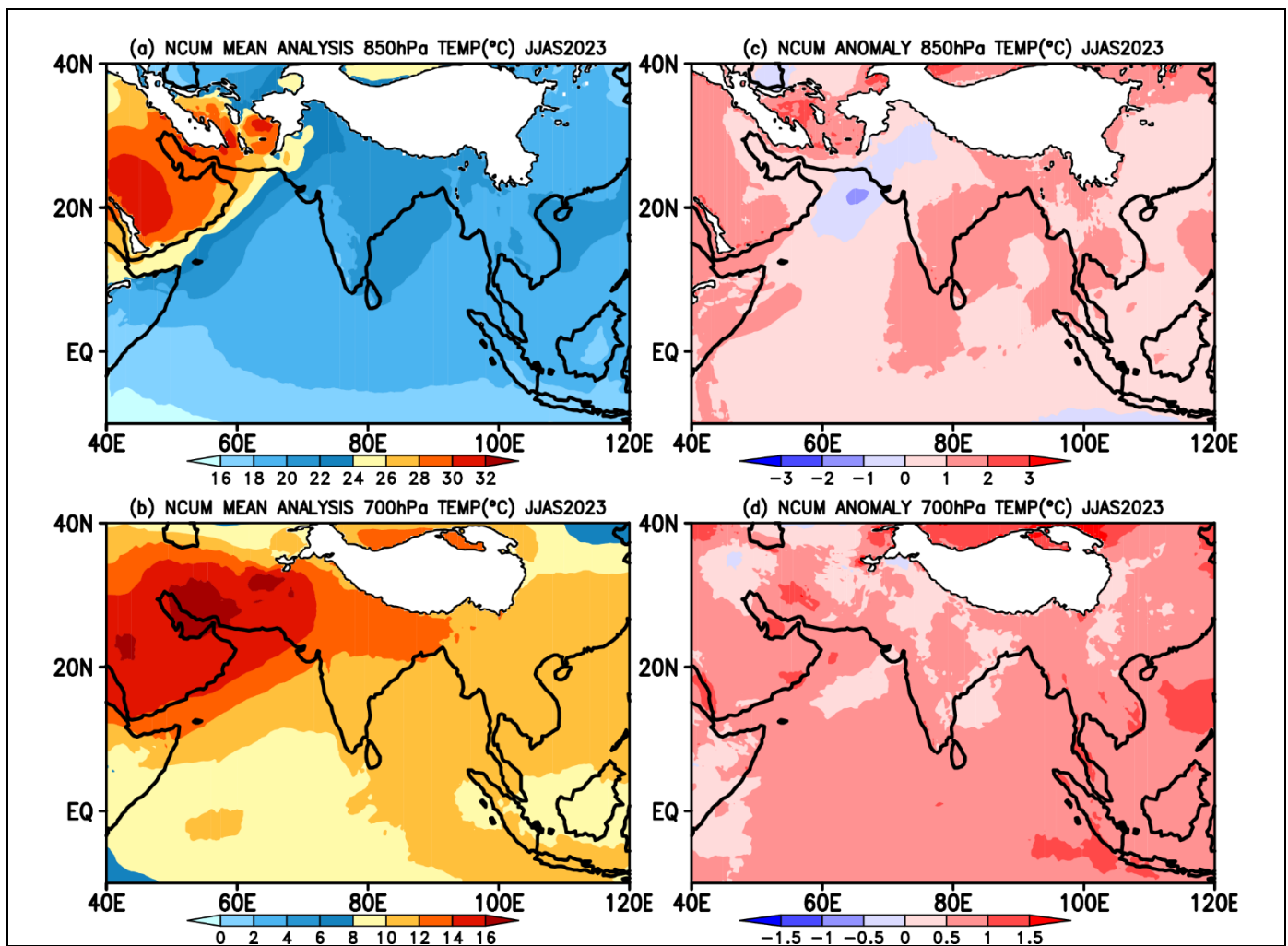
Figure 3. Mean winds at (a) 850 hPa and (b) 700 hPa in the NCUM-G analysis during JJAS 2023 (m/s). The right panels show the anomaly circulations at (c) 850 hPa and (d) 700 hPa levels.

Figure 4. Mean winds at (a) 500 hPa and (b) 200 hPa in the NCUM-G analysis during JJAS 2023 (m/s). Right panels show the anomaly circulations at (c) 500 hPa and (d) 200 hPa levels.

The spatial distribution of seasonal mean temperature and anomalies at 850 and 700 hPa levels are shown in Figure 5. The mean daily temperature at lower levels (i.e., at 850 and 700 hPa levels) is below 21^0C over the Indian subcontinent and adjoining Seas excluding the north-west part of India and the Arabian Sea (Figures 5a, b). The positive anomalies (1-2^0C; red) are widespread, except over the north-west part of India and the Arabian Sea (Figure 5c). The negative anomalies (1 to -2^0C at 850 hPa) over the northern Arabian Sea could be due to weak westerlies at 850 hPa (Figure 3c) and strong northeasterly flow from land, particularly at 700 hPa (Figure 3d). At 700 hPa, positive temperature anomalies are seen over the entire domain (Figure 3d). Mean temperature and anomalies at 500 and 200 hPa levels are shown in Figure 6. The mean temperature is obviously maximum at 500 hPa over the Tibetan region associated with a high sensible heat flux resulting in an anticyclone during the summer monsoon period. The positive anomalies ($>1^0$C at 500 hPa and $>2^0$C at 200 hPa) are seen as widespread over the entire domain (Figures 6c, d).

The lower tropospheric mean and anomaly Relative Humidity at 850 and 700 hPa levels are shown in Figures 7a-d. The mean RH is high (>60%) at 850 and 700 hPa (Figures 7a, b) over the Indian land region and neighboring Seas typically indicating the humid monsoon climate. The mean RH values exceed 80% at 850 hPa over India's west coast, central, and northeastern regions. The RH anomaly at 850 hPa (Figure 7c) is significantly positive (blue) indicating a wet anomaly in the analysis over the part of the northern Arabian Sea. However, the RH anomaly is negative (red) indicating a dry anomaly over the Bay of Bengal and large parts of the equatorial Indian Ocean (central and eastern). At 850 hPa level, the dry RH anomaly could be partly explained as due to weaker southwesterly monsoon flow (Figure 3c) over a large area covering the Bay of Bengal and large parts of the equatorial Indian Ocean. At 700 hPa level (Figure 7d), the RH anomaly is positive (blue) over the entire domain, except for isolated regions of North West (NW) India and SE Asia, which may not be explained fully by the wind anomaly shown in Figure 3d.

Figure 5. Mean Temperature (Degree Celsius, ^{0}C) at (a) 850 hPa and (b) 700 hPa in the NCUM-G analysis during JJAS 2023. Right panels show the Temperature anomalies at (c) 850 hPa and (d) 700 hPa levels.
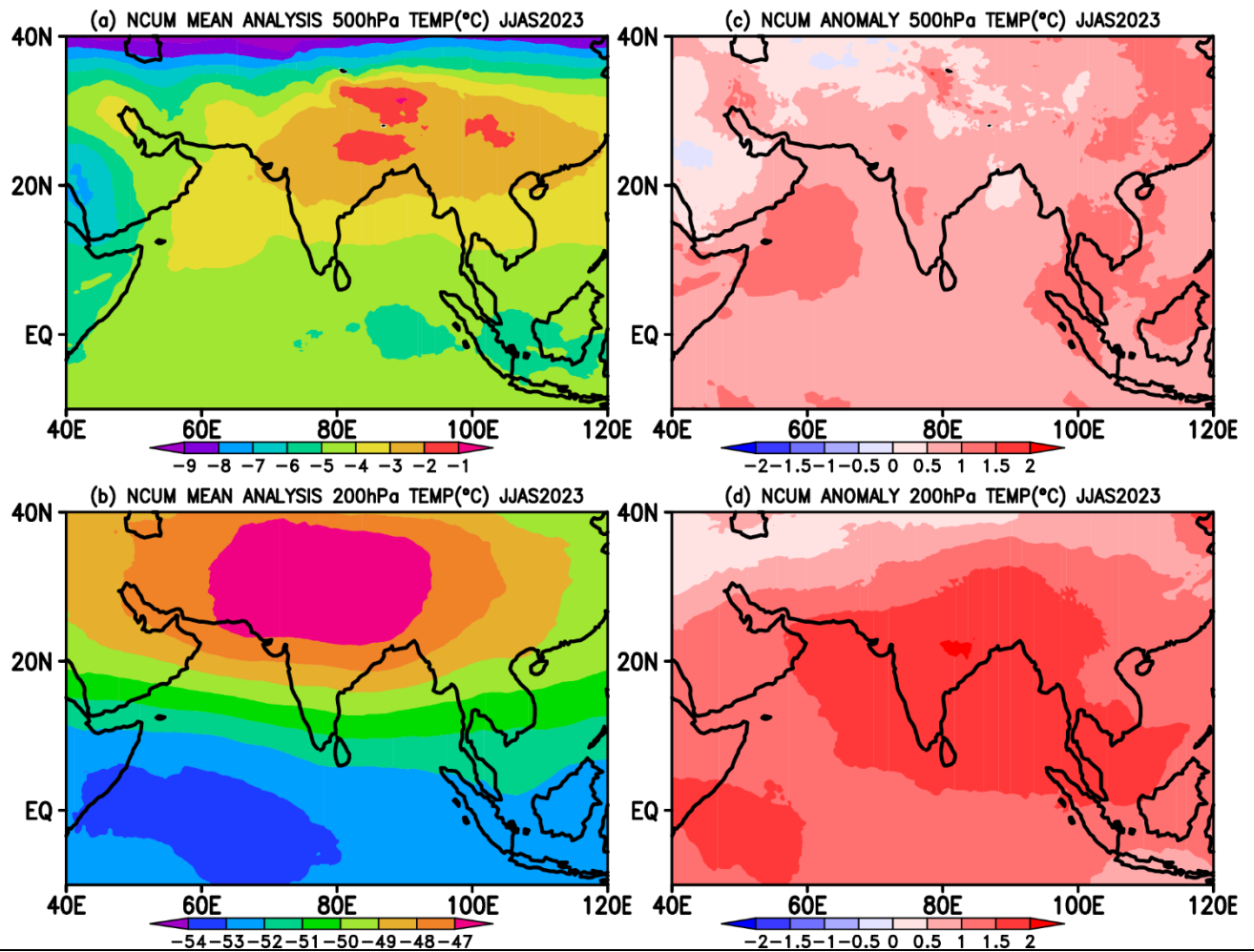
Figure 6. Mean Temperature (Degree Celsius, ^{0}C) at (a) 500 hPa(b) 200 hPa in the NCUM-G analysis during JJAS 2023. The right panels show the Temperature anomalies at (c) 500 hPa and (d) 200 hPa levels.

Figure 7. Mean Relative Humidity (%) at (a) 850 hPa and (b) 700 hPa in the NCUM-G analysis during JJAS 2023. The right panels show the anomalies in Relative Humidity at (c) 850 hPa and (d) 700 hPa.
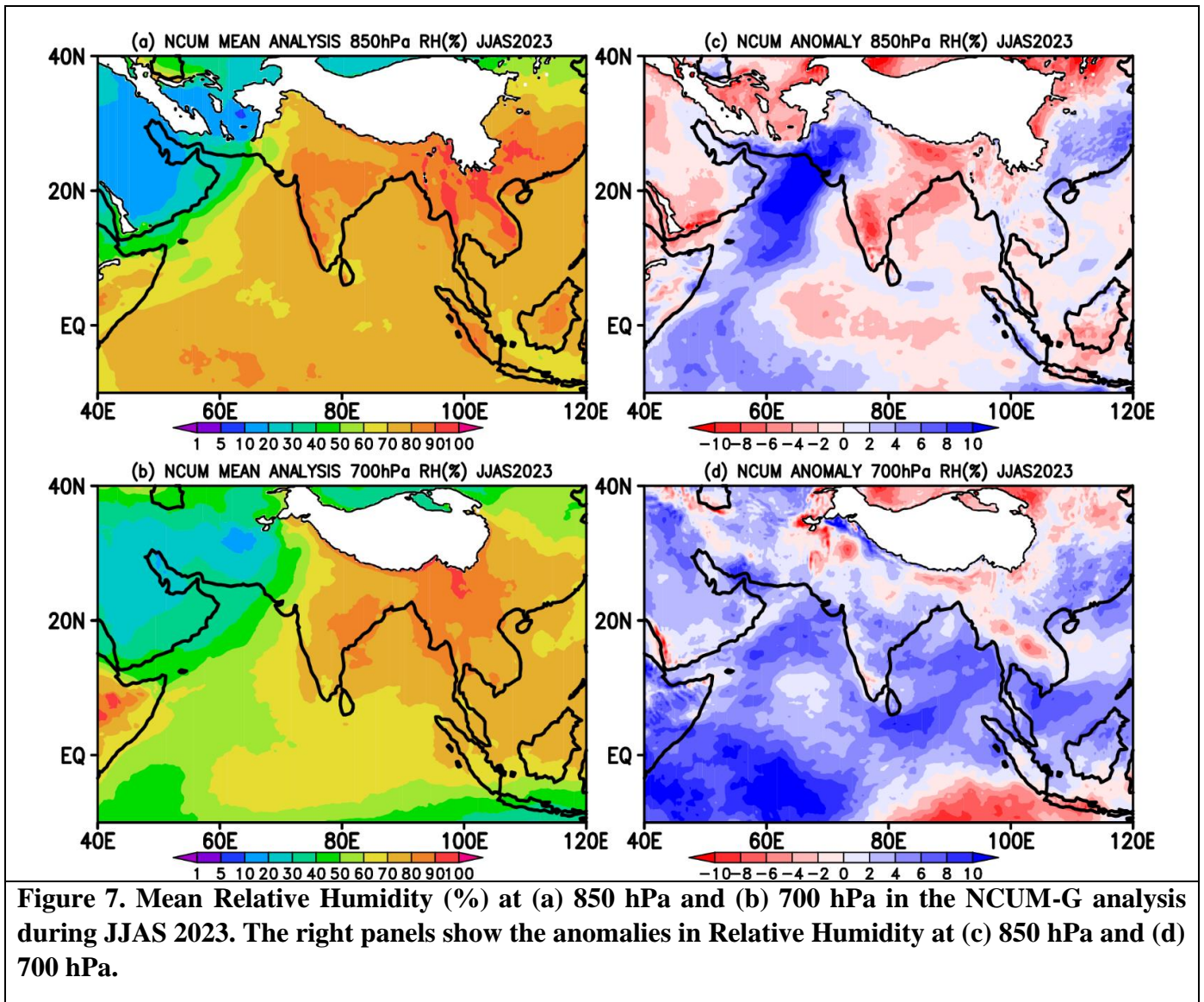
4. Systematic Errors in NCUM-G Forecasts

This section discusses systematic errors in the Day-1 (24 hr), Day-3 (72 hr), and Day-5 (120 hr) forecasts relative to model analysis for Winds and Temperature at 850, 700, 500, and 200 hPa levels; and Relative Humidity at 850 and 700 hPa levels (Figures 8-13).

4.1. *Winds at 850, 700, 500, and 200 hPa levels*

At 850 hPa level (Figures 8a-d), the systematic errors in the forecast indicate three important features (a) A westerly & southwesterly bias over the Indian region and neighboring seas suggesting stronger monsoon flow in forecasts. The magnitude of the positive bias is increasing from Day-1 to Day-5 (Figures 8b-d). Interestingly the forecast winds are not covering the Somali coast; instead, the strong cross-equatorial flow is more prominently seen over open Arabian Sea, especially in Day-3 and Day-5. (b) An easterly bias over the

eastern equatorial Indian Ocean indicating a weakened westerly/southwesterly flow in the forecasts. The pattern of biases (positive and negative) over the Bay of Bengal and the anticyclonic anomaly in Figure 8c, d, suggests a slight northward shift in the monsoon flow over the Bay of Bengal. (c) The westerly bias along the west coast of India can be seen shifting northwestwards in Day-5 with the strongest bias over the northern Arabian Sea and western India in Day-3 and Day-5.

At 700 hPa level (Figures 9a-d), the westerly bias over the Indian peninsula and Bay of Bengal is prominent extending over SE Asia. Negative bias (red) over the northern and western Arabian Sea indicates weakened monsoon flow, particularly in the Day-3 and Day-5 forecasts. The weaker cross-equatorial flow can also be seen off the African coast. Additionally, the negative bias over the eastern equatorial Indian Ocean, prominent at 850 hPa is also pronounced at 700 hPa level (Figures 8 and 9).

At 500 hPa level (Figures 10a-d) the pattern and sign of biases over the western and eastern equatorial Indian Ocean are more or less similar. Over the northern Arabian Sea, positive bias (blue) indicates strong northeasterly flow from NW India where anomalous cyclonic flow is evident on Day-3 and Day-5. At 200 hPa (Figures 11a-d), the positive easterly bias (blue) extends over the Indian peninsula and neighboring Arabian Sea and Bay of Bengal and the magnitude of this bias increases with forecast lead time. The negative westerly bias (red) occupies the entire equatorial region of the domain suggesting a weakened tropical easterly jet as forecast length increases.

Figure 8. (a) Mean winds and systematic errors (m/s) in (b) Day-1, (b) Day-3, and (d) Day-5 forecasts at 850 hPa during JJAS 2023.

Figure 9. (a) Mean winds and systematic errors (m/s) in (b) Day-1, (b) Day-3, and (d) Day-5 forecasts at 700 hPa during JJAS 2023.
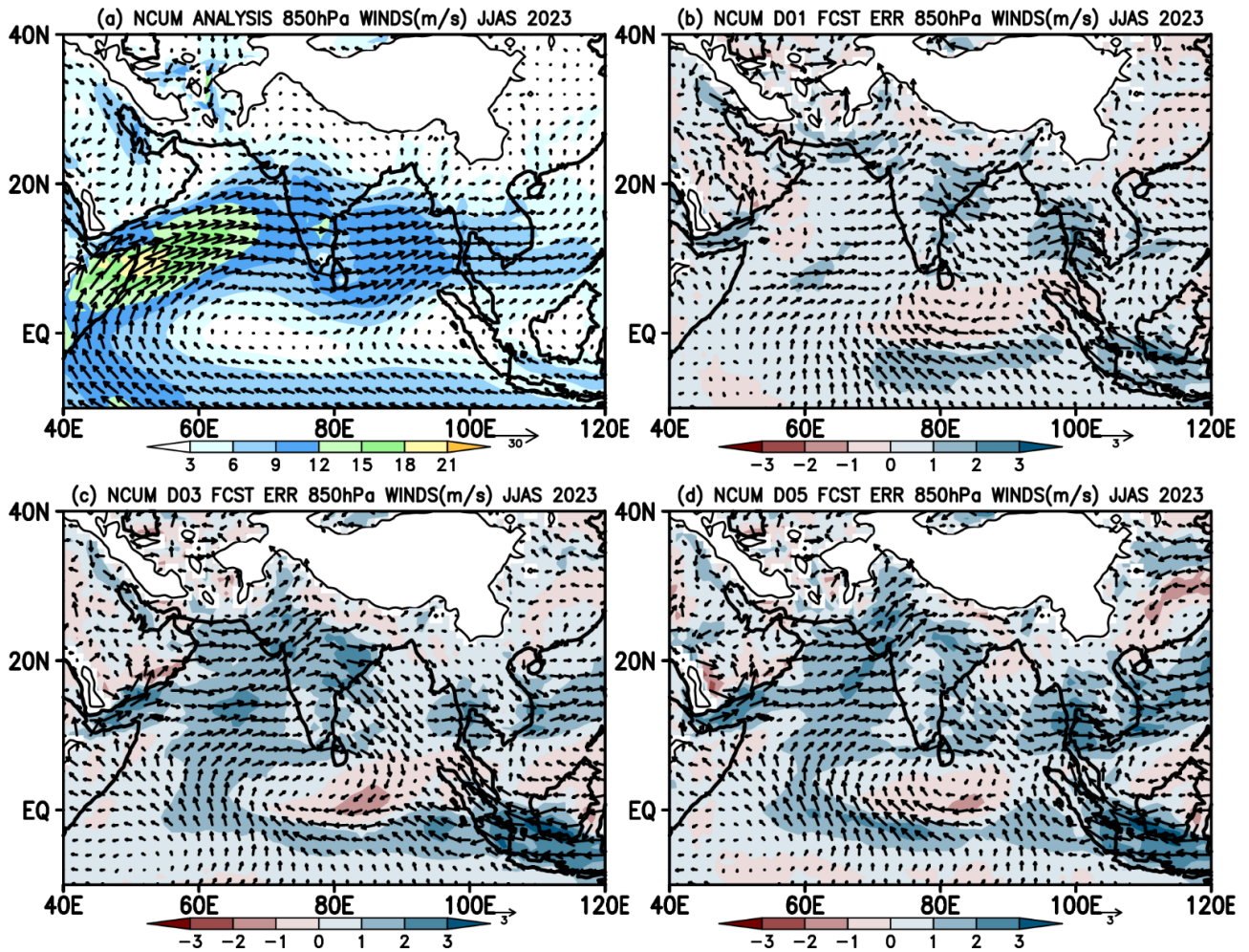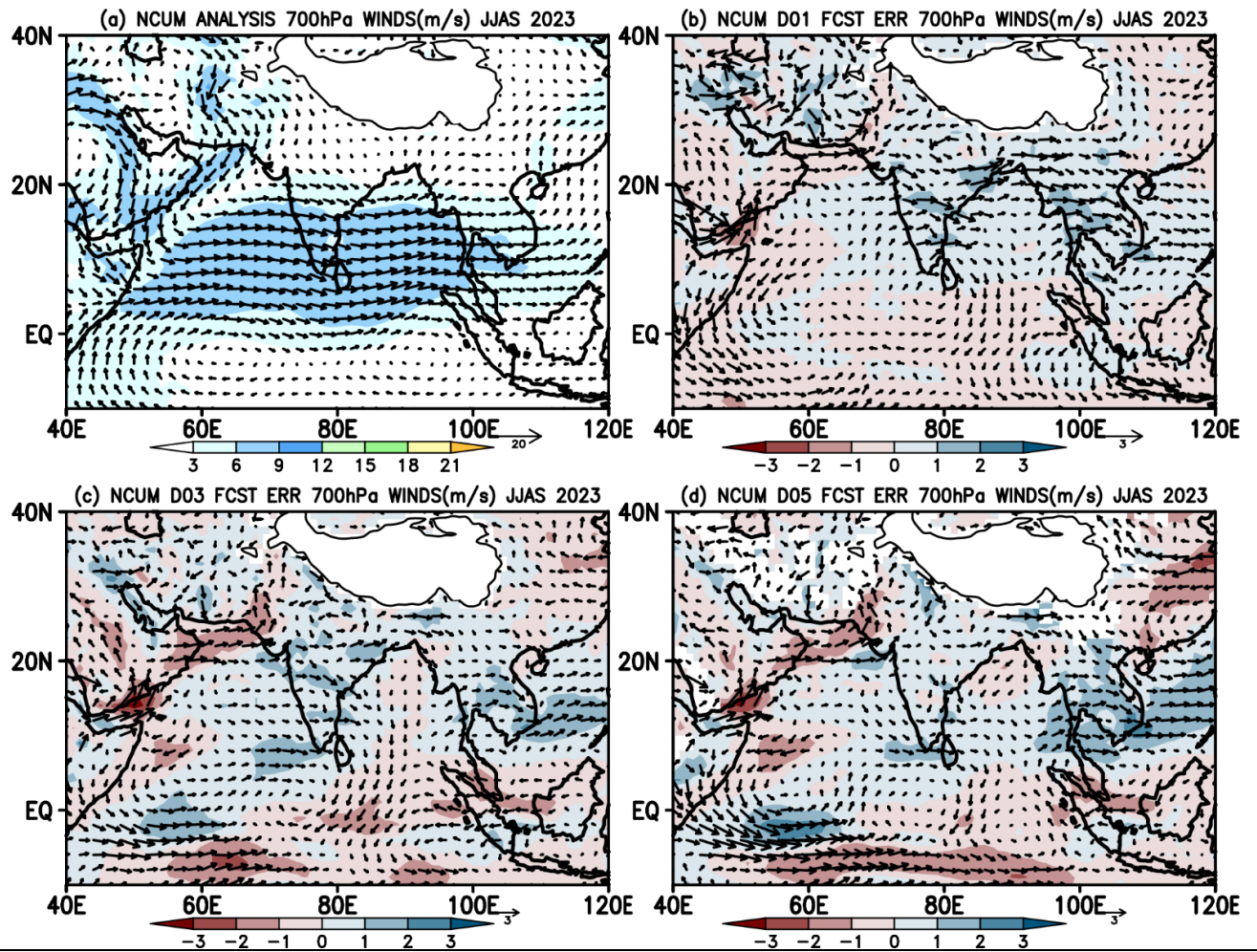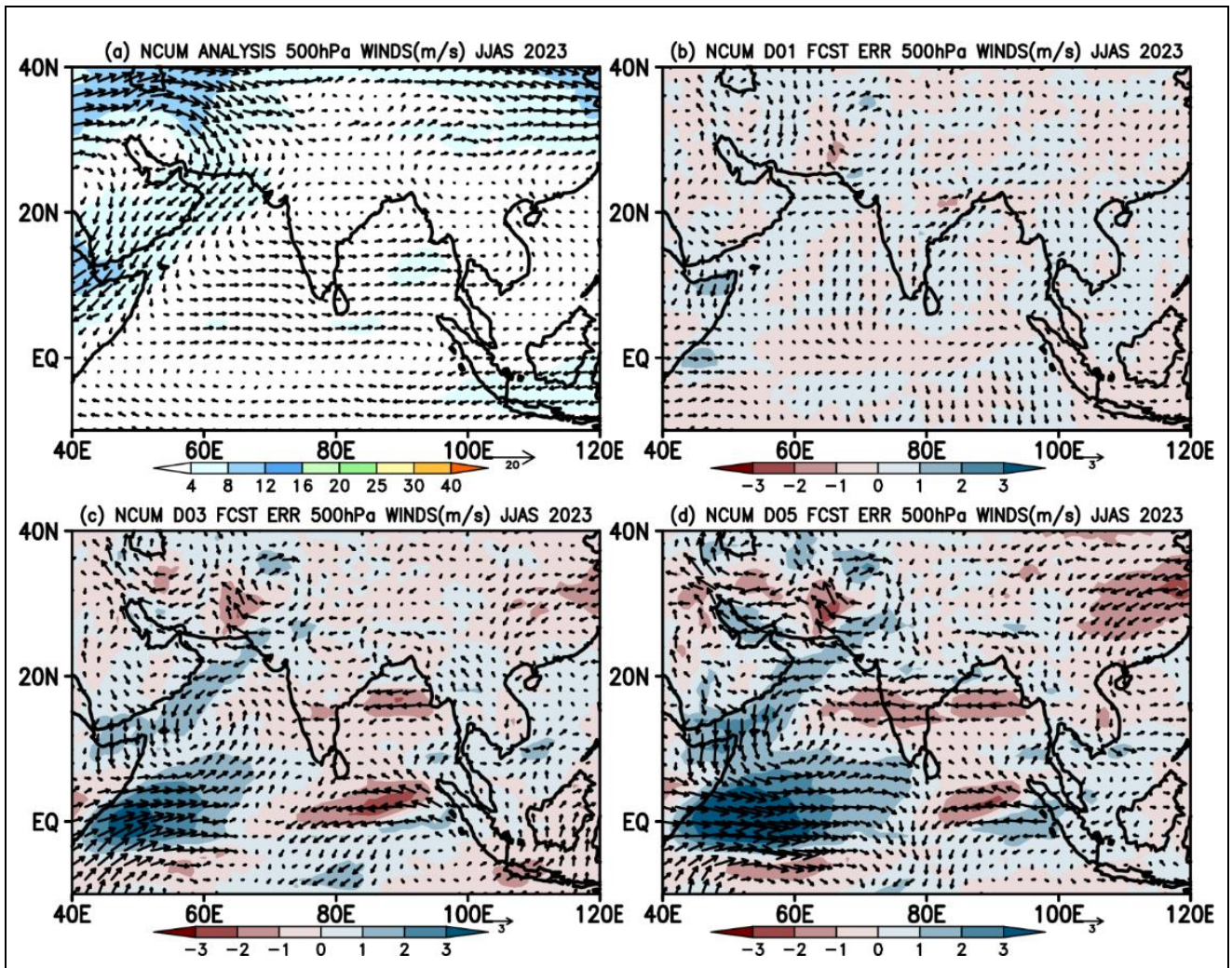
Figure 10. (a) Mean winds and systematic errors (m/s) in (b) Day-1, (b) Day-3, and (d) Day-5 forecasts at 500 hPa during JJAS 2023.
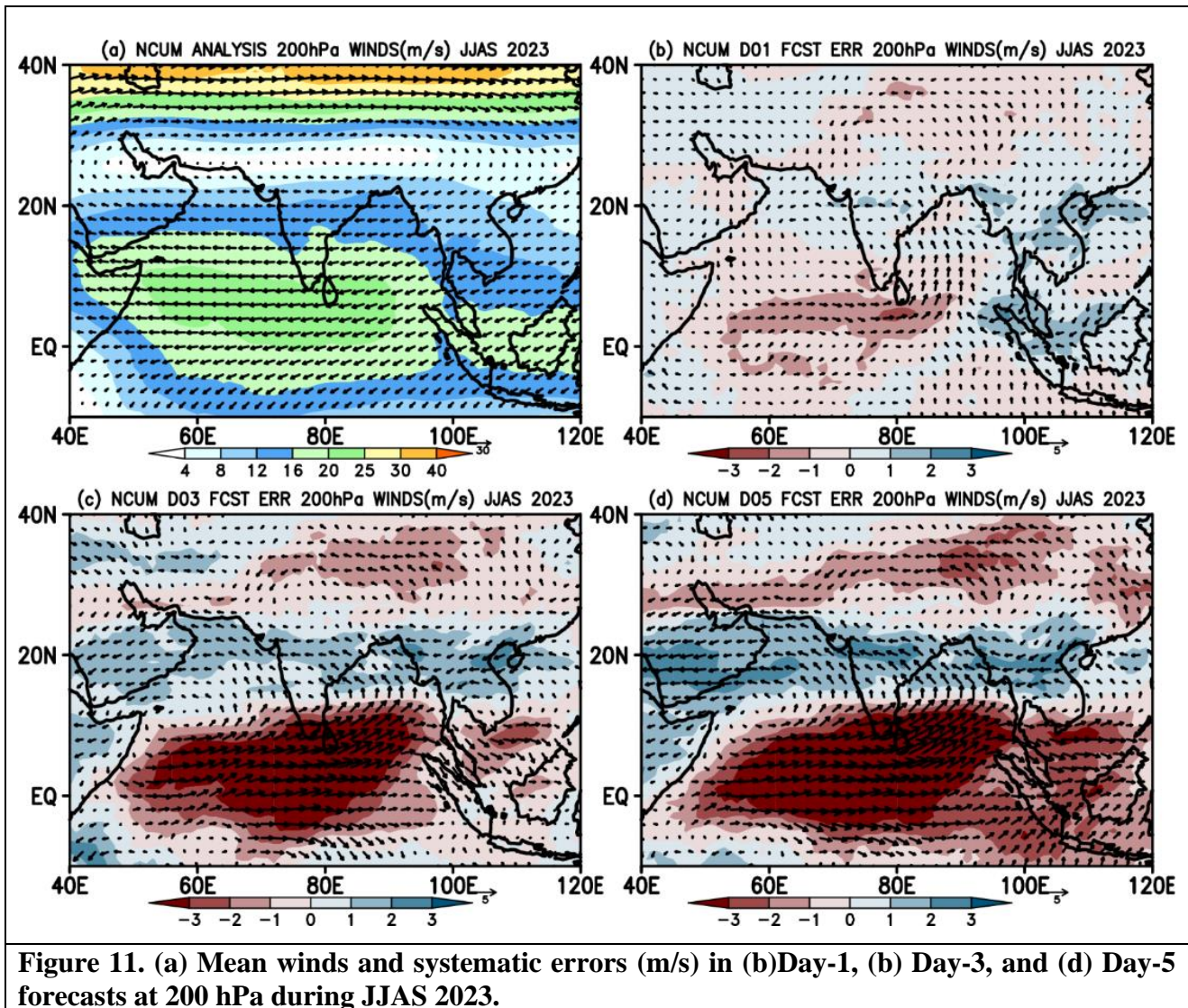
Figure 11. (a) Mean winds and systematic errors (m/s) in (b)Day-1, (b) Day-3, and (d) Day-5 forecasts at 200 hPa during JJAS 2023.

4.2. *Temperature and Relative Humidity*

At 850 hPa level, (Figures 12a-d) systematic errors in temperature forecasts indicate (a) a warm bias (>0.5°C) over north India particularly over the Indo-Gangetic plain (IGP) region and the neighboring Arabian Sea, Bay of Bengal, and around the South China Sea regions. (b) Strong warm bias (>1°C) is prominent in Day-3 and Day-5 forecasts over NW India. (c) Mild cold bias (about -0.5°C) over west coast of India. At 700 hPa (Figure S1; see appendix) and 500hPa (Figure S2; see appendix) the warm (*cold*) bias over the land (*sea*) regions persists by and large with reduced magnitude, excluding the easter Indian Ocean at 500 hPa and peninsular India at both levels. At 200 hPa (Figure S3; see appendix), the land and sea regions partly feature cold bias in all the forecasts, except over the equatorial Indian Ocean, with magnitudes of about 0.5^0C.

Figure 13 shows the systematic errors in Relative Humidity at the 850 hPa level. The forecasts prominently exhibit negative (red) dry bias over the Arabian Sea, NW India, IG plains, and head BoB in all the lead times.

These dry biases are also seen at 700 hPa (Figure S4, see appendix). Consistent with bias in RH, it is found that total precipitable water (PWAT) (see appendix Figure S5) also shows dry bias. In summary, the forecasts have a moist and dry bias in the lower troposphere, and the magnitude of bias increases with forecast lead time. It is rather difficult to corroborate all the moist and dry biases based on the wind biases alone. Hence, vertically integrated moisture transport (VIMT) is assessed in next section.
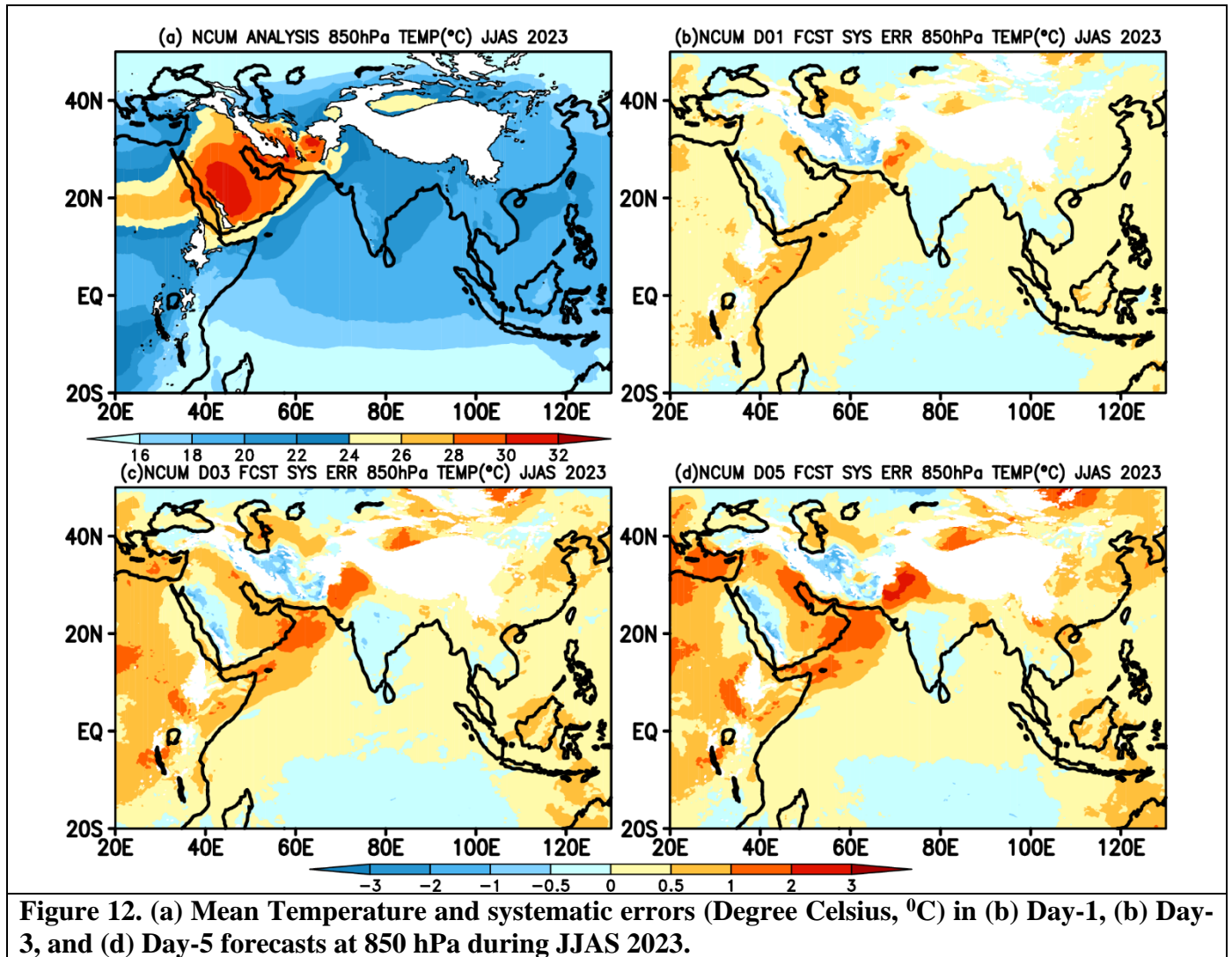

Figure 12. (a) Mean Temperature and systematic errors (Degree Celsius, ^{0}C) in (b) Day-1, (b) Day-3, and (d) Day-5 forecasts at 850 hPa during JJAS 2023.
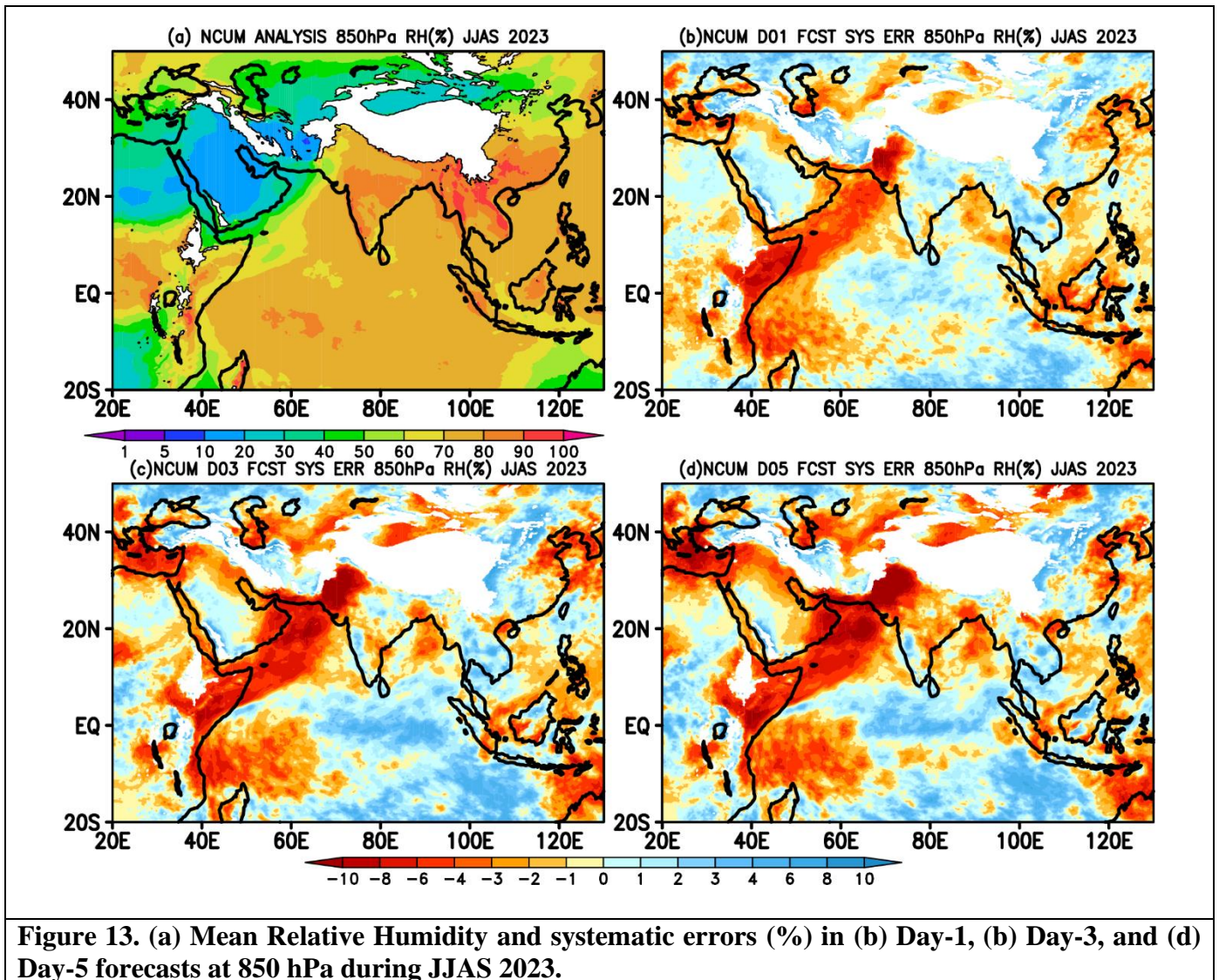
Figure 13. (a) Mean Relative Humidity and systematic errors (%) in (b) Day-1, (b) Day-3, and (d) Day-5 forecasts at 850 hPa during JJAS 2023.

4.3. *Vertically Integrated Moisture Transport (VIMT)*

To further assess the role of biases in winds and moisture at different levels, systematic errors in VIMT are computed based on wind components (*U, V*) and specific humidity (*q*) at all levels (surface – 300 hPa). The analyses mean VIMT and systematic errors during JJAS 2023 are presented in Figures 14a-d. The biases in the forecasts show positive (blue) over the entire Indian land region, Arabian Sea, and the Bay of Bengal. The Day-3 and Day-5 forecasts show negative bias (red) over the eastern equatorial Indian ocean consistent with the wind biases at 850, 700, and 500 hPa shown in Figures 8-10. Despite the strong dry bias indicated by systematic errors in RH (Figure 13), it can be inferred that the strong positive biases in winds (Figure 8-10) have offset the impact of dry bias in the forecasts over India. It is also worth noting that over the IG plains, negative bias in VIMT is prominent, with increasing error magnitudes as the forecast lead time increases.
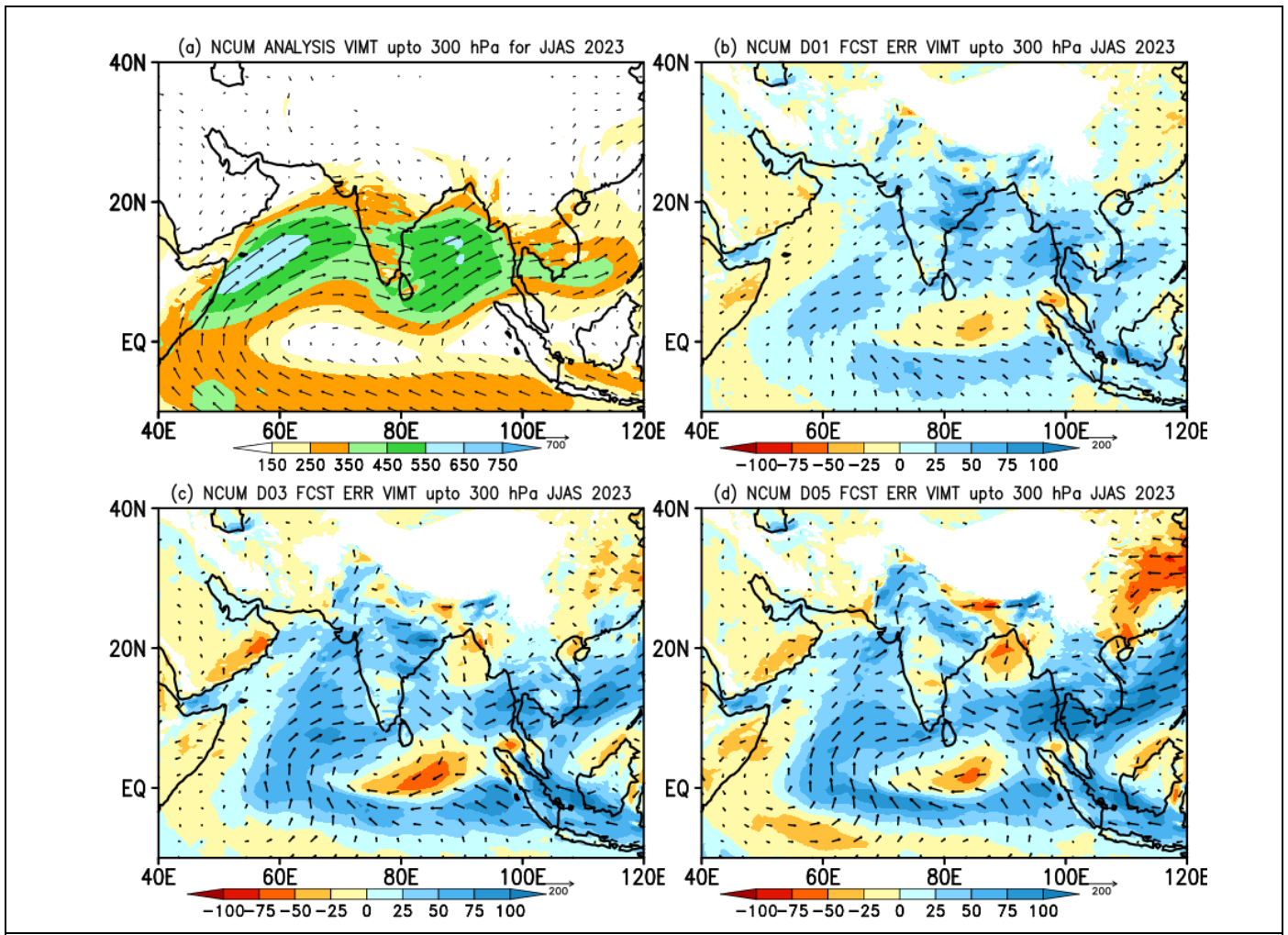
Figure 14. (a) Mean VIMT and systematic errors in (b) Day-1, (c) Day-3, and (d) Day-5 NCUM-G forecasts.

4.4. *RMSE in Wind and Temperature over India 2018-2023*

The forecast errors at 850 and 200 hPa winds and temperature are quantified in terms of RMSE computed against the analysis over India in Figure 15. The results of JJAS 2023 are compared with scores from recent monsoons (2018-2023). Although there are some year-to-year variations in the RMSE, the lowest RMSE is evident during JJAS 2022 at all lead times, however, a slight increase is seen in JJAS 2023 RMSE compared to JJAS 2022 (except for Temp at 200 hPa, Figure 15).
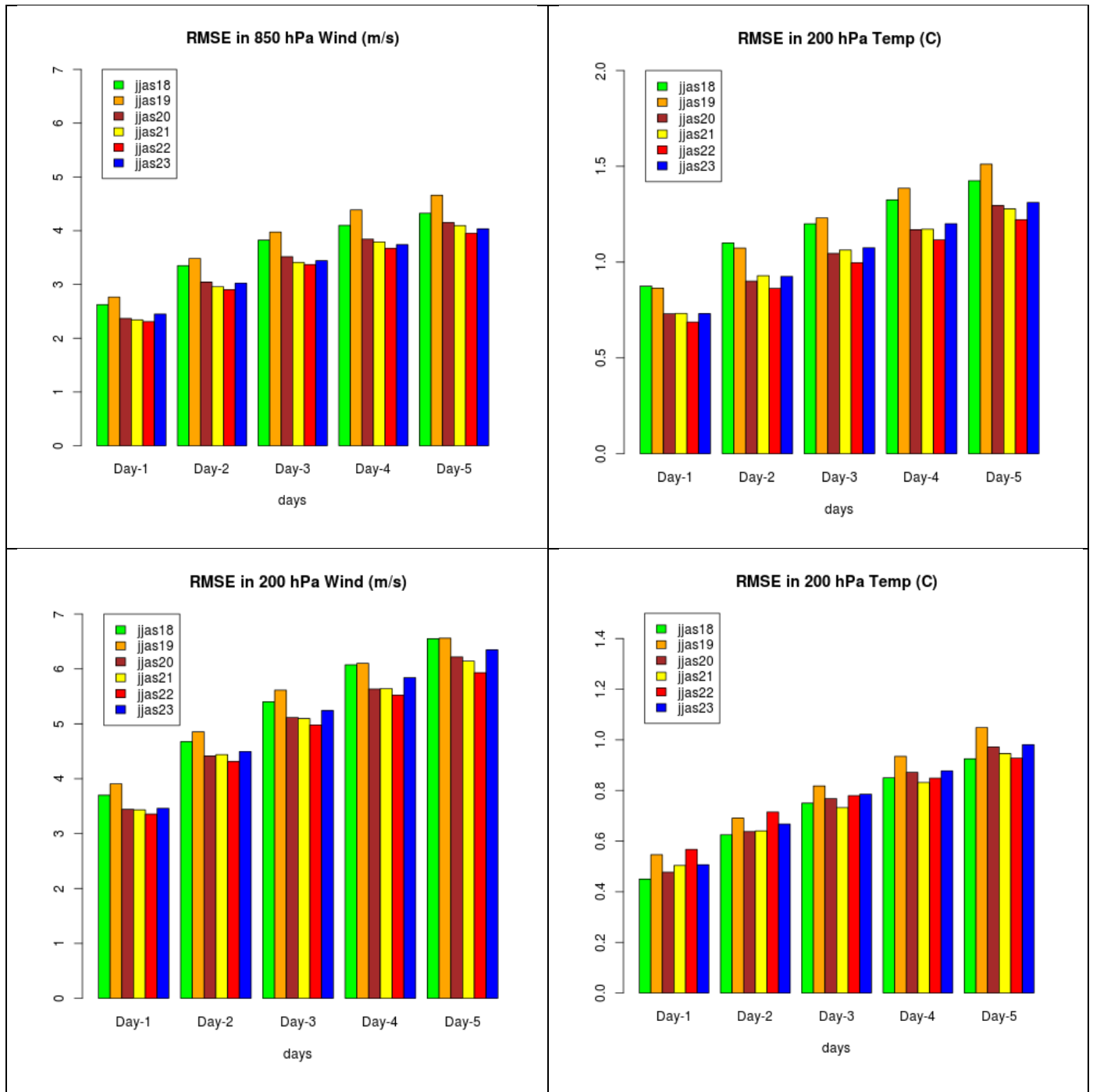
Figure 15. RMSE in the NCUM-G forecast at 850 & 200 hPa in (left panel) wind and (right panel) temperature during recent years (2018-2023).

5. Rainfall Forecast Verification during JJAS 2023

Verification of NCUM-G model rainfall forecasts is presented in this section for JJAS 2023. The 24-hour accumulated rainfall forecasts are verified against the NCMRWF-IMD merged Satellite and gauge rainfall analysis. The discussion presented in this section is aimed at highlighting the model biases and accuracy over India using mean error (ME), RMSE, correlation, forecast rainfall frequency at different thresholds, etc. Further, this section also quantifies forecast skill using standard verification metrics, namely, the probability of detection (POD), the probability of detection (FAR), critical success index (CSI), BIAS, Peirce's skill score (PSS) which are described in standard text books (Wilks 2011, Jolliffe and Stephenson 2012) and new Symmetric extremal dependence index (SEDI) (Stephenson et al. 2008, Ashrit et al. 2015, Sharma et al. 2022).
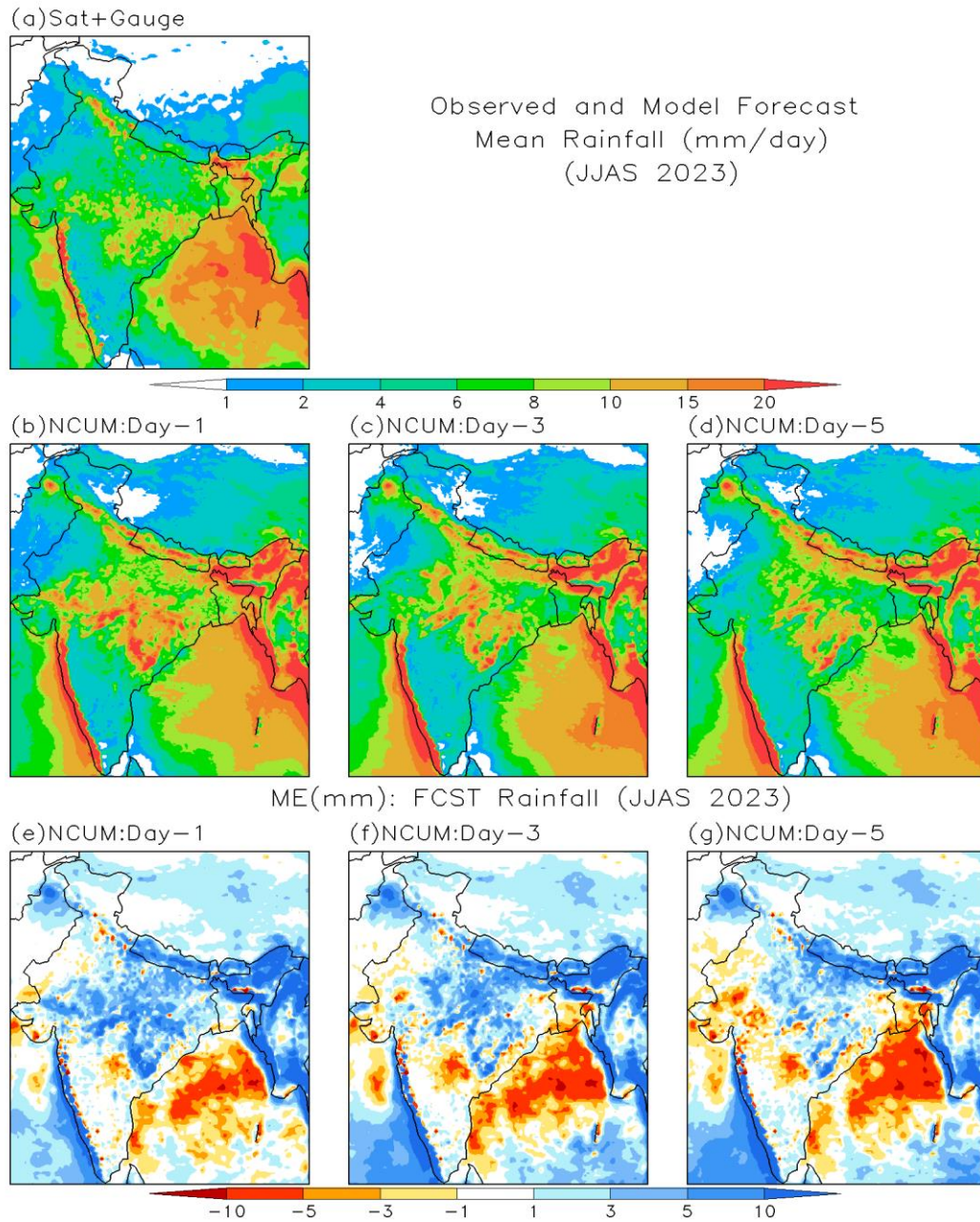
5.1. *Mean, Mean Error, RMSE, and Correlation*

The observed and forecast mean monsoon rainfall during JJAS 2023 is shown in Figure 16. Observations indicate the highest mean rainfall exceeding 10 mm/day is seen over the west coast, head Bay of Bengal, and parts of Northeast (NE) India. Another region of high rainfall 6-10 mm/day is prominent over the core monsoon region where the synoptic systems during monsoon bring in heavy rains (Figure 16a). The panels in the middle row, Figures 16b-d show Day-1, Day-3, and Day-5 forecast rainfall averaged during the JJAS 2023. The observed peak rainfall amounts (>10mm/day) along the Western Ghats and the Arakan coast are well predicted in all the forecast lead times. However, it is found that the NCUM-G forecast shows higher rainfall amounts all over the West Coast and NE India. In addition, the forecasts overestimate the isolated high rainfall amounts (>10mm/day) over the core monsoon regions, indicating the overestimation of observed rainfall over land and the neighboring seas. On the contrary, forecast rainfall shows a large underestimation over the Bay of Bengal region, which is noteworthy. The reduced rainfall amounts (<6mm/day) over the eastern parts of the peninsula and northwest India are predicted fairly well in the model. The panels in the bottom row (Figures 16e-g) show mean error (ME) in predicted rainfall indicating wet bias (blue) all along the west coast, over the Arabian Sea, and over central India. Dry bias (orange/red) is prominent over the Bay of Bengal and the amplitude of dry bias is enhancing w.r.t lead time. Over the Indian land region, dry bias can be seen over parts of Gujarat, western India, parts of the central peninsula, and isolated regions along the west coast. The east-west gradient over the west coast in the ME (i.e., wet (dry) bias to the west (east)) indicates a westward shift in the rainfall over the west coast in the forecasts. Similarly, wet (dry) bias over core monsoon regions, NE India, and Arakan coast (parts of peninsula and adjoining Bay of Bengal) indicates a northward and eastward shift in the forecast rainfall over core monsoon regions, NE India, and Arakan coast.

The excessive forecast rainfall in the model over hilly regions of the west coast, NE India, and the Himalayas is attributed to an enhanced model grid resolution of 12km. The wet bias (blue) over central India and the core

monsoon zone can be partly explained as resulting from the positive bias in VIMT discussed in Figure 14. While the dry bias over the Bay of Bengal could be associated partially by the moderate negative bias (~-25) in VIMT over that region and the wet bias over the Arabian Sea is in very good agreement with the positive VIMT.

To further quantify and summarize the rainfall forecast performance over India, a spatial map of RMSE and correlation is presented in Figure 17. RMSE gives the average forecast error weighted according to squared error. While it does not indicate the direction of the forecast errors, it gives greater emphasis on relatively larger errors. It can be noted that the forecasts feature large errors over regions of high rainfall amounts along the west coast, Himalayan belt, Bay of Bengal, central India, and NE regions. Additionally, RMSE is high over parts of the core monsoon regions and Bay of Bengal, which can be seen to increase with forecast lead time. However, the map of correlation (Figure 17) shown in the bottom panels suggests a sharp decline in the forecast skill from Day-1 to Day-5.

Figure 16. Accumulated JJAS rainfall (mm) in (a) Observations and (b) Day-1, (c) Day-3, and (d) Day-5 forecasts. Bottom panels (e), (f), and (g) show Mean Error (ME) in Day-1, Day-3, and Day-5 forecasts, respectively.
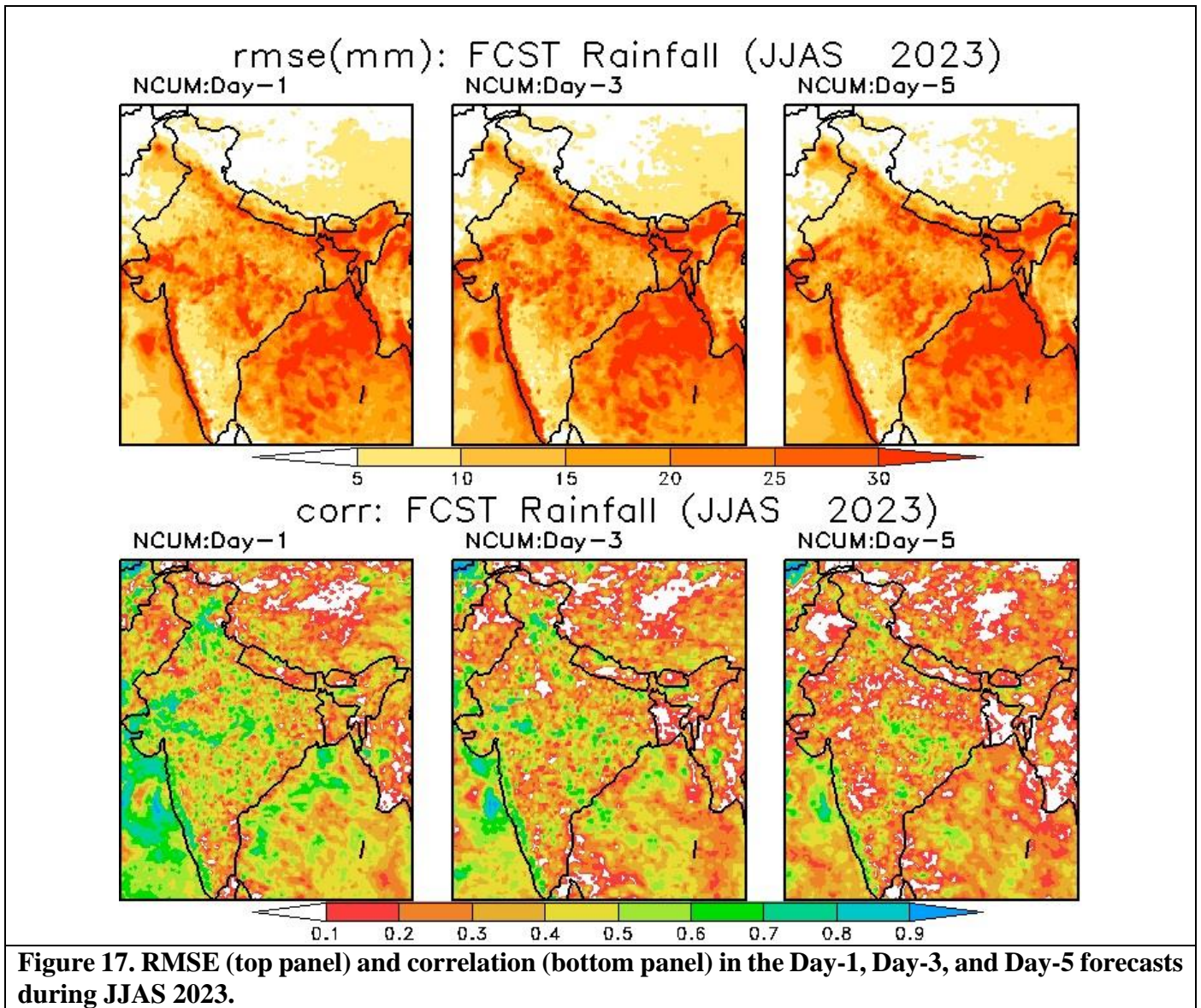
Figure 17. RMSE (top panel) and correlation (bottom panel) in the Day-1, Day-3, and Day-5 forecasts during JJAS 2023.

5.2. *Frequency of Rainy Days, Moderate Rain Days, and Heavy Rain Days*

To further assess the source of wet rainfall bias over the land regions in the model forecasts and observed, counts for observed and forecasted rainfall >1mm/day (rainy day) are presented in Figure 18. The observations show (a) a high number of rainy days (>80 days; orange shade) along the west coast and NE India and (b) 60-80 days (yellow shade) over the core monsoon regions. Over the dry regions of NW India and the eastern peninsula, the number of rainy days is lower than 40-60 days (green & blue) (Figure 18a). The model forecasts show an exceedingly higher number (>60 days) of rainy days over most parts of India (Figures 18b-d).

Similar counts for observed and forecasted rainfall exceeding thresholds 15.6 mm/day ("moderate rainy days") and 64.5 mm/day ("heavy rainy days") are presented in Figures 19 and 20, respectively. Figures 19b-d shows that the model forecasts have a higher (60-80) number of moderate rainfalls over the west coast and NE India. Over the dry regions of NW India, central, and eastern peninsula, the model predicts a far lower number of moderate rainy days. For the "heavy rainy days" (>64.5 mm/day) category (Figure 20a-d), forecasts have a higher count along the west coast, over NE India, and core monsoon regions (to some extent). Thus, it can be concluded that *a significant part of rainfall biases over the Indian land region is due to the model's tendency to frequently predict higher rainfall amounts.*

Figure 18. (a) Observed and forecasted (b) Day-1, (c) Day-3, and (d) Day-5 number of rainy days (i.e., rainfall >1mm/day) during Jun-Sept 2023.

Figure 19. Same as in Figure 18, but for rainfall threshold above 15.6 mm/day during JJAS 2023.

Figure 20. As in Figure 18, but for rainfall threshold above 64.5 mm/day during JJAS 2023.
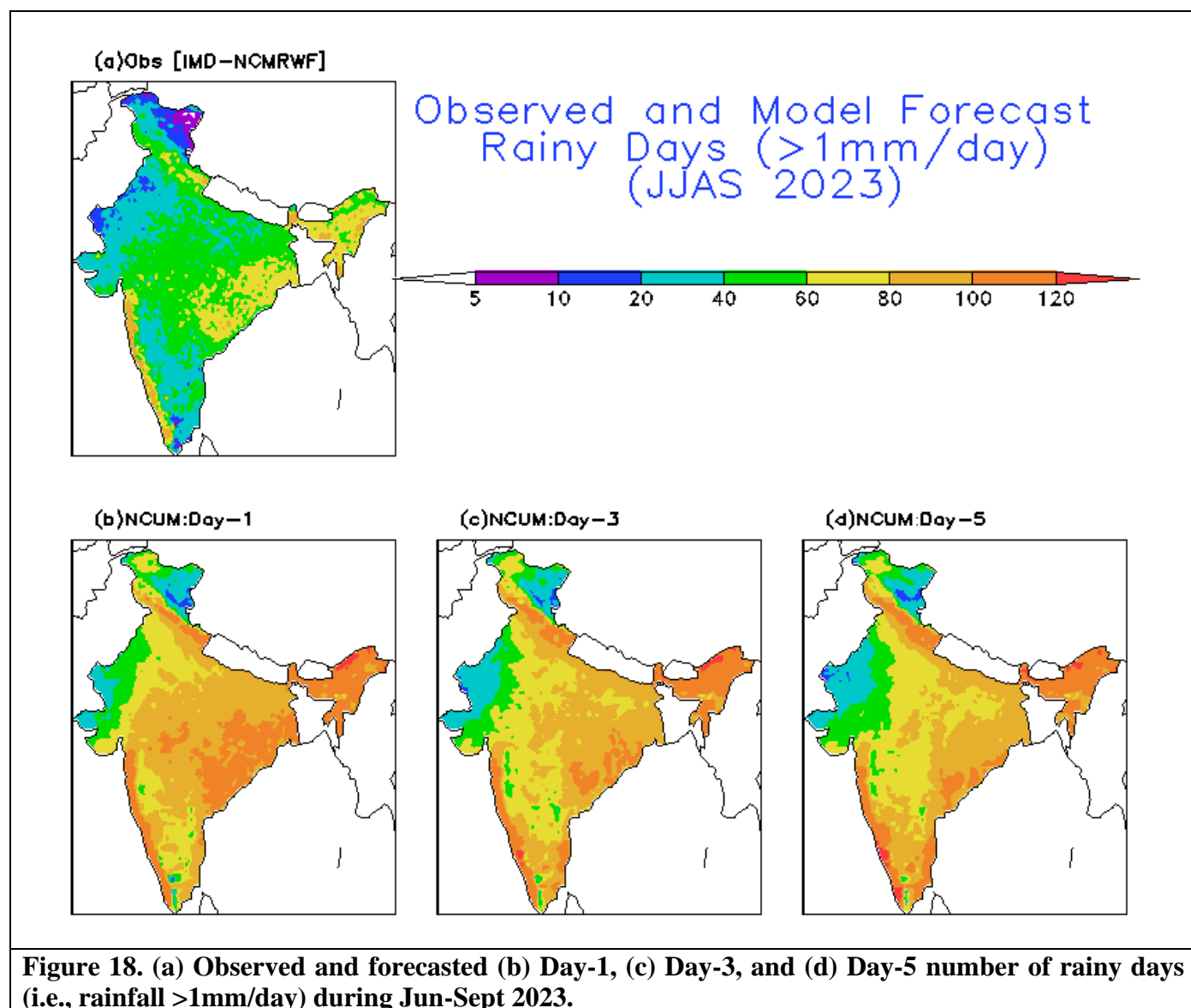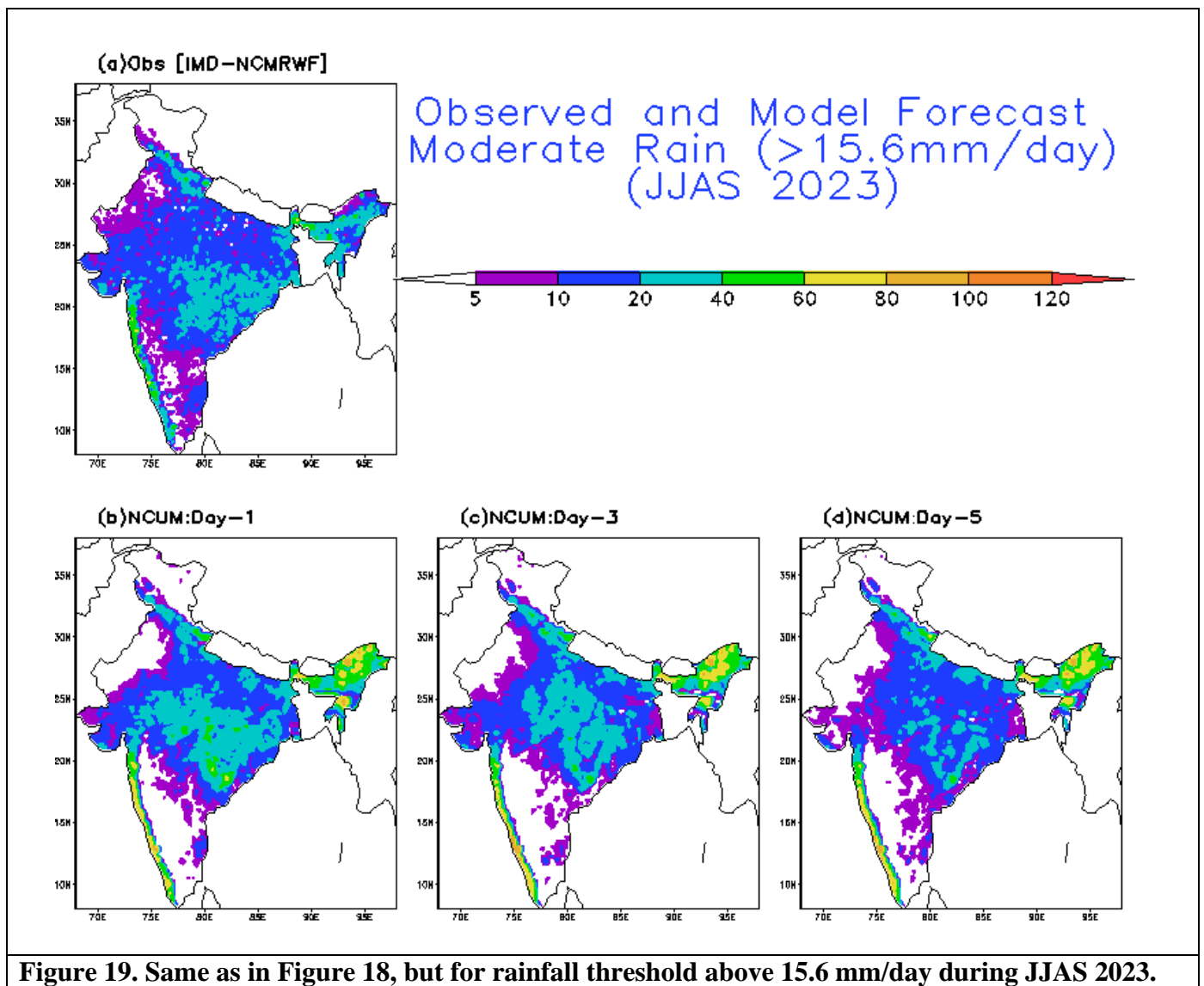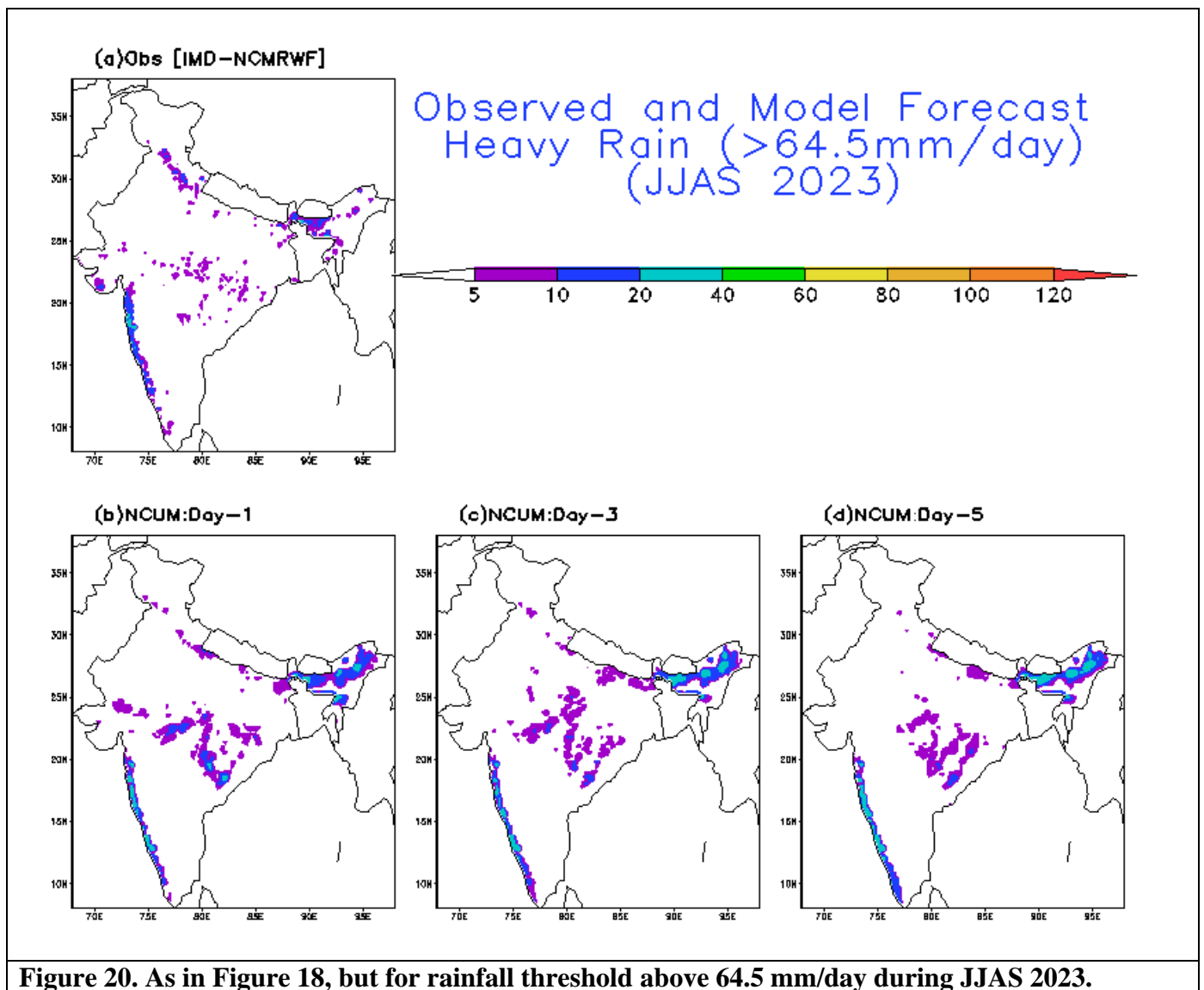
5.3. *Categorical Scores of Rainfall forecasts*

To further quantify the model rainfall forecasts, categorical skill scores are computed over the Indian subcontinent. The categorical approach of verifying quantitative precipitation forecast (QPF) is based on the 2 x 2 contingency table which is evaluated for different rainfall thresholds. A detailed description of the verification metrics computed using the 2 x 2 contingency table is presented in Appendix (Tables S1 and S2) and the results for JJAS 2023 are shown in Figure 21. Verification scores are shown for rainfall of up to 30mm/day. For rainfall threshold of up to 9 mm/day, the forecasts have POD >0.5 (& FAR <0.6) in the Day-1 forecast. After 9mm/day, POD and FAR show a decrease and increase in scores, respectively. The BIAS score (frequency bias) indicates that forecasts overestimate the frequency upto 9mm/day or lower. The values

of CSI, PSS, and SEDI all are high for rainfall up to 9mm/day suggesting reasonable skill. However, the skill is not bias-free. For higher amounts (9-30mm/day), there is no frequency bias, but the skill is low as indicated by CSI, PSS, and SEDI (Figure 21).
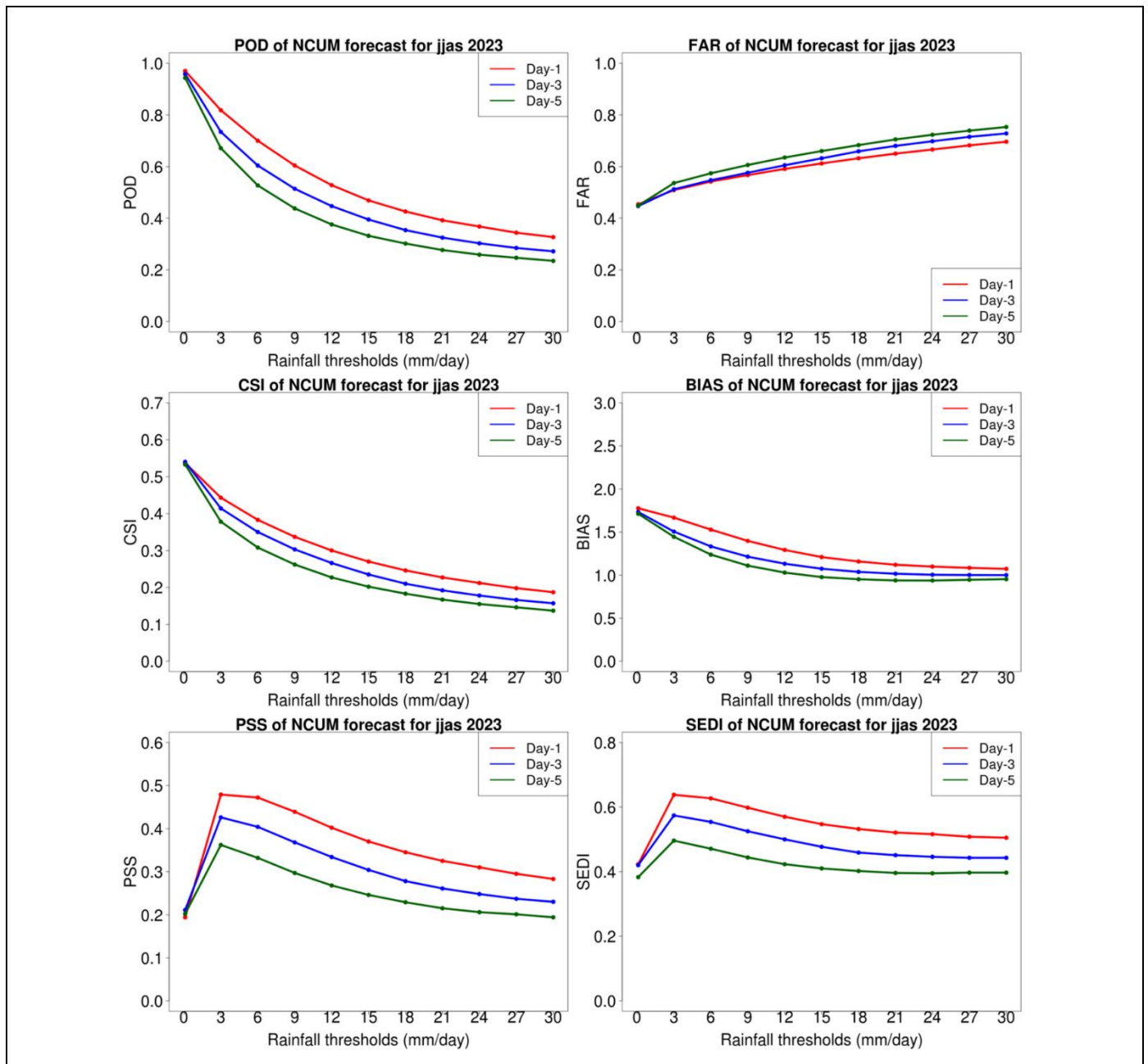
Figure 21. Categorical all India Rainfall scores POD (*top left*), FAR (*top right*), CSI (*middle left*), BIAS (*middle right*), PSS (*bottom left*), and SEDI (*bottom right*).

6. Verification of Onset, Active/Break Spells, and Synoptic Features

6.1. *Onset of Monsoon: Onset Circulation Index (OCI)*

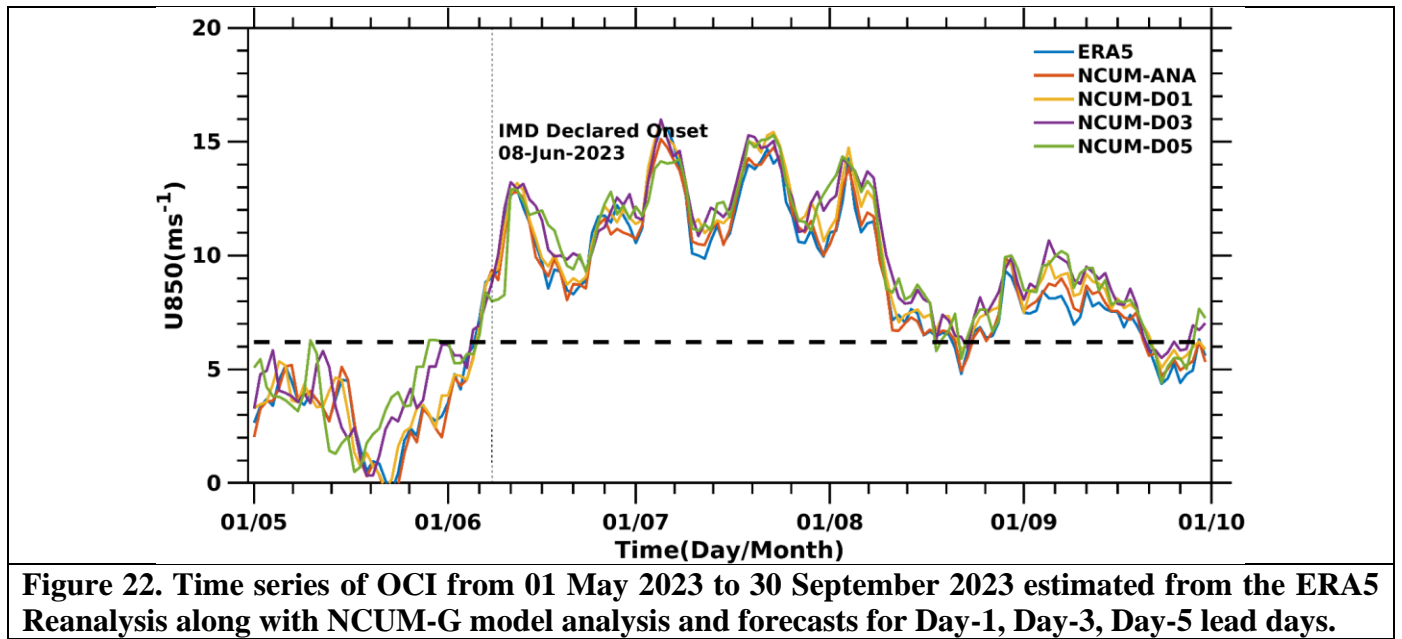In this part, we determine the onset date using the NCUM Global model forecasts. Identifying the monsoon onset is challenging due to various meteorological factors. The IMD, for example, defines onset based on variables like rainfall in Kerala, wind field, and outgoing longwave radiation (source: https://mausam.imd.gov.in/imd_latest/contents/onset.php). Past studies attempted to establish simpler definitions by correlating with IMD criteria. Wang et al. (2001) introduced a circulation index, the difference between 850hPa wind fields over specific regions, showing a strong correlation (0.79) with IMD onset date and Indian monsoon rainfall variability (0.74). Later, they developed another index using 850 hPa zonal wind over the Southern Arabian Sea (SAS) region (Wang et al., 2009), known as the onset circulation index (OCI), correlating at 0.81 with IMD onset date from 1947-2007. This OCI index is applied to identify the 2023 monsoon onset over Kerala. The onset date is considered the first day when OCI exceeds 6.2 m/s, persisting for 7 consecutive days. This threshold aligns with the climatological mean onset date of 1 June in Kerala, where the 850-hPa zonal wind averaged over SAS is 6.2 m/s on that day (Wang et al., 2009). The 7-day persistence ensures that strong westerlies are not solely induced by synoptic events.

Here, we used the NCUM-G model forecasts for Day-1, Day-3, and Day-5, along with NCUM-G analysis and ERA5 reanalysis for comparison. Figure 22 below shows how the OCI time series evolves over time in NCUM-G analysis (NCUM-ANA) with forecasts and ERA5 reanalysis. The IMD declared a late onset for 2023 on June 8, as shown in Figure 22 (vertical dashed line). The temporal evolution of OCI from NCUM-G closely matches ERA5 reanalysis and NCUM-ANA analysis. According to the ERA5 and NCUM-ANA winds, the onset date is June 6, 2023. The NCUM model forecasts for Day-1, Day-3, and Day-5 also indicate onset on June 6, 5, and 6, 2023, respectively. So, the onset date from ERA5 and NCUM model analysis is a bit earlier than IMD's declared onset. NCUM forecasts suggest a similar onset as the model analysis. One reason for the slightly early onset in NCUM analysis and forecasts is the stronger southwesterly winds due to its high spatial resolution. The systematic error of model wind forecasts (Figure 8) shows that wind strength increases as the forecast length increases. Therefore, the expected date in model forecasts using the above index suggests an earlier onset.

Figure 22. Time series of OCI from 01 May 2023 to 30 September 2023 estimated from the ERA5 Reanalysis along with NCUM-G model analysis and forecasts for Day-1, Day-3, Day-5 lead days.

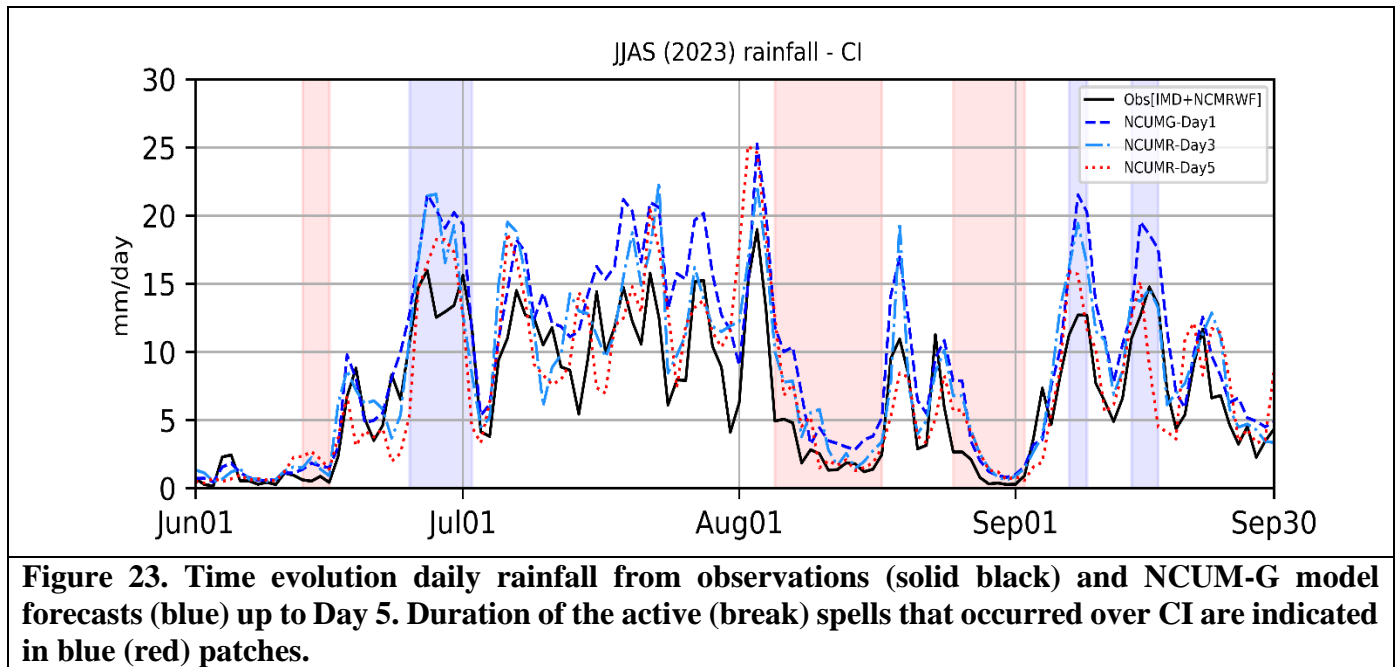## 6.2. *Monsoon active and break spells – 2023*

During monsoon season a major component of variability exists from the intra-seasonal oscillation of active (enhanced convection) and break (subdued or no convection) spells over the Indian subcontinent. Active and break spells over the Indian subcontinent during monsoon season (June through September, JJAS) 2023 were identified from NCMRWF and IMD merged gridded daily rainfall data over central India (15-25^0N, 72-85^0E; CI) following the methodology given by Rajeevan et al (2010). Based on the criterion 3 active and 3 break spells were identified during monsoon JJAS 2023. The timing and the duration of the active and break spells are listed in Table 2. During JJAS 2023, intense and prolonged break spells are identified during the peak monsoon month of August. Active spells over CI occurred during September indicating the revival of monsoon after a prolonged break. During the peak monsoon month (i.e., during August) CI experienced break conditions. Lack of formation of synoptic systems (depression and deep depressions) during July and August (except a deep depression in 1-3 August over BoB) decreased the seasonal rainfall as a whole over the Indian subcontinent during JJAS 2023.

Table 2: List of Active and break spells over Central India (CI) during JJAS 2023

S. No.	Active	Break
1.	25 June – 01 July 2023	13-16 June 2023
2	7-9 September 2023	05-19 August 2023
3.	14-16 September 2023	25August – 02 September 2023

6.3.   *Active and Break spells in NCUM-G model forecasts*

In this section, we have assessed the NCUM-G model rainfall forecast in the representation of active and break spells during the monsoon 2023. For this analysis, we have considered daily rainfall data from the observations averaged over CI model forecasts. The temporal evolution of rainfall time series over the core monsoon region (Figure 23) shows good agreement despite having small discrepancies in rainfall amplitudes especially during the second and third weeks of July 2023 in forecasts.

Figure 23. Time evolution daily rainfall from observations (solid black) and NCUM-G model forecasts (blue) up to Day 5. Duration of the active (break) spells that occurred over CI are indicated in blue (red) patches.

6.4.   *Active and break composites*

The spatial maps of active and break days composite from observations and model forecast are shown in Figures 24 and 25 respectively. The observed rainfall composite during active spell days shows rainfall maxima over the west coast, CI, and Bay of Bengal (BoB), Arakan coast (Figure 24a). Seasonal mean rainfall over CI and over BoB are relatively high compared to the other regions and also the rainfall maxima over CI is slightly south of the mean position of the monsoon trough, which is noteworthy. These enhanced rainfall regions are overestimated in the rainfall forecasts during monsoon 2023. However, with lead time overestimation of rainfall is seen over west coast and CI regions (Figures 24c and 24d). Along the East coast and Northern Bay of Bengal the underestimation in magnitude and rainfall area is very prominent. In all the forecast days rainfall is underestimated (overestimated) over Northern (southern) parts of BoB region (Figure 24c and 24d). In addition, the rainfall area and magnitudes over the equatorial regions are also underestimated

in model forecasts perhaps this could be due to the misrepresentation of convection and low-pressure systems in NCUM-G.

The break composite shows no rainfall over most of the Indian land region. A rainfall maximum is located along the foothills and North-eastern parts (Figure 25a). Model forecasts also exhibit suppressed convection over most of the Indian region, except over the foothills of the Himalayas (Figures 25b-25d). The convection over the foothill and northeastern region from model forecasts exhibit large magnitudes in the forecasts (Figures 25c and 25d), in addition rainfall forecasts over Equatorial Indian Ocean and head Bay of Bengal and are also underestimated both in magnitude and areal extent. In crux, though the active/break mean composites are reasonably represented in NCUM-G model forecasts, the spatial biases in rainfall persist need attention.
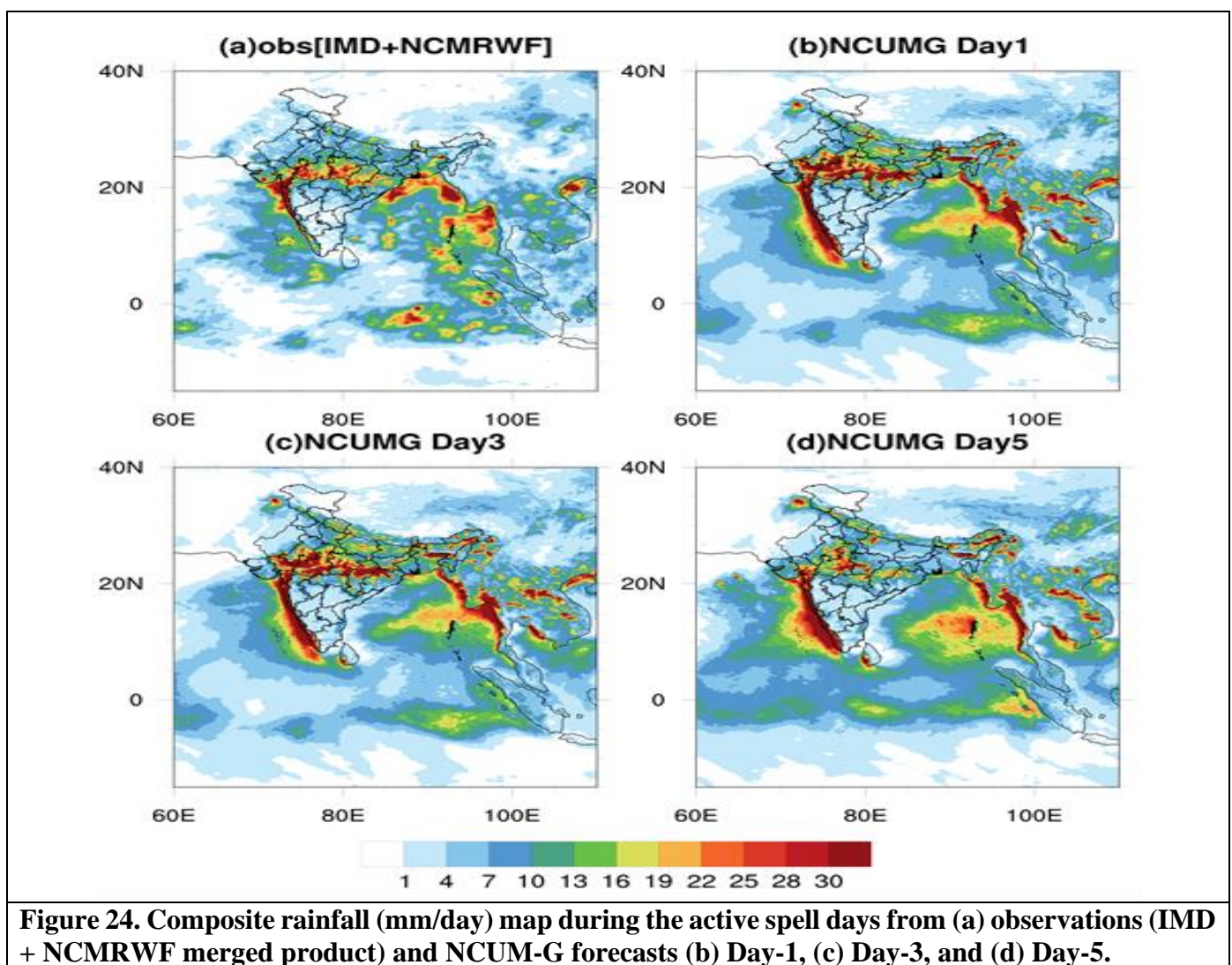
Figure 24. Composite rainfall (mm/day) map during the active spell days from (a) observations (IMD + NCMRWF merged product) and NCUM-G forecasts (b) Day-1, (c) Day-3, and (d) Day-5.
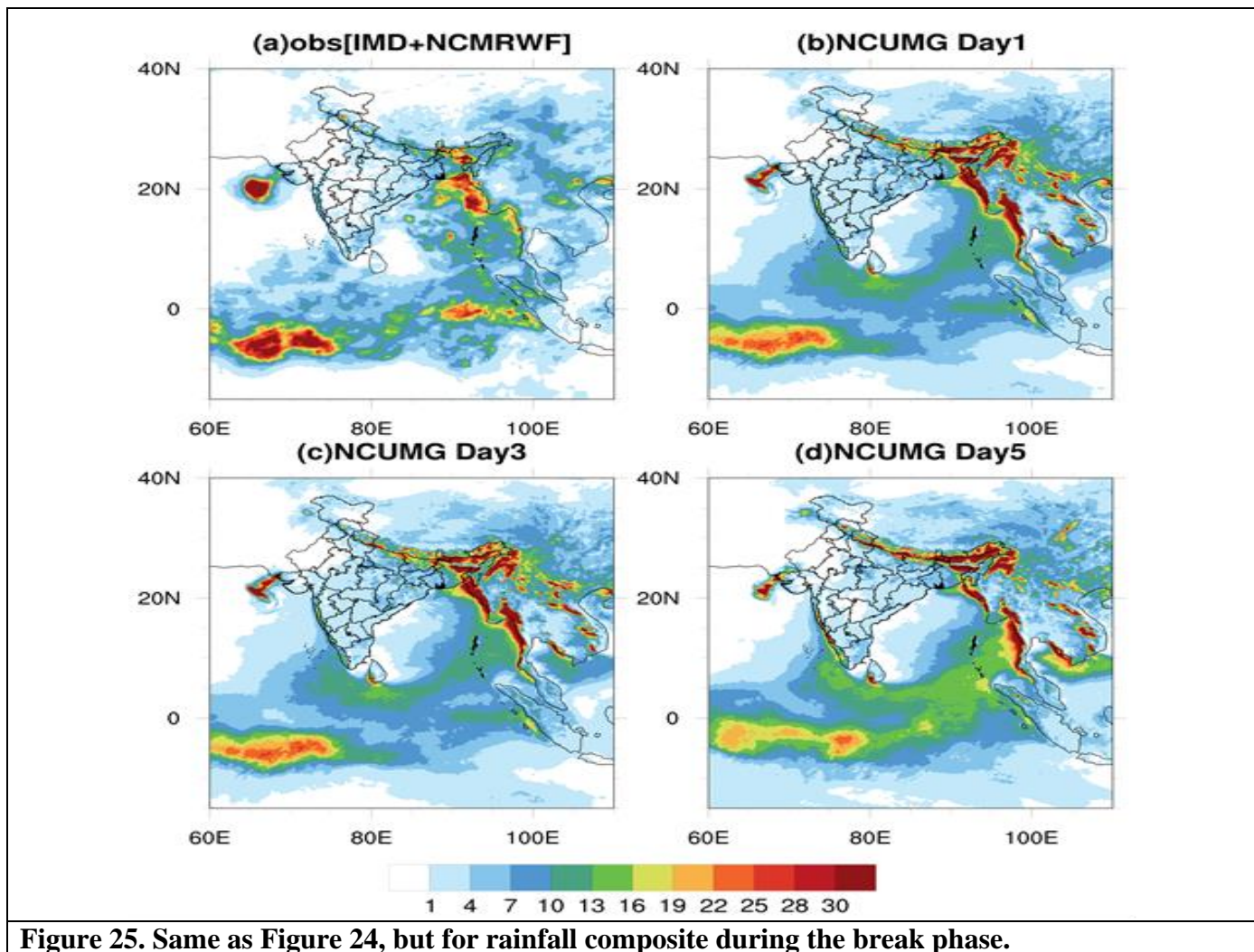
Figure 25. Same as Figure 24, but for rainfall composite during the break phase.

6.5.   *Synoptic features*

During the JJAS 2023 monsoon season, fifteen (15) low-pressure systems (LPS) were formed over the Indian region as listed in Table 3. These low-pressure systems contributed to receiving a substantial amount of rainfall during the JJAS period. Among these LPSs, one of them intensified into depression (i.e., on 30th Sep) and one into a deep depression (i.e., during 01-03 Aug) over BoB. Further, the LPS that formed over the Arabian Sea (AS) on 6th Jun 2023 has intensified into an extremely severe cyclonic storm (ESCS) "BIPARJOY", on same day (i.e., 6th June 2023). The storm continued to move Northeastward and on 16th Jun it made landfall in Naliya, Gujarat, India. Later on, June 19, this cyclone was downgraded to a depression and subsequently to a well-defined low-pressure area. A detailed verification is presented in the subsequent section 6.5.1, while the verification of a monsoon depression (case study) is discussed in section 6.5.2 from the NCUM-G model forecasts.

Table 3: *List of Low-Pressure Areas (LPAs) during JJAS 2023.*

S. No.	Month	Low Pressure Areas (LPAs)	
		Total	**Duration**
1.	JUN	3	❖ An LPA formed over AS during 6 – 19 Jun, associated with the extremely severe cyclonic storm (ESCS) "BIPARJOY". ❖ Two well marked LPAs formed over BoB during 9 – 11 Jun and 25 – 30 Jun.
2.	JUL	5	❖ One LPA formed over Land during 10 - 11 Jul. ❖ Four LPAs formed over BoB --- Out of 4, 2 LPAs formed during 16 - 17 Jul and 20 - 22 Jul, and the other two systems intensified into well-marked LPAs during 25-28 Jul and 29- 31 Jul.
3.	AUG	2	❖ A deep depression formed over BoB during 01-03 Aug. ❖ One low-pressure area formed over BoB during 17-20 Aug.
4.	SEP	5	❖ Four LPAs formed --- Out of 4, 1 LPA formed over AS, and the other three systems intensified into well-marked LPAs over BoB. ❖ A depression formed over BoB on 30th Sep 2023.

6.5.1. Verification of 'BIPARJOY' Cyclone Over Arabian Sea (Jun 06-18, 2023)

This section briefly summarizes the verification of NCUM model forecasts for the recent Extremely Severe Cyclonic Storm (ESCS) "Biparjoy" from June 6 to 18, 2023, over the Arabian Sea. Originating from a Low-Pressure Area in southeast AS on June 5, 2023, "Biparjoy" moved northwards, making landfall between Mandvi (Gujarat) and Karachi (Pakistan) on June 15, 2023, as a Very Severe Cyclonic Storm (VSCS) with a maximum sustained wind speed of 115-125 kmph. By June 16, it weakened to a Severe Cyclonic Storm (SCS), then to a Cyclonic Storm (CS) and further into a Depression (DD) on June 17, tracking northeastward. Finally, on June 18, it weakened into a well-marked low-pressure area over Central Parts of Northeast Rajasthan and its vicinity. Verification of the forecast tracks and intensity is presented for all NCMRWF Unified Models; NCUM-G (12km grid resolution), NEPS-G mean (12km grid resolution), and NCUM-R (4km grid resolution) for both 00UTC and 12UTC runs. Forecast verification is presented for model-predicted tracks and intensity against IMD best track data.

The Spatial maps of wind direction and magnitude (shading) for NCUM-G analysis and forecasts during 16th June 2023 (landfall) time are shown in Figure 26. Here for better legibility, Day-1, Day-3, and Day-5 forecasts are presented along with the analysis. It is clear from Figure 26 that Day-1 forecasts from NCUM-G are well-matching with the analysis (Figure 26 (top panel)). However, system forecasts in Day-3 and Day-5 are relatively intense with wind magnitudes reaching >30m/s.
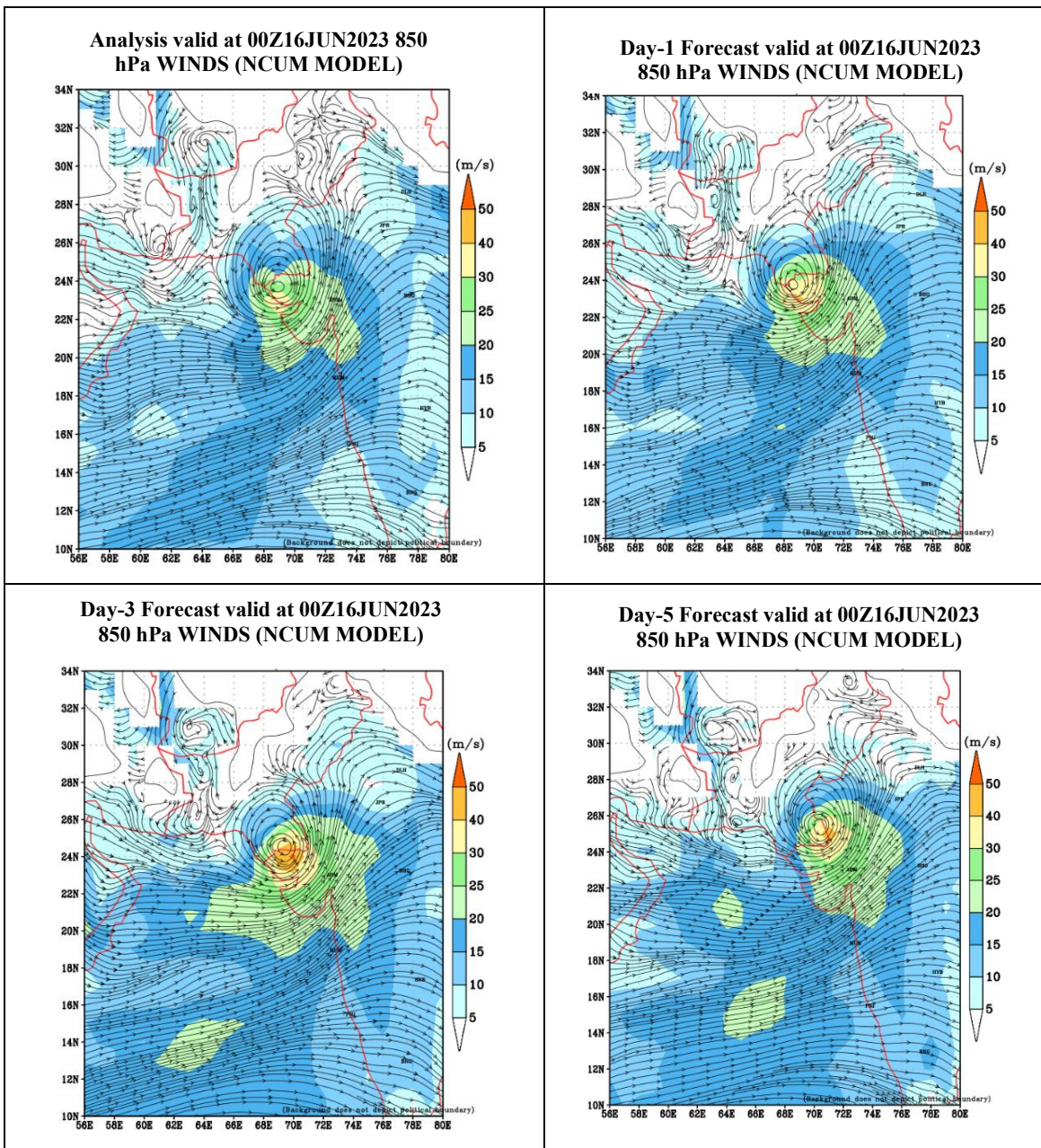
Figure 26. Spatial maps of analysis, Day-1, Day-3, and Day-5 forecasts of wind speed (shading; units m/s) and direction from NCUM-G during the 'Biparjoy' cyclone on 16th June 2023.

6.5.1.1. *Forecast Tracks and Strike Probability*

The observed and predicted tracks based on 00UTC of 12th June 2023 are shown in Figure 27 (top). All the predicted tracks indicated that ESCS "Biparjoy" would track towards Gujarat and adjoining Pakistan region. The strike probability (Figure 27; bottom) based on the 22 member NEPS-G ensemble indicates that the cyclone would approach the Gujarat coast in forecast based on 12th June 2023.

Figure 27. Observed & forecasted tracks of Arabian Sea ESCS 'Biparjoy'. Forecast tracks, strike probability, and EPS grams are based on IC 00UTC 12th June 2023.
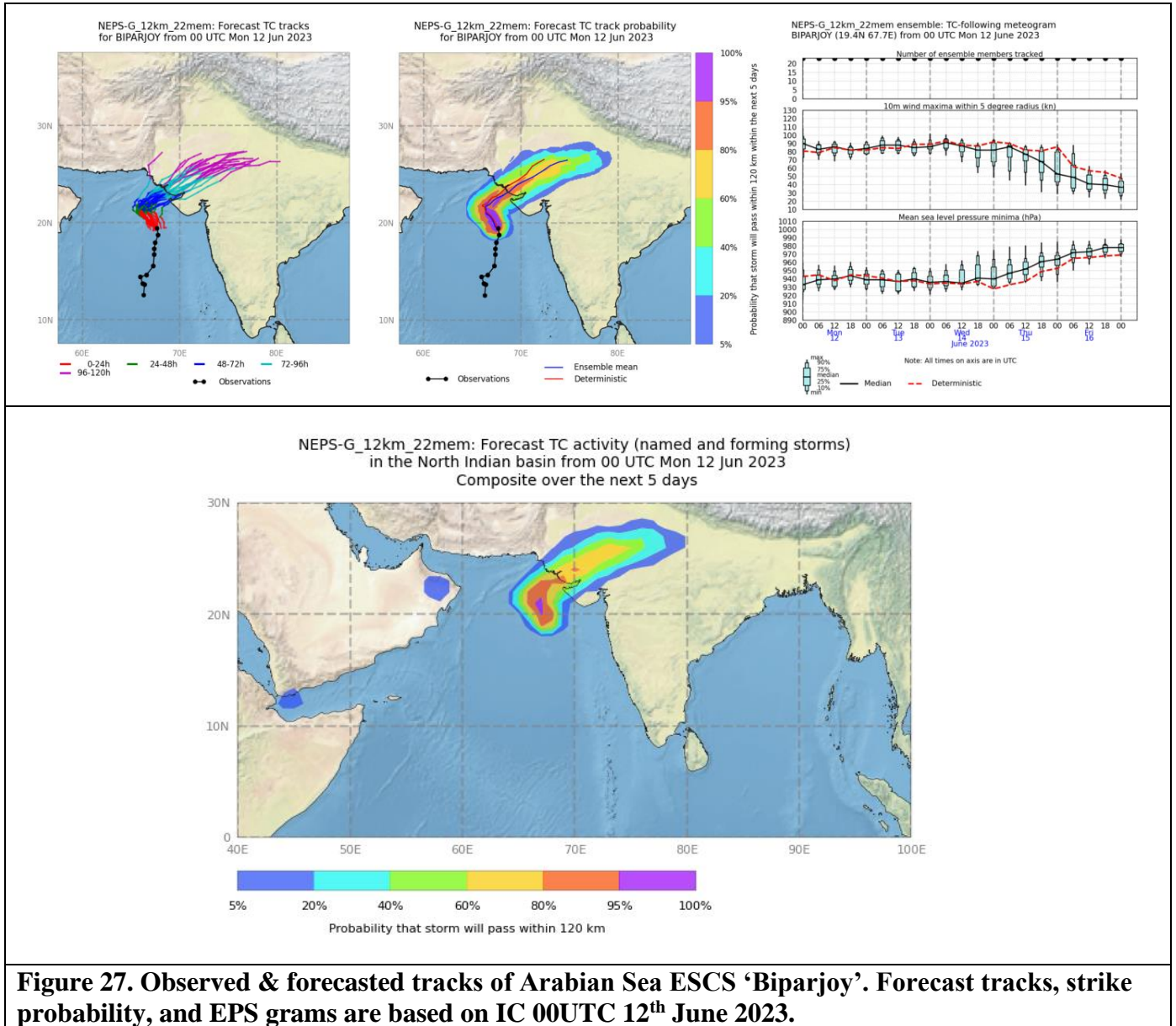
6.5.1.2. Forecast Track Errors

The NCUM-G, NCUM-R, and NEPS-G model forecasts have been used in the verification. The Track forecast verification statistics shown in Table 4 are based on model runs (NCUM-G and NCUM-R) with ICs from 06th to 18th Jun 2023 including 00 and 12UTC. For NEPS-G track verification model runs with ICs from 06th to 16th June have been used. Mean initial position error is least 32 km in NCUM-G and 35 km in NCUM-R with slightly higher error of 43 km in NEPS-G (ensemble mean). NCUM-G features DPE< 100 km up to 60 hrs.

The track error components, Direct Position Error (DPE), Along Track Error (ATE), and Cross Track Error (CTE) are shown in Figure 28. DPE & ATE are highest in NCUM-R at all lead times up to 72hrs. Beyond 72hrs, NEPS-G forecast tracks have higher error.

Table 4: *Forecast Track Errors NCUM-R, NCUM-G, and NEPS-G (numbers in the adjacent column in italics indicate number of forecast points validated)*

Fcst Hour	DPE					
	NCUM-R	No of Fcst. verified	NCUM-G	No of Fcst. verified	NEPS-G	No of Fcst. verified
0	35	*26*	32	*26*	43	*22*
12	44	*26*	48	*26*	51	*22*
24	69	*25*	53	*25*	60	*22*
36	91	*24*	68	*24*	77	*22*
48	109	*23*	84	*23*	94	*22*
60	135	*22*	96	*22*	113	*22*
72	159	*21*	111	*21*	142	*21*
84			129	*20*	178	*20*
96			158	*19*	223	*19*
108			193	*18*	257	*18*
120			212	*17*	282	*17*
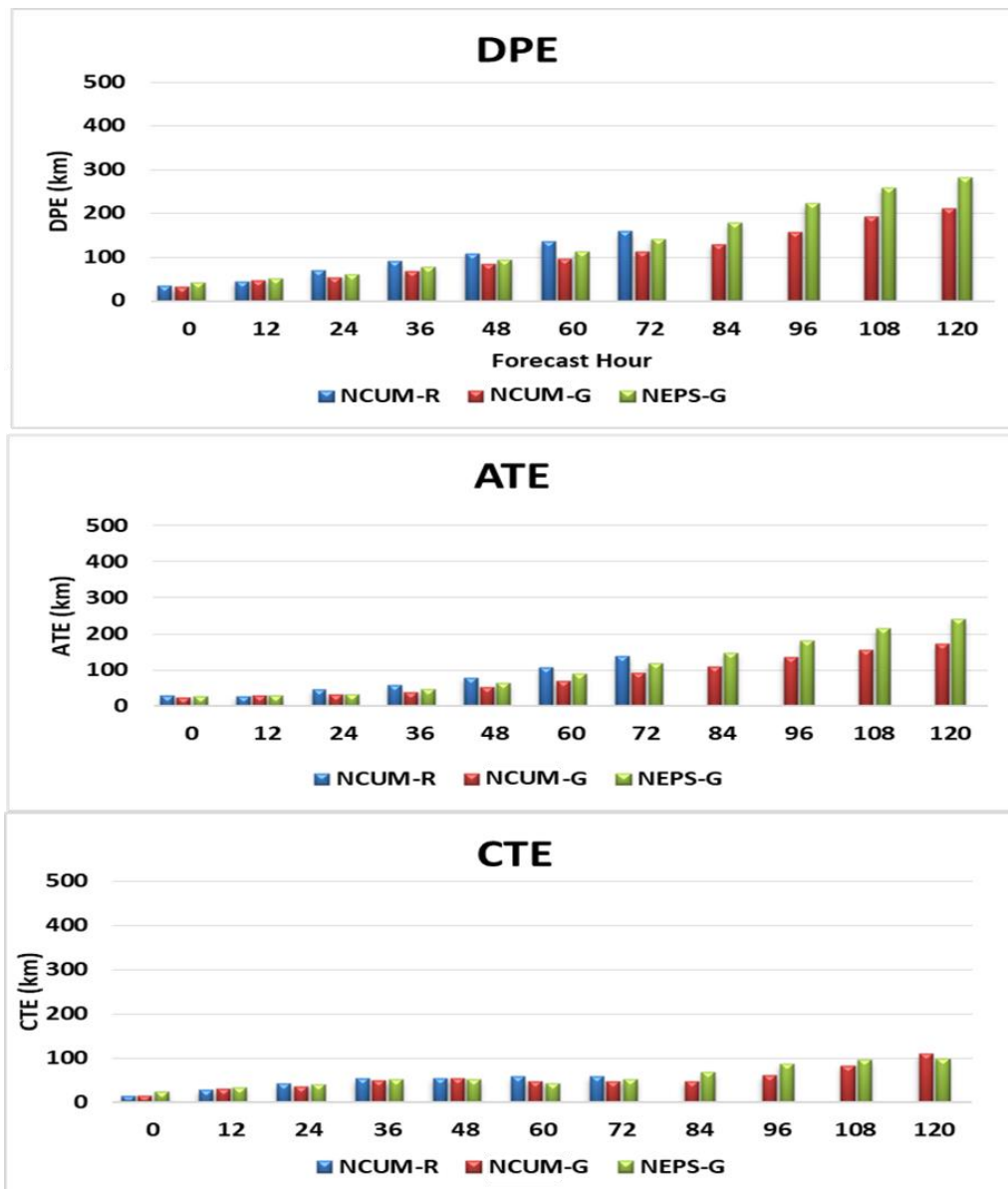
Figure 28. Track forecast errors (top panel) Direct position error (DPE), (middle panel) along track error (ATE), and (bottom panel) cross track error (CTE) in km.

6.5.1.3. *Forecast Intensity errors (Min SLP and Max Wind)*

The mean absolute error (MAE) in the forecast of central pressure (CP)/minimum Sea Level Pressure (min SLP) and maximum sustained wind (MSW) for NCUM-R and NCUM-G models is shown in Figure 29. The average error in CP is significantly lower (<10 hPa) in NCUM-R forecasts than in NCUM-G. Similarly, the MAE in MSW is lower in NCUM-R for all lead times (after 12hr) as compared to NCUM-G. This is also reflected in Figure 30, where NCUM-R forecasts have very realistic representation of MSW and MinSLP with different ICs.
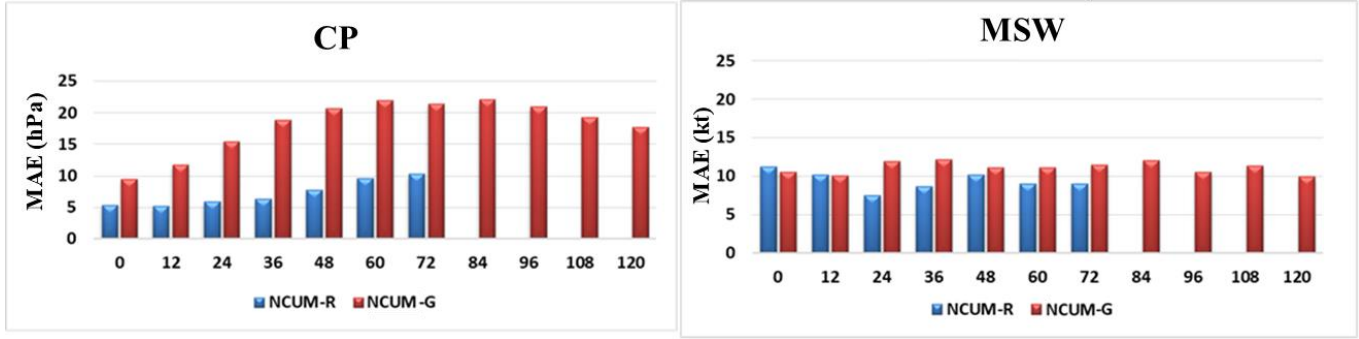
Figure 29. Mean Absolute Error (MAE) in CP (hPa) and MSW (kt) at different forecast lead times.
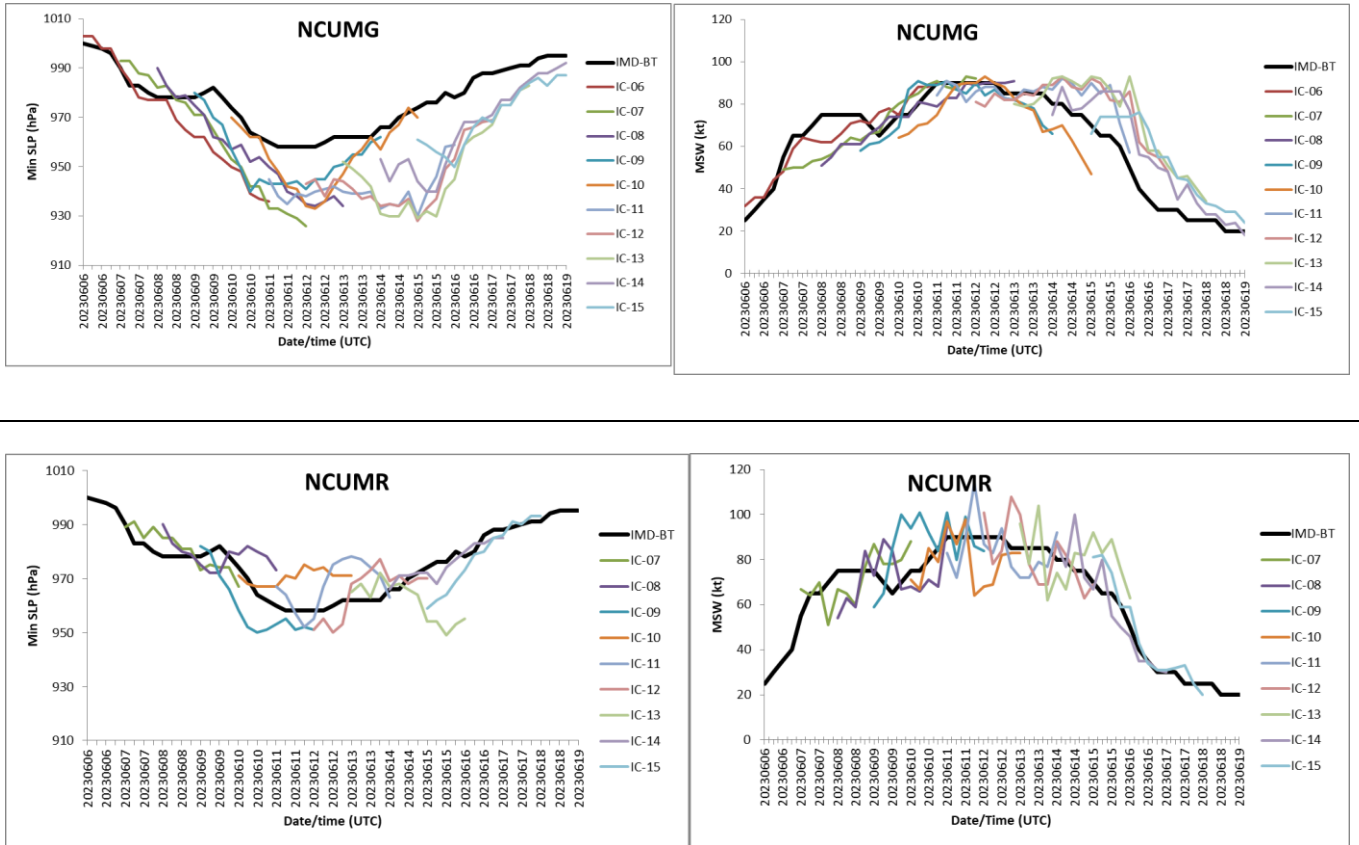
Figure 30. Intensity given by MSW (left) & Min SLP (right) in NCUM-G (top) and NCUM-R (bottom) forecasts with different initial conditions from 6th to 15th Jun 2023.

6.5.1.4. Forecast Landfall Error

As per the IMDs best track data the ESCS "Biparjoy" landfall time is 16-17 UTC on 15th Jun 2023 near 23.28⁰N and 68.56⁰E. The forecast landfall errors have been computed using the first forecast position on the land (Table 5). The forecast landfall time error is -6 to -12 hours in NCUM-G from 12UTC10Jun till 00UTC12Jun. Subsequently the errors are small ranging from 0 to -6hrs. On the other hand, NEPS-G shows a landfall time error mostly ranging from -6 to -12hrs. NCUM-R forecasts show 0 landfall time error on all days. Landfall position error was lowest (<50 km) in NCUM-R from 00UTC14th June onwards.

Table 5. Error in the forecasted landfall time and position (Forecast time – Observed time) [-ve depicts early landfall and +ve shows delay in landfall]

		NCUM-R		NCUM-G		NEPS-G	
IC	Fcst length (h)	Position	Time	Position	Time	Position	Time
2023061012	120			9	-12	52	-3
2023061100	108			20	-12	16	0
2023061112	96			25	-6	26	-12
2023061200	84			23	-6	18	-12
2023061212	72			72	0	36	-6
2023061300	60	0	0	53	-3	61	-6
2023061312	48	58	0	109	0	86	-6
2023061400	36	8	0	51	-6	84	-6
2023061412	24	16	0	60	0	54	-6
2023061500	12	22	0	42	0	46	0
2023061512	0	39	0	35	0	26	0

6.5.1.5. Verification of Strike Probability

Cyclone strike probability is the probability of locating cyclone within 120 km of any grid point. The verification of strike probability is presented using Relative Operating Characteristics (ROC) and Reliability diagram (attributes diagrams). It must be noted that the verification of strike probability is presented for a period from 6-18 Jun 2023.The Reliability diagram gives a comparison of forecast probability against the observed frequencies. A perfect match will show all points along the diagonal line. Points above diagonal suggest underestimation (lower forecast probabilities) while points below the diagonal suggest over estimation (higher forecast probabilities).

For the case of ESCS "Biparjoy", the verification of strike probability obtained from NEPS-G is carried out using the best track data. Figure 31 shows the reliability and ROC plots for the strike probability verification. In the Reliability diagram, the points are along the diagonal thus indicating near best performing model. The

ROC curve of NEPS-G shows that the model has skill as the curve is away from the diagonal line of no resolution. The AROC (area under the ROC) is 0.73 which is also indicative of reasonably good resolution in the model.
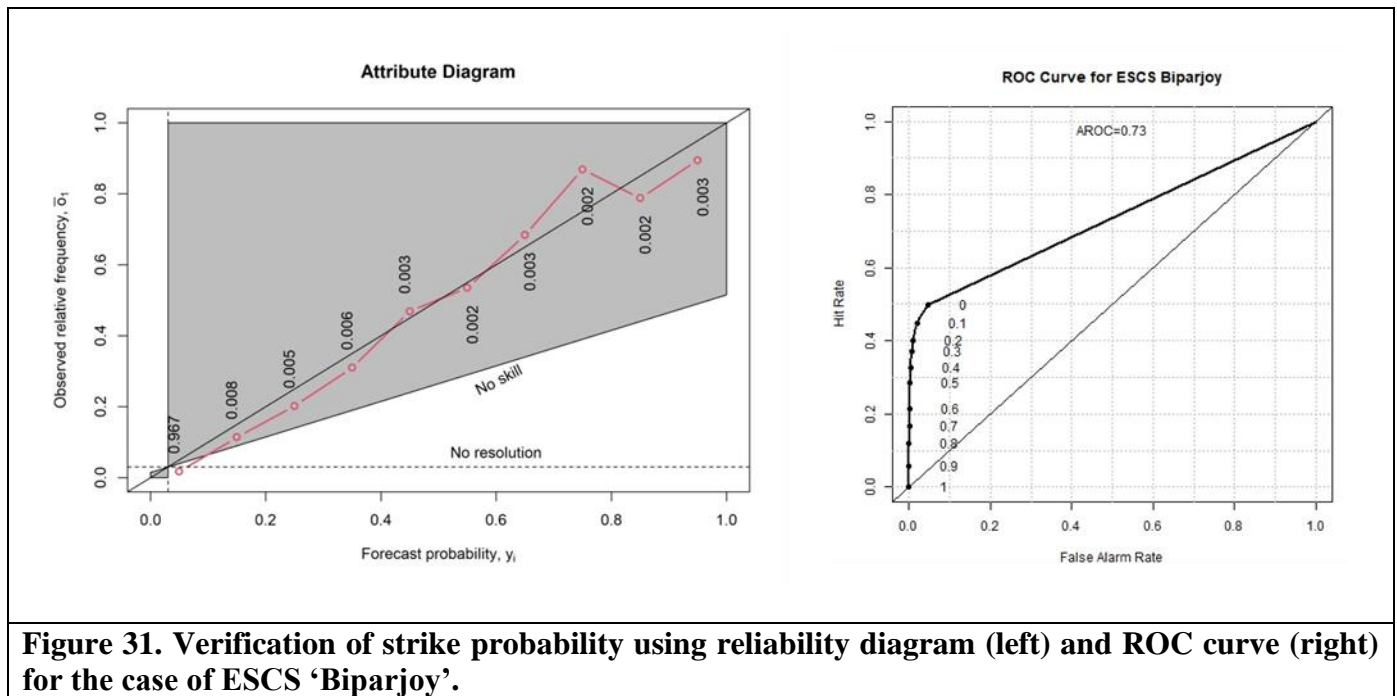

Figure 31. Verification of strike probability using reliability diagram (left) and ROC curve (right) for the case of ESCS 'Biparjoy'.

6.5.2 Low Pressure System in JJAS 2023

The 2023 southwest monsoon season witnessed numerous extreme rainfall events as reported by IMD. In June, Rajasthan experienced extremely heavy rainfall, attributed to the extremely severe cyclonic storm "BIPARJOY". July witnessed extremely heavy rainfall events in Konkan & Goa, Coastal Karnataka, Uttarakhand, Himachal Pradesh, and Telangana, primarily due to the presence of low-pressure systems. Due to the formation of one deep depression and one low pressure region over the Bay of Bengal, extremely heavy rainfall events were more common in August over Odisha and Gangetic West Bengal. Moving into September, the extremely heavy rainfall events were more realized over Madhya Pradesh, Bihar and West Uttar Pradesh due to the formation of low-pressure areas over the Bay of Bengal. Overall, Monsoon 2023 registered a 5.6% deficit from the long-term average, placing it within the 'normal' rainfall category, as per the IMD.

Out of all the LPAs during the southwest monsoon season (JJAS), 2023 listed in Table 3, we have chosen an LPA case for this report. Here we verify an LPA that occurred during 16 - 17 Jul 2023. The low-pressure system (LPS) that occurred over the Bay of Bengal region on 17th July 2023 is shown in Figure 32. On 17th

Jul 2023, a low-pressure area lies over west Jharkhand and adjoining north Chhattisgarh & north interior Odisha; and the associated cyclonic circulation has caused wide-spread rainfall activity over eastern parts of Indian region (Figure 32). Compared to NCUM-G analysis (Figure 32), the Day-1 forecast shows the LPS over the head Bay of Bengal and a well-marked trough is extending along the east coast. In contrast, the Day-3 forecast in NCUM-G exhibits more intense LPS and shifted more towards the inland. With lead time the shift is further towards northwest towards land regions (Figure 32). The strength of low-level jet not varying much in the forecast times and maximum wind speeds are situated over the Arabian sea region. Another noteworthy feature is that the strength of the LPS, as evidenced by the density and orientation of isobars, is enhancing in all the forecast timings.
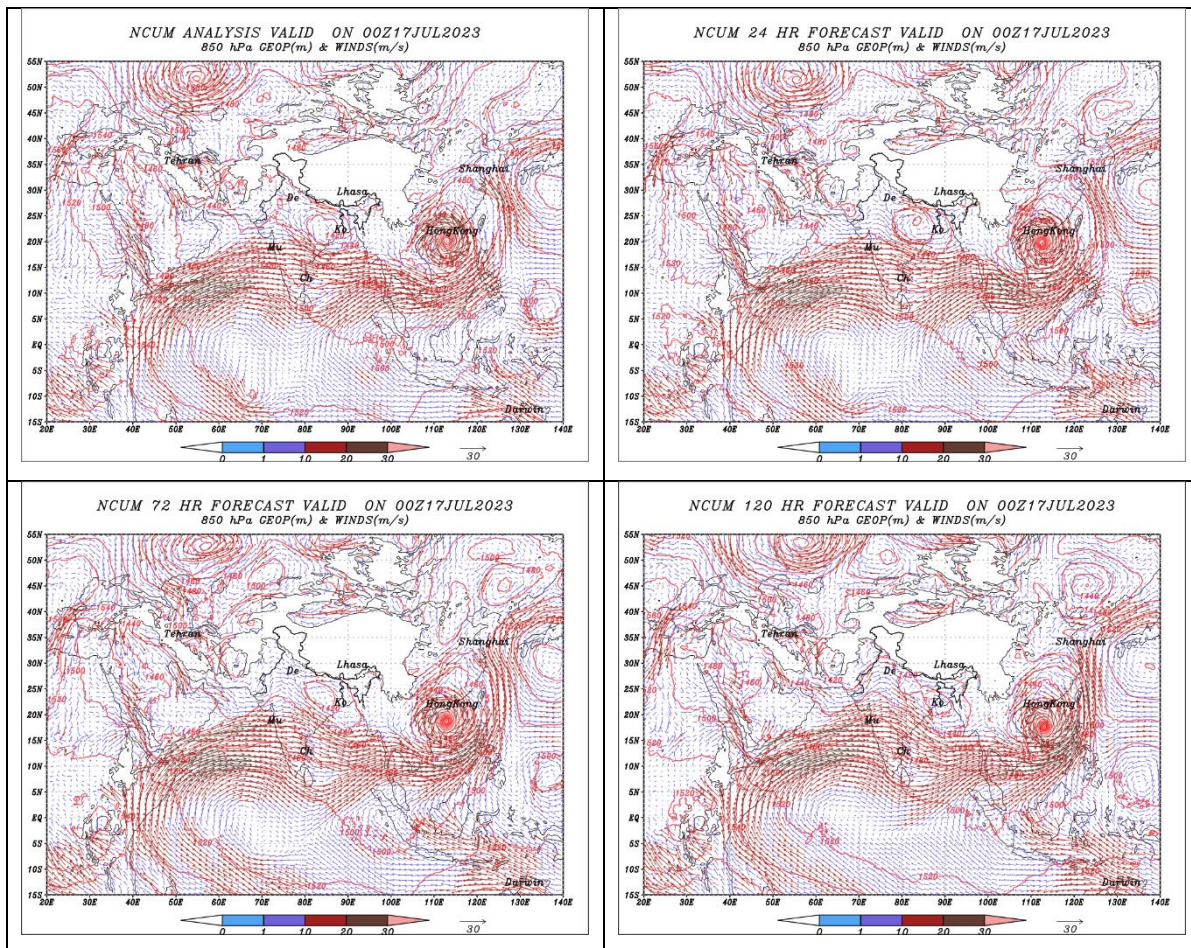
Figure 32. Spatial maps of Analysis, Day-1, Day-3, and Day-5 forecasts of wind speed (shading; units m/s), direction (blue vectors), and geopotential height contours at 850 hPa level from NCUM-G during the Low-pressure system (LPS) occurred on 17th July 2023.

6.6. Heavy Rainfall occurrences in NCUM-G

In this section, we evaluate the performance of the NCUM-G forecasts in representing rainfall frequencies. Figure 33 displays the spatial distribution of maximum rainfall at each grid, showcasing the highest rainfall received during the season for comparison between observed and forecasted values. Over the land region, we focus on rainfall events exceeding 10cm/day. Observations reveal a distinct near east-west belt over central India and the Himalayan foothills, with both regions experiencing higher rainfall events exceeding 20cm/day at isolated locations. To further assess the model's performance, we present average rainfall time series for the selected regions (depicted in the box in the left panel of Figure 33), highlighting where the maximum rainfall occurred during the season. The right panel of Figure 33 illustrates the mean rainfall for these regions, providing insights into high rainfall spells across different geographic areas. Our goal is to comprehensively understand the NCUM-G model's forecasting accuracy for regions exhibiting high rainfall maxima. Figure 34 examines into rainfall frequencies across four different regions (as indicated in the left panel of Figure 33). Normalized frequencies of rainfall for thresholds up to 5 cm/day are presented in Figures 34(a-e). The plots reveal that, during the JJAS 2023 period, NCUM-G tends to overestimate the frequency of rainy days, particularly for rainfall thresholds up to 2cm/day, across most regions—except for Mumbai and the Northeast, where NCUM-G overestimates by approximately 30-40cm/day.
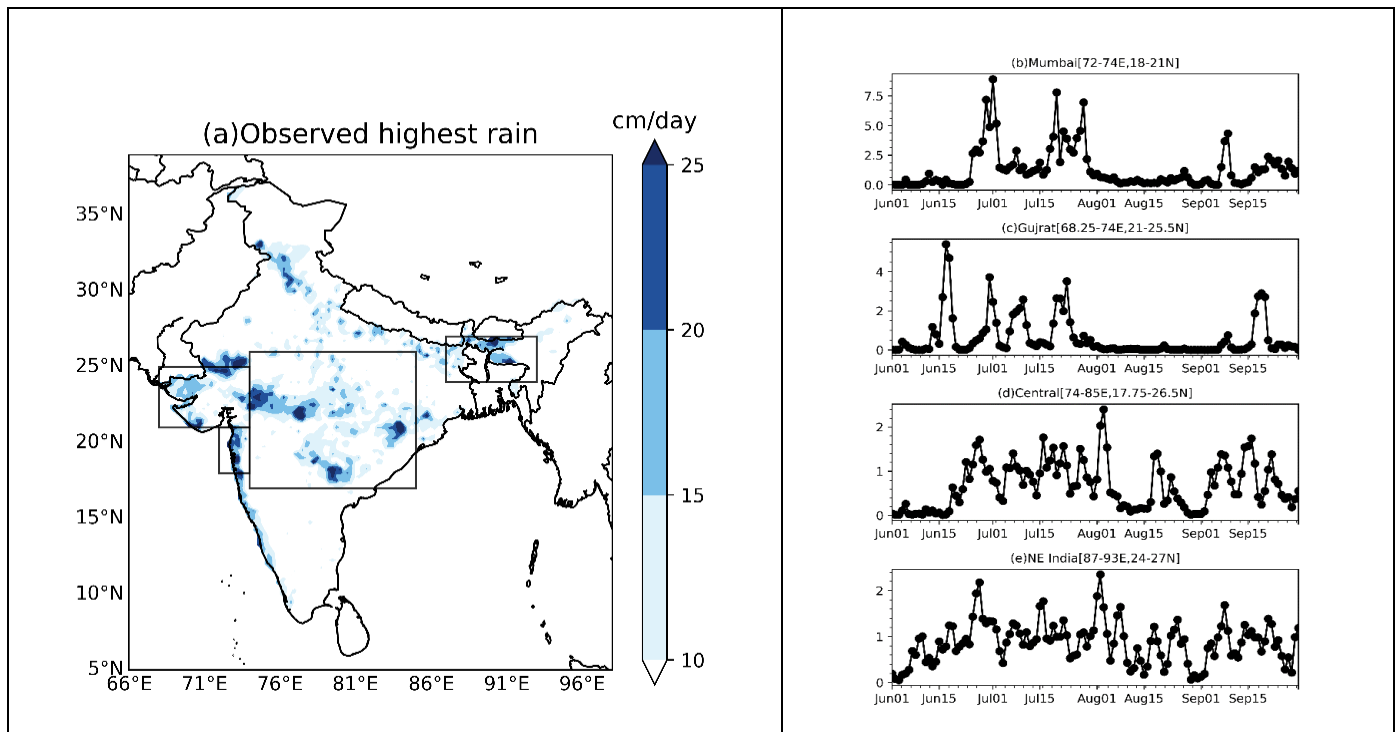

Figure 33. (left panel) The spatial distribution of observed highest rain across Indian subcontinent. (right panel) The averaged rainfall over four different regions (outlined in (a)) selected for the estimation of rainfall skill from NCUM-G.

Figure 34. Observed and forecast rainfall frequencies over four regions of India in NCUM-G forecasts.
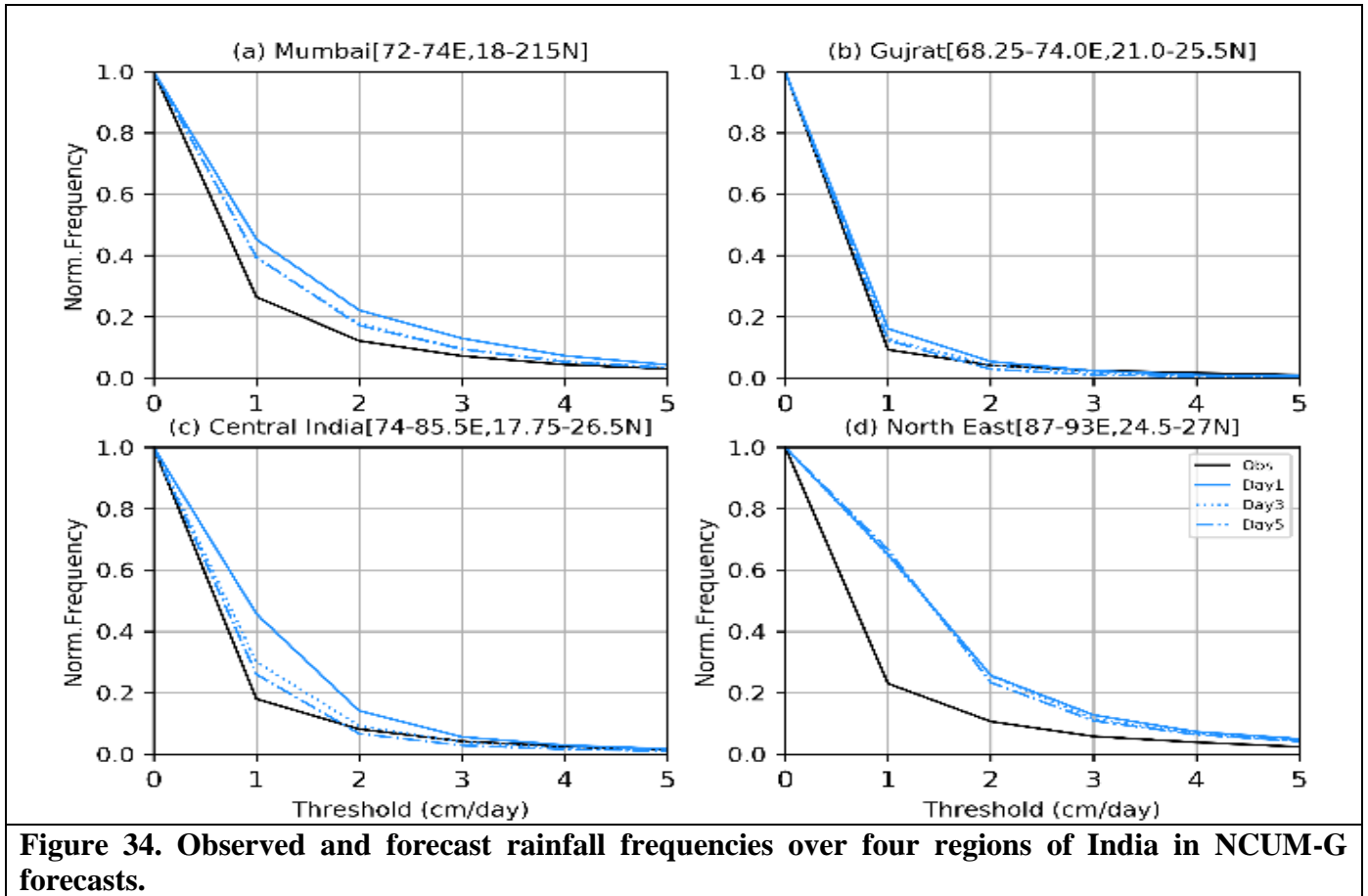
6.7. Investigation of sources of Rainfall Biases in NCUM-G

Here we briefly discuss the sources of rainfall biases in NCUM-G forecasts. Figure 35 shows Day-1; Day-3 and Day-5 rainfall & 850 hPa wind biases in NCUM-G for monsoon JJAS 2023. Note that here biases are computed against rainfall from GPM and ERA-5 wind analysis products. For better legibility, winds from both reanalysis and forecasts are re-gridded to 1.5 x 1.5-degree resolution. Like any other models NCUM-G model forecasts also exhibit biases in key variables. The spatial biases in the NCUM-G show a prominent difference in both rainfall and 850hPa winds. For instance, wet bias is seen in NCUM-G over the west coast, foothills of the Himalayas, Equatorial Indian Ocean (EIO) and some parts over Central India (CI). The magnitude of these rainfall biases is increasing with lead time from Day-1 to Day-5 (Figure 35). Further, in NCUM-G forecasts dry biases are seen over the Head BoB and the magnitude of these rainfall biases enhance with lead time, perhaps due to the misrepresentation in low pressure systems in NCUM-G rainfall forecasts. In addition, the presence of low-level anti-cyclonic circulation reduces the mean westerlies over BoB resulting in dry biases (Figure 35).

Figure 35. Rainfall and wind biases in NCUM-G during (a) Day-1; (b) Day-3 and (c) Day-5 during JJAS 2023.
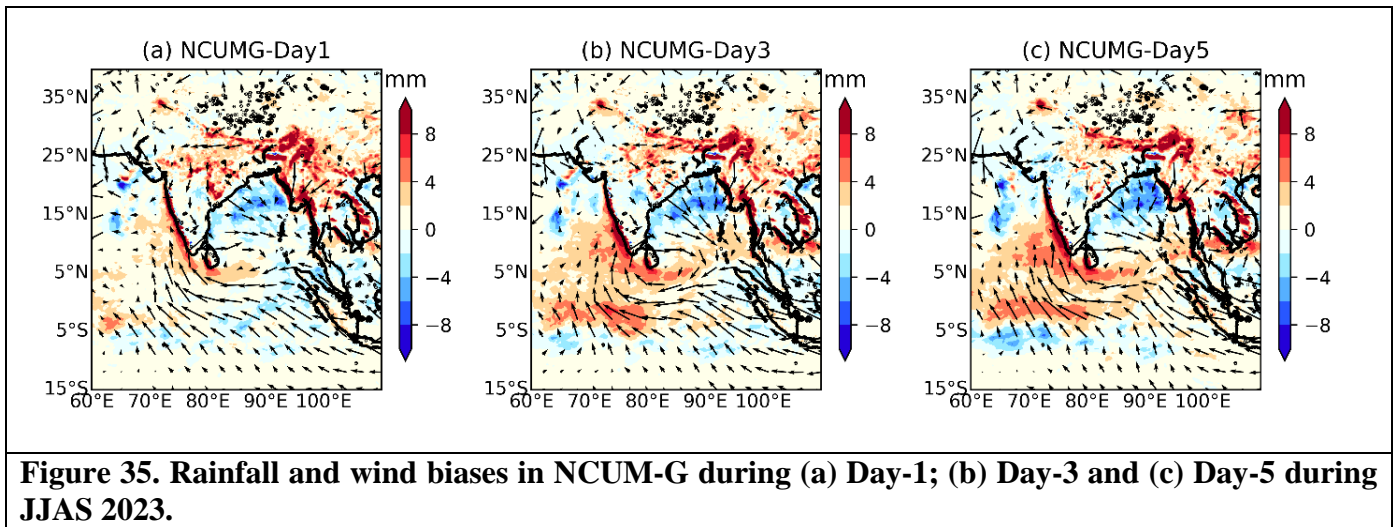
To further establish the connection between rainfall discrepancies and key meteorological factors, Figure 36 illustrates vertical profiles of temperature (T), specific humidity (q), and vertical velocity (w) averaged over central India (CI) and the Bay of Bengal (BOB). These profiles highlight biases in key variables across different forecast lead times, with the understanding that biases are computed based on the model's own analysis. While there is a consistent alignment in the bias profiles for temperature across forecast lead times, slight variations are observed in specific humidity (q) and vertical velocity (w) profiles. Temperature biases indicate colder air at boundary layer levels and relatively warmer air in the free tropospheric level (300-500 hPa), presenting a dipole-like structure in model forecasts for both CI and BOB. Specific humidity biases reveal dry conditions around the boundary layer, which is expected given the model's tendency to underestimate boundary layer processes. The vertical profiles of vertical velocity in NCUM-G consistently show underestimation in forecast leads compared to analysis at all levels above 600 hPa. Additionally, the double peak observed in Day-1 'w' bias is absent in forecast lead times over CI. The underestimation of 'w' observed at upper tropospheric levels results in a large-scale descent, coupled with stable conditions, may contribute to the dry biases over the Bay of Bengal in model forecasts. Interestingly, this phenomenon is less evident in the vertical profiles over land regions of India, suggesting the influence of other factors such as remote responses, advection, surface fluxes, etc., leading to wet biases.
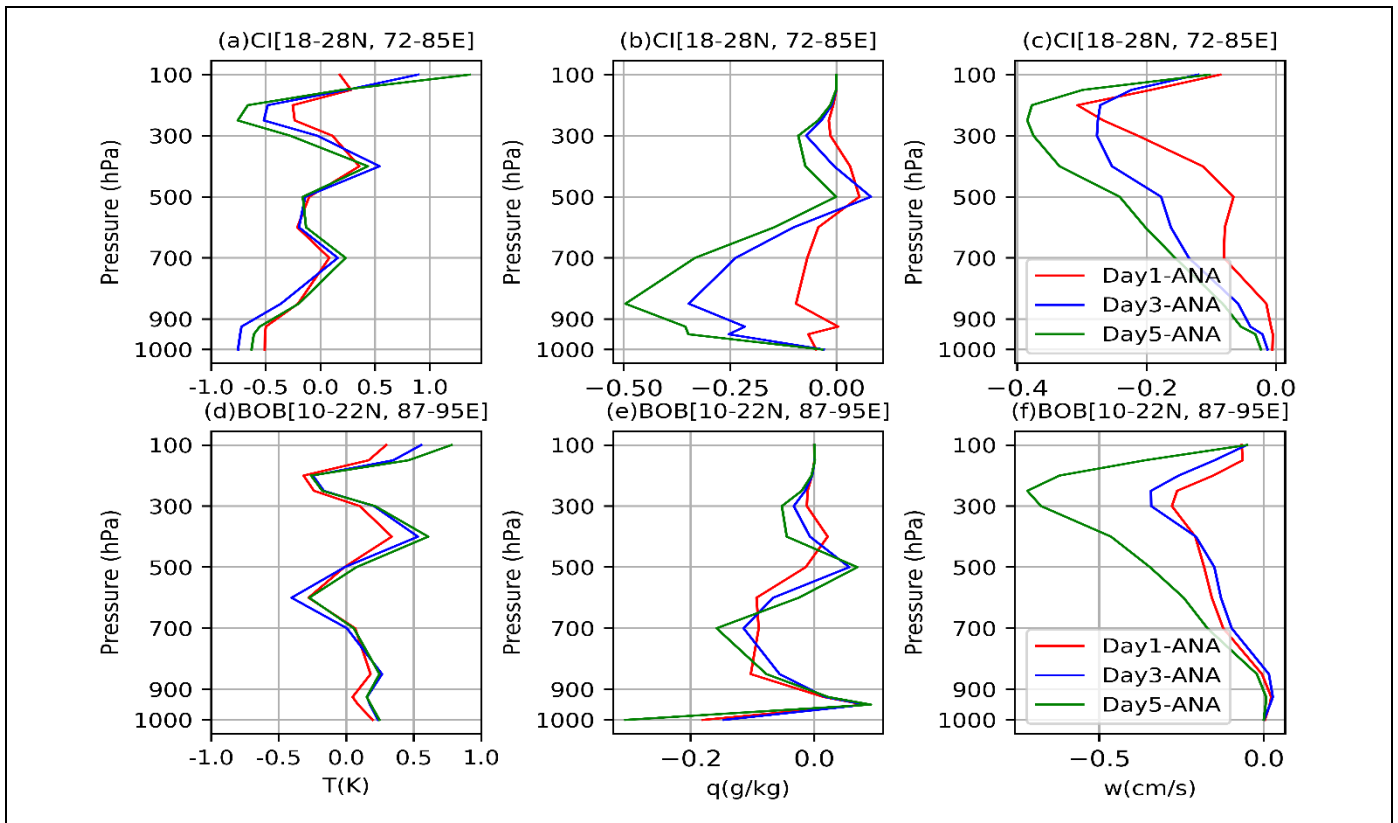
Figure 36. Mean vertical profiles of biases in T, *q*, and *w* averaged over CI (top panel) and BOB (bottom panel).

7. Sub-seasonal variability of monsoon rainfall 2023

Rainfall during the monsoon season in India is extremely important for farming and brings many socio-economic benefits. That's why in the previous sections (section 5 and section 6), we talked about how the rainfall varies in space and time and looked at the mistakes the models make. We found that the model's daily rainfall matches pretty well with what's really happening, but there are some small errors from day to day. Figure 23 shows how these errors change every day, especially in the main monsoon region. Generally, the errors range from +/-10mm per day, with the model predicting more rain than what actually falls. Also, when we look at how the rainfall changes over time, we see some quick and slow variations, along with changes caused by weather patterns. We already know that monsoon rainfall in South Asia mainly varies in three ways: i) Synoptic scale (<7 days); ii) Quasi-biweekly scale (QBWO;10-20days); iii) Low-frequency instar-seasonal scale (ISO;30-60days) (ref: Krishnamurti and Bhalme, 1976).

Synoptic variability encompasses various systems, including monsoon troughs, low-pressure systems, monsoon depressions, cyclones, offshore vortices, etc. In this section, we initially present the synoptic variance derived from both model simulations and observational data (IMD+NCMRWF merged rainfall

product). The time series of monsoon rainfall at each grid point is subjected to a band-pass filter of 3-7 days for the JJAS 2023 period, and the variance is then computed from these filtered anomalies. Figure 37 illustrates the synoptic variance observed and forecasted by the model. It is evident that both observed and model variance are pronounced over central India and the complex Himalayan region. This enhanced variance is particularly associated with the movement of the monsoon trough and monsoon depressions. Additionally, the observed variance is prominent in the northern Bay of Bengal and along the west coast of India. The sharp variance in the Bay of Bengal is likely linked to strong convection and the development of low-pressure systems such as cyclones, while the increased variance on the west coast is primarily attributed to offshore vortices. Comparing the model-derived synoptic variance to observations, we observe a slight overestimation over central India and the complex Himalayan region. Notably, the variance in the western ghats on the leeward side is exceptionally high in the NCUM-G forecast, a feature absents in the observations. Furthermore, the high variance observed in the northern Bay of Bengal is also not adequately captured in the model forecasts. Consequently, the NCUM-G model severely underestimates synoptic variance over oceanic regions. However, it is crucial to highlight that the observed high variance over the northern Arabian Sea is likely associated with the cyclonic storm "BIPARJOY," which occurred from June 6th to 18th, 2023. This cyclone, one of the enduring cyclones over the Arabian Sea, significantly contributes to the synoptic variance seen in Figure 37a. Moreover, the model forecasts reasonably predict this variance in different forecast lead-times, particularly associated with the cyclone.

Figure 37. The spatial distribution of the synoptic variance (mm2) of rainfall for JJAS 2023 from (a) Observed and NCUM-G (b) Day-1 (c) Day-3, (d) Day-5 forecasts.
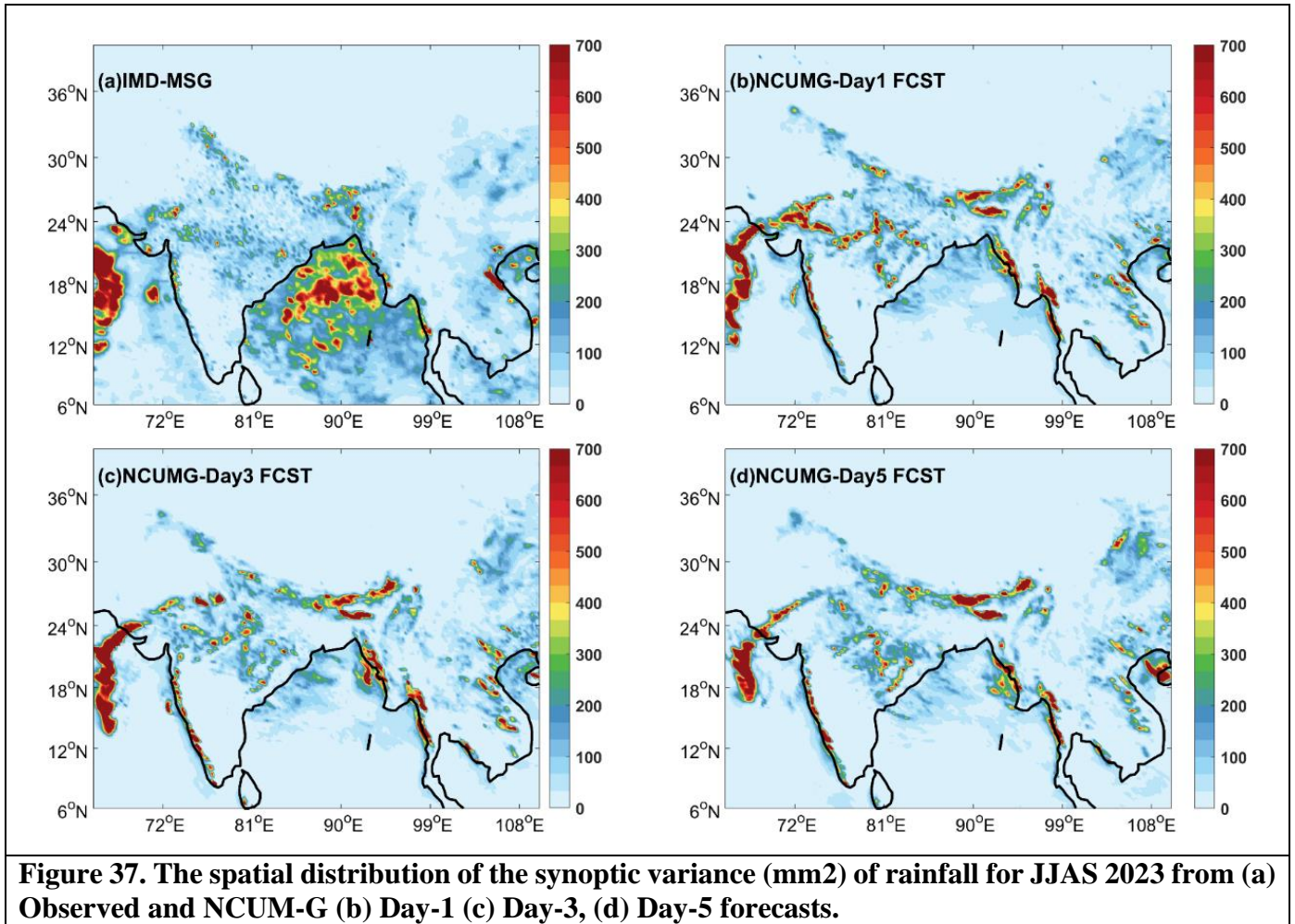
Figure 38 presents a spectral analysis of rainfall to understand the energy patterns of intraseasonal variability in the Indian region. Previous studies have identified two modes, QBWO (around 14 days) and ISO (along with a 20–30-day oscillation), in the intraseasonal scale of Indian monsoon rainfall. The spectrum in Figure 38 illustrates these modes alongside synoptic variability in monsoon rainfall. It's important to note that the model forecasts significantly overestimate both QBWO and ISO modes, especially in Day-3 and Day-5 forecast lead times. Unfortunately, Figure 38 doesn't provide time information about when these modes are strong. To address this, we conducted a wavelet analysis of daily average rainfall over Indian land regions, which preserves time information and shows the evolution of these two modes.
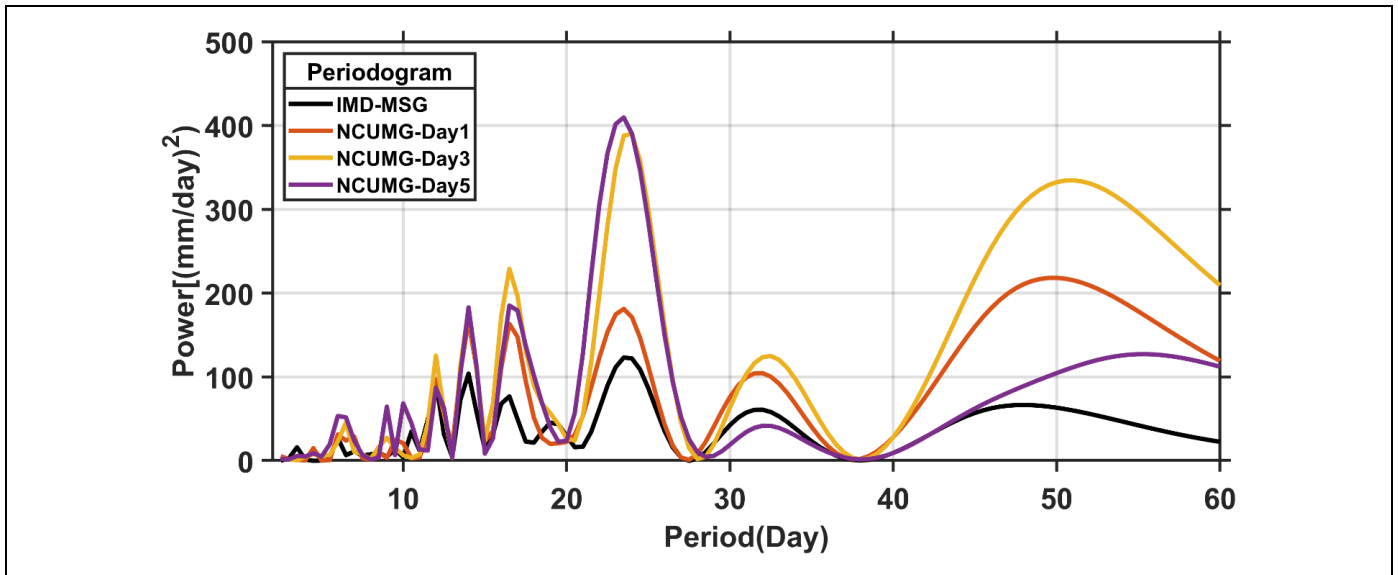
Figure 38. The spectral analysis of JJAS 2023 daily rainfall averaged over the Indian region from Observed and NCUM-G forecasts.

In Figure 39, the wavelet spectra of both observed and model forecast data are presented across various lead days. Specifically, Figure 39a illustrates the observed spectra, revealing a distinct peak in low-frequency oscillations, notably the Quasi-Biweekly Oscillation (QBWO), during the starting and retrieval phases of the monsoon, with a 95% confidence level. During the 2023 monsoon, the Intra-Seasonal Oscillation (ISO) does not exhibit significant characteristics. Comparatively, the model spectra in Figure 39b and Figure 39c, corresponding to Day-1 and Day-3 forecasts, respectively, align quite well with the observations. Both the QBWO and ISO are captured prominently by the model, reflecting the patterns observed in the actual data. However, it is noteworthy that as forecast lead-times progress, there is an observable increase in ISO amplitudes. Additionally, a crucial observation develops concerning the phase of the QBWO in the model forecasts relative to the observed data. There exists a slight disparity in the phases that stands significant implications for rainfall forecasts. This discrepancy suggests that while the model captures the overall patterns accurately, subtle differences in the timing of certain oscillations may influence the accuracy of precipitation predictions. This emphasizes the importance of refining model parameters to enhance the temporal synchronization between observed and forecasted meteorological phenomena.
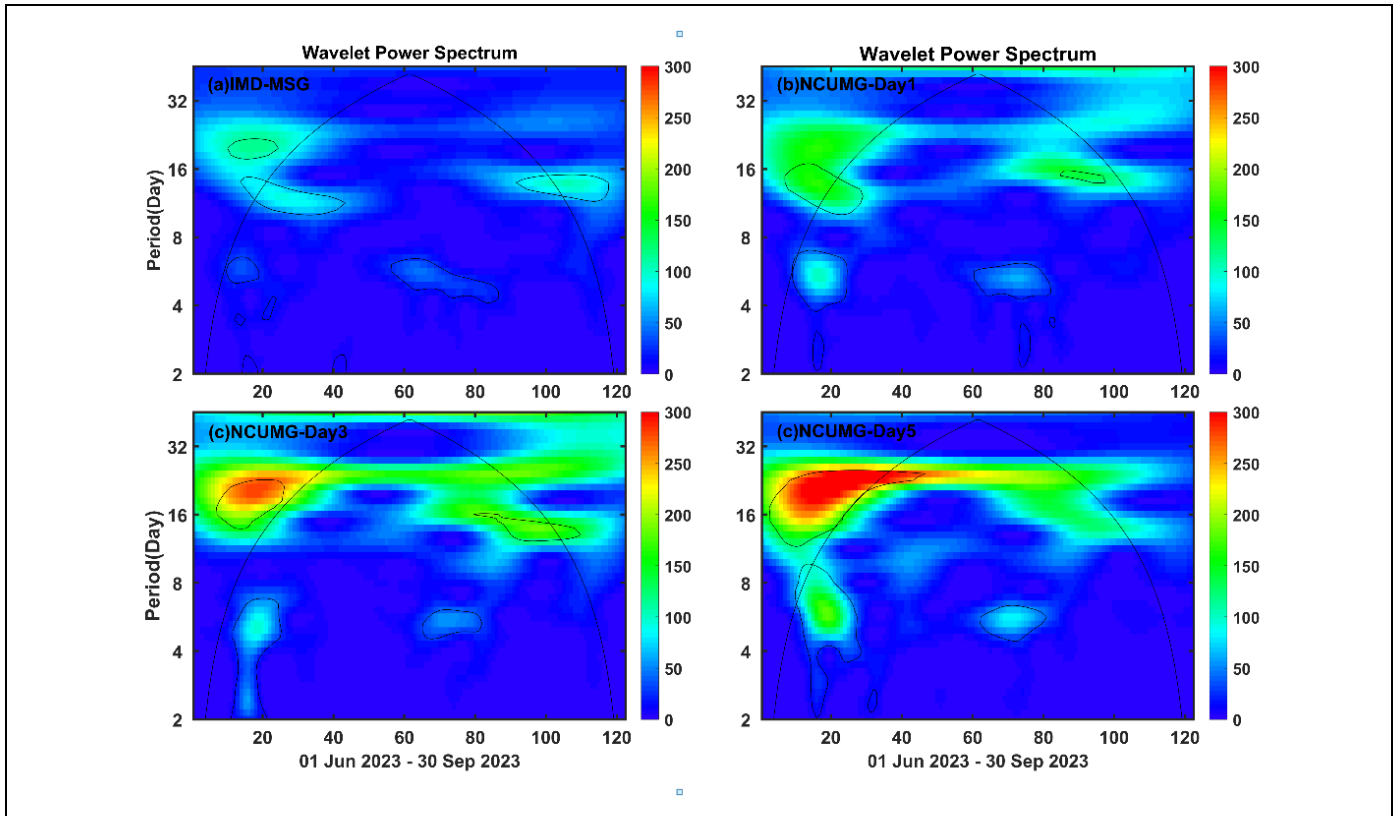
Figure 39. Wavelet Spectrum of Daily area-averaged rainfall over the Indian region from (a) Observed and NCUM-G (b) Day-1 (c)Day-3, and (d)Day-5 forecasts. The dashed line indicates the cone of influence; anything above is dubious. The solid lines indicate the 95% confidence interval based on chi-squared statistics.

Moreover, the observed spectra in Figure 39a show substantial synoptic variability lasting less than 7 days. Notably, the lower frequency side of this synoptic variability consistently aligns well with observations across all lead times. Examining Figure 16, the overall overestimation or underestimation of mean monsoon rainfall in various regions within the model forecasts can be primarily attributed to the model's handling of the ISO and QBWO modes in comparison to observed data. Given their significance as prominent northward and westward propagating rainfall bands, the ISO and QBWO contribute significantly to precipitation over the South Asian monsoon region, along with synoptic variance. The discrepancy in the model's representation of the spatial and temporal patterns of these modes, especially the synoptic variability, becomes evident, particularly over oceanic regions and, more specifically, the Bay of Bengal. The model's limitations in capturing these features have implications for accurately forecasting rainfall over these critical areas, highlighting the need for enhanced modeling precision to better characterize the complexities of monsoon dynamics.

8. Summary and Conclusions

This report documents the performance of the NCMRWF model forecasts during the winter season of JJAS 2023. The verification results are presented to address both forecasters and model developers. The information on biases in the forecast winds, temperature, humidity, rainfall, etc., is crucial for the forecasters to interpret the model guidance for forecasting. The diagnostic analysis of intra-seasonal features such as active/break spells, monsoon onset, and synoptic scale variability is also presented. Additionally, information on recent improvements in the model skill adds to confidence in the model forecasts. The results of the study can be summarized below.

8.1. NCUM-G Mean analysis and anomalies during JJAS 2023

❖ *The anomaly winds show (a) weak cross-equatorial flow and (b) south-easterly anomaly winds over the AS. Over the AS the negative anomaly indicated in red shade also suggests (c) weaker south-westerlies, (d) weaker westerlies/south-westerlies over north-eastern Indian region and head BoB. At 700 hPa level, the mean winds show most of the features very similar to flow at 850 hPa. In addition, Northeasterly flow is prominent over the horn of Africa and adjoining AS which was not seen at 850 hPa. Another feature to be noted at 700 hPa level is the strong cross equatorial and south westerly winds. The wind anomalies at 700 hPa show an anomalous cyclonic circulation over the AS indicating a stronger monsoon current over the AS. Over the equatorial Indian Ocean, specifically in southern latitudes, the SW winds are weaker in NCUM-G analysis resulting in strong anomalous easterlies/south-easterlies. Similarly, over the Indian land region, the easterly anomalies over north-eastern India indicate weak westerly winds relative to ERA-5 climatology. At 500 hPa, weaker south-westerlies indicated by negative anomalies over the Bay of Bengal. In contrast, positive anomalies are observed over across the western parts of India and extending into adjoining Arabian Sea. The anomalous winds at 200 hPa indicate weaker than normal easterlies/northeasterly over the AS, southern Bay of Bengal, peninsular India, and parts of SE Asia, as indicated by a negative anomaly in red shade.*

❖ *The positive anomalies (1-2^0C; red) are widespread, except over the north-west part of India and the Arabian Sea. The negative anomalies (1 to -2^0C at 850 hPa) over the northern Arabian Sea could be due to weak westerlies at 850 hPa and strong northeasterly flow from land, particularly at 700 hPa. At 700 hPa, positive temperature anomalies are seen over the entire domain. The positive anomalies ($>1^0$C at 500 hPa and $>2^0$C at 200 hPa) are seen as widespread over the entire domain.*

❖ *The RH anomaly at 850 hPa is significantly positive (blue) indicating a wet anomaly in the analysis over the part of the northern AS. However, the RH anomaly is negative (red) indicating a dry anomaly over the BoB and large parts of the equatorial Indian Ocean (central and eastern). At 850 hPa level, the dry RH anomaly could be partly explained as due to weaker southwesterly monsoon flow over a large area covering the BoB and large parts of the equatorial Indian Ocean. At 700 hPa level, the RH anomaly is positive (blue) over the entire domain, except for isolated regions of NW India and SE Asia, which may not be explained fully by the wind anomaly.*

8.2. NCUM-G Systematic Errors

❖ *At 850 hPa level, the systematic errors in the forecast indicate three important features (a) A westerly & southwesterly bias over the Indian region and neighboring seas suggesting stronger monsoon flow in forecasts. The magnitude of the positive bias is increasing from Day-1 to Day-5. Interestingly the forecast winds are not covering the Somali coast; instead, the strong cross-equatorial flow is more prominently seen over open AS, especially in Day-3 and Day-5. (b) An easterly bias over the eastern equatorial Indian Ocean indicating a weakened westerly/southwesterly flow in the forecasts. The pattern of biases (positive and negative) over the BoB and the anticyclonic anomaly, suggests a slight northward shift in the monsoon flow over the BoB. (c) The westerly bias along the west coast of India can be seen shifting northwestwards in Day-5 with the strongest bias over the northern AS and western India in Day-3 and Day-5.*

❖ *At 700 hPa level, the westerly bias over the Indian peninsula and BoB is prominent extending over SE Asia. Negative bias (red) over the northern and western Arabian Sea indicates weakened monsoon flow, particularly in the Day-3 and Day-5 forecasts. The weaker cross-equatorial flow can also be seen off the African coast. Additionally, the negative bias over the eastern equatorial Indian Ocean, prominent at 850 hPa is also pronounced at 700 hPa level.*

❖ *At 500 hPa level (Figures 10a-d) the pattern and sign of biases over the western and eastern equatorial Indian Ocean are more or less similar. Over the northern Arabian Sea, positive bias (blue) indicates strong northeasterly flow from NW India where anomalous cyclonic flow is evident on Day-3 and Day-5. At 200 hPa, the positive easterly bias (blue) extends over the Indian peninsula and neighboring Arabian Sea and Bay of Bengal and the magnitude of this bias increases with forecast lead time. The negative westerly bias (red) occupies the entire equatorial region of the domain suggesting a weakened tropical easterly jet as forecast length increases.*

❖ *At 850 hPa level, systematic errors in temperature forecasts indicate (a) a warm bias (>0.5°C) over north India particularly over the IGP region and the neighboring AS, BoB, and around the South China Sea regions. (b) Strong warm bias (>1°C) is prominent in Day-3 and Day-5 forecasts over NW India. (c) Mild cold bias (about -0.5°C) over west coast of India. At 700 hPa and 500hPa the warm (cold) bias over the land (sea) regions persists by and large with reduced magnitude, excluding the easter Indian Ocean at 500 hPa and peninsular India at both levels. At 200 hPa, the land and sea regions partly feature cold bias in all the forecasts, except over the equatorial Indian Ocean, with magnitudes of about 0.5^0C.*

❖ *The forecasts prominently exhibit negative (red) dry bias over the AS, NW India, IG plains, and head BoB in all the lead times. These dry biases are also seen at 700 hPa. Consistent with bias in RH, it is found that PWAT also shows dry bias. Overall, the forecasts have a moist and dry bias in the lower troposphere, and the magnitude of bias increases with forecast lead time.*

❖ *The biases in the VIMT forecasts show positive (blue) over the entire Indian land region, AS, and the BoB. The Day-3 and Day-5 forecasts show negative bias (red) over the eastern equatorial Indian ocean consistent with the wind biases at 850, 700, and 500 hPa. Despite the strong dry bias indicated by systematic errors in RH, it can be inferred that the strong positive biases in winds have offset the impact of dry bias in the forecasts over India. It is also worth noting that over the IG plains, negative bias in VIMT is prominent, with increasing error magnitudes as the forecast lead time increases.*

❖ *There are some year-to-year variations in the RMSE during 2018-2023, the lowest RMSE is evident during JJAS 2022 at all lead times, however, a slight increase is seen in JJAS 2023 RMSE compared to JJAS 2022 (except for Temp at 200 hPa).*

8.3. Forecast Verification during JJAS 2023

❖ *The NCUM-G forecast shows higher rainfall amounts all over the West Coast and NE India. In addition, the forecasts overestimate the isolated high rainfall amounts (>10mm/day) over the core monsoon regions, indicating the overestimation of observed rainfall over land and the neighboring seas. On the contrary, forecast rainfall shows a large underestimation over the Bay of Bengal region, which is noteworthy. The reduced rainfall amounts (<6mm/day) over the eastern parts of the peninsula and northwest India are predicted fairly well in the model.*

❖ *Mean error (ME) in predicted rainfall indicating wet bias (blue) all along the west coast, over the AS, and over central India. Dry bias (orange/red) is prominent over the BoB and the amplitude of dry bias is enhancing w.r.t lead time. Over the Indian land region, dry bias can be seen over parts of Gujarat, western India, parts of the central peninsula, and isolated regions along the west coast. The east-west gradient over the west coast in the ME (i.e., wet (dry) bias to the west (east)) indicates a westward shift in the rainfall over the west coast in the forecasts. Similarly, wet (dry) bias over core monsoon regions, NE India, and Arakan coast (parts of peninsula and adjoining BoB) indicates a northward and eastward shift in the forecast rainfall over core monsoon regions, NE India, and Arakan coast.*

❖ *RMSE gives the average forecast error weighted according to squared error. While it does not indicate the direction of the forecast errors, it gives greater emphasis on relatively larger errors. It can be noted that the forecasts feature large errors over regions of high rainfall amounts along the west coast, Himalayan belt, BoB, central India, and NE regions. Additionally, RMSE is high over parts of the core monsoon regions and BoB, which can be seen to increase with forecast lead time. However, the map of correlation shown in the bottom panels suggests a sharp decline in the forecast skill from Day-1 to Day-5.*

❖ *The observations show (a) a high number of rainy days (>80 days; orange shade) along the west coast and NE India and (b) 60-80 days (yellow shade) over the core monsoon regions. Over the dry regions of NW India and the eastern peninsula, the number of rainy days is lower than 40-60 days (green & blue). The model forecasts show an exceedingly higher number (>60 days) of rainy days over most parts of India. Over the dry regions of NW India, central, and eastern peninsula, the model predicts a far lower number of moderate rainy days, however, a higher (60-80) number of moderate rainy days over the west coast and NE India. For the "heavy rainy days" (>64.5 mm/day) category, forecasts have a higher count along the west coast, over NE India, and core monsoon regions (to some extent).*

❖ *For rainfall threshold of up to 9 mm/day, the forecasts have POD >0.5 (& FAR <0.6) in the Day-1 forecast. After 9mm/day, POD and FAR show a decrease and increase in scores, respectively. The BIAS score (frequency bias) indicates that forecasts overestimate the frequency upto 9mm/day or lower. The values of CSI, PSS, and SEDI all are high for rainfall up to 9mm/day suggesting reasonable skill. However, the skill is not bias-free. For higher amounts (9-30mm/day), there is no frequency bias, but the skill is low as indicated by CSI, PSS, and SEDI.*

8.4. Verification of Onset, Active/Break Spells, and Synoptic Features

❖ *Variability in rainfall patterns is studied, with a focus on synoptic, quasi-biweekly, and low-frequency instar-seasonal scales. Synoptic variability, including monsoon troughs and cyclones, is analyzed, showing model overestimations, especially in central India and the Himalayas.*

- ❖ *Spatial synoptic variance distribution for JJAS 2023 indicates notable disparities between observed and model forecasts.*
- ❖ *Spectral analysis showing model overestimations in QBWO and ISO modes in Day-3 and Day-5 forecasts. To address the lack of time information a wavelet analysis is conducted, emphasizing the need to refine model parameters for better temporal synchronization. Wavelet spectra reveals discrepancies in QBWO phases between observed and model forecasts. The model captures overall patterns accurately, but subtle timing differences may impact precipitation predictions.*
- ❖ *The limitations in representing spatial and temporal patterns, especially over oceanic regions and the Bay of Bengal, emphasize the need for enhanced modeling precision in forecasting monsoon dynamics.*
- ❖ **Cyclone 'Biparjoy'**
    - ❖ ***Initial Position Error****: Mean initial position error is least 32 km in NCUM-G and 35 km in NCUM-R with slightly higher error of 43 km in NEPS-G (ensemble mean)*
    - ❖ ***Direct Position Error****: NCUM-G features DPE <100 km up to 60 hrs. DPE & ATE are highest in NEPS-R (NEPS-G) at all lead times up to 72hrs (after 72hrs).*
    - ❖ ***Landfall Position & Time error****: The forecast landfall time error is -6 to -12 hours in NCUM-G from 12Z10Jun till 00Z12Jun. Subsequently the errors are small ranging from 0 to -6h. On the other hand, NEPS-G shows a landfall time error mostly ranging from -6 to -12h. NCUM-R forecasts show 0 landfall time error on all days. Landfall position error was lowest (<50km) in NCUM-R from 00Z14th June onwards.*
    - ❖ ***Intensity verification (NCUM-G & NCUM-R)****: The Mean Sea Level Pressure Error (MSPE) in NCUM-R forecasts is significantly lower (<10hPa) than in NCUM-G. Similarly, the Maximum Sustained Wind Error (MSWE) is lower in NCUM-R for all lead times (after 12hrs) as compared to NCUM-G.*
    - ❖ ***Verification of strike probability (NEPS-G)****: The reliability diagram shows NEPS-G strike probability has near perfect reliability. With an AROC of 0.73, the strike probability forecasts have reasonable skill.*

References

1. Ashrit, R., Sharma, K., Dube, A., Iyengar, G. R., Mitra, A. K. and Rajagopal. E. N. 2015: Verification of short-range forecasts of extreme rainfall during monsoon; Mausam 66 375–386, 607 https://metnet.imd.gov.in/mausamdocs/16633˙F.pdf.

2. Auligne, T., McNally, A. P., Dee, D. P., 2007: Adaptive bias correction for satellite data in a numerical weather prediction system.Q J ROY METEOR SOC, 133, 631-642. https://doi.org/10.1002/qj.56

3. Barker, D., 2011: Data assimilation-progress and plans, MOSAC-16, 9-11 November 2011, Paper16.6.

4. Cameron, J., Bell, W., 2018: The testing and planned implementation of variational bias correction (VarBC) at the Met Office 21.

5. Clayton, A.M., Lorenc, A.C., Barker, D.M., 2013: Operational implementation of a hybrid ensemble/4D-Var global data assimilation system at the Met Office: Hybrid Ensemble/4D-Var Data Assimilation. Q.J.R. Meteorol. Soc. 139, 1445–1461.https://doi.org/10.1002/qj.2054.

6. Harris, B.A., Kelly, G., 2001: A satellite radiance-bias correction scheme for data assimilation. Q.J Royal Met. Soc. 127, 1453–1468.https://doi.org/10.1002/qj.49712757418.

7. Hersbach H, Bell B, Berrisford P, et al. 2020: The ERA5 global reanalysis. Q J R Meteorol Soc. 2020;146:1999–2049. https://doi.org/10.1002/qj.3803

8. Jolliffe, I. T., and D. Stephenson, 2012: Forecast Verification: A Practitioner's Guide in Atmospheric Science, John Wiley & Sons, Ltd.

9. Kumar Sumit, A. Jayakumar, M. T. Bushair, Buddhi Prakash J., Gibies George, Abhishek Lodh, S. Indira Rani, Saji Mohandas, John P. George and E. N. Rajagopal 2019: Implementation of New High Resolution NCUM Analysis-Forecast System in Mihir HPCS. NMRF/TR/01/2019, 17p.

10. Kumar Sumit, M. T. Bushair, Buddhi Prakash J., Abhishek Lodh, Priti Sharma, Gibies George, S. Indira Rani, John P. George, A. Jayakumar, Saji Mohandas, Sushant Kumar, Kuldeep Sharma, S. Karunasagar, and E. N. Rajagopal 2020: NCUM Global NWP System: Version 6 (NCUM-G:V6), NMRF/TR/06/2020.

11. Kumar Sumit, Gibies George, Buddhi Prakash J., M. T. Bushair, S. Indira Rani and John P. George 2021: NCUM Global DA System: Highlights of the 2021 upgrade, NMRF/TR/05/2021.

12. Krishnamurti, T. N., &Bhalme, H. N. (1976). Oscillations of a MonsoonSystem. Part I. Observational Aspects, Journal of Atmospheric Sciences,33(10), 1937-1954. DOI:https://doi.org/10.1175/1520-0469(1976)033<1937:OOAMSP>2.0.CO;2

13. Lorenc, A.C., 2003. Modelling of error covariances by 4D-Var data assimilation. Q.J.R. Meteorol. Soc. 129, 3167–3182.https://doi.org/10.1256/qj.02.131

14. Levine, R.C. and Martin, G.M. (2018) On the climate model simulation of Indian monsoon low-pressure systems and the effect of remote disturbances and systematicbiases. Climate Dynamics, 50, 4721– 4743

15. Mamgain, A., Sarkar, A., Dube, A., Arulalan, T., Chakraborty, P., George, J. P., and Rajagopal, E. N., 2018: Implementation of Very High Resolution (12 km) Global Ensemble Prediction System at NCMRWF and its Initial Validation, NMRF/TR/02/2018, 21p.

16. Mitra, A. K., A. K. Bohra, M. N. Rajeevan and T. N. Krishnamurti, 2009: Daily Indian precipitation analyses formed from a merged of rain-gauge with TRMM TMPA satellite derived rainfall estimates, J. of Met. Soc. of Japan, 87A, 265-279.

17. Mitra, A. K., I. M. Momin, E. N. Rajagopal, S. Basu, M. N. Rajeevan and T. N. Krishnamurti, 2013, Gridded Daily Indian Monsoon Rainfall for 14 Seasons: Merged TRMM and IMD Gauge Analyzed Values, J. of Earth System Science, 122(5), 1173-1182.

18. Rabier, F., Thépaut, J.-N., Courtier, P., 1998. Extended assimilation and forecast experiments with a four-dimensional variational assimilation system. Q.J Royal Met. Soc. 124, 1861– 1887.https://doi.org/10.1002/qj.49712455005

19. Rabier, F., Järvinen, H., Klinker, E., Mahfouf, J.-F., Simmons, A., 2007. The ECMWF operational implementation of four-dimensional variational assimilation. I: Experimental results with simplified physics. Q.J.R. Meteorol. Soc. 126, 1143–1170.https://doi.org/10.1002/qj.49712656415

20. Rajeevan, M., Gadgil, Sulochana and Bhate, Jyoti, 2010, "Active and break spells of the Indian Summer Monsoon", Journal of Earth System Science, 119, 3, 229-247.

21. Rani, S.I., Taylor, R., Sharma, P., Bushair, M.T., Jangid, B.P., George, J.P., Rajagopal, E.N., 2019. Assimilation of INSAT-3D imager water vapour clear sky brightness temperature in the NCMRWF's assimilation and forecast system. J Earth Syst Sci 128, 197.

22. Rawlins, F., Ballard, S.P., Bovis, K.J., Clayton, A.M., Li, D., Inverarity, G.W., Lorenc, A.C., Payne, T.J., 2007. The Met Office global four-dimensional variational data assimilation scheme. Q.J.R. Meteorol. Soc. 133, 347–362.https://doi.org/10.1002/qj.32

23. Sarkar, A., Chakraborty, P., George, J. P., and Rajagopal, E. N., 2016: Implementation of Unified Model Based Ensemble Prediction System at NCMRWF (NEPS), NMRF/TR/02/2016, 26p.

24. Sharma, K., Ashrit, R., Kumar, S. et al. Unified model rainfall forecasts over India during 2007–2018: Evaluating extreme rains over hilly regions. J Earth Syst Sci 130, 82 (2022). https://doi.org/10.1007/s12040-021-01595-1

25. Stephenson D.B., B. Casati, C.A.T. Ferro and C.A. Wilson, 2008: The extreme dependency score: a non-vanishing measure for forecasts of rare events. Meteorol. Appl., 15, 41-50.

26. Wang, B., Wu, R., & Lau, K-M. (2001). Interannual Variability of theAsian Summer Monsoon: Contrasts between the Indian and the Western NorthPacific–East Asian Monsoons, Journal of Climate, 14(20), 4073-4090.DOI:https://doi.org/10.1175/1520-0442(2001)014<4073:IVOTAS>2.0.CO;2

27. Wang, B., Ding, Q., & Joseph, P. V. (2009). Objective Definition of the Indian Summer Monsoon Onset, Journal of Climate, 22(12), 3303-3316.DOI:https://doi.org/10.1175/2008JCLI2675.1

28. Walters, D., and co-authors: The Met Office Unified Model Global Atmosphere 6.0/6.1 and JULES Global Land 6.0/6.1 configurations, Geosci. Model Dev., 10, 1487–1520, https://doi.org/10.5194/gmd-10-1487-2017, 2017.

29. Walters, D., Baran, A.J., Boutle, I., Brooks, M., Earnshaw, P., Edwards, J., Furtado, K., Hill, P., Lock, A., Manners, J. and Morcrette, C., 2019. The Met Office Unified Model global atmosphere 7.0/7.1 and JULES global land 7.0 configurations. Geoscientific Model Development, 12(5), pp.1909-1963.

30. Wilks D S 2011 (eds) Statistical methods in the atmospheric 807 sciences; 3rd edn, Elsevier, 676p
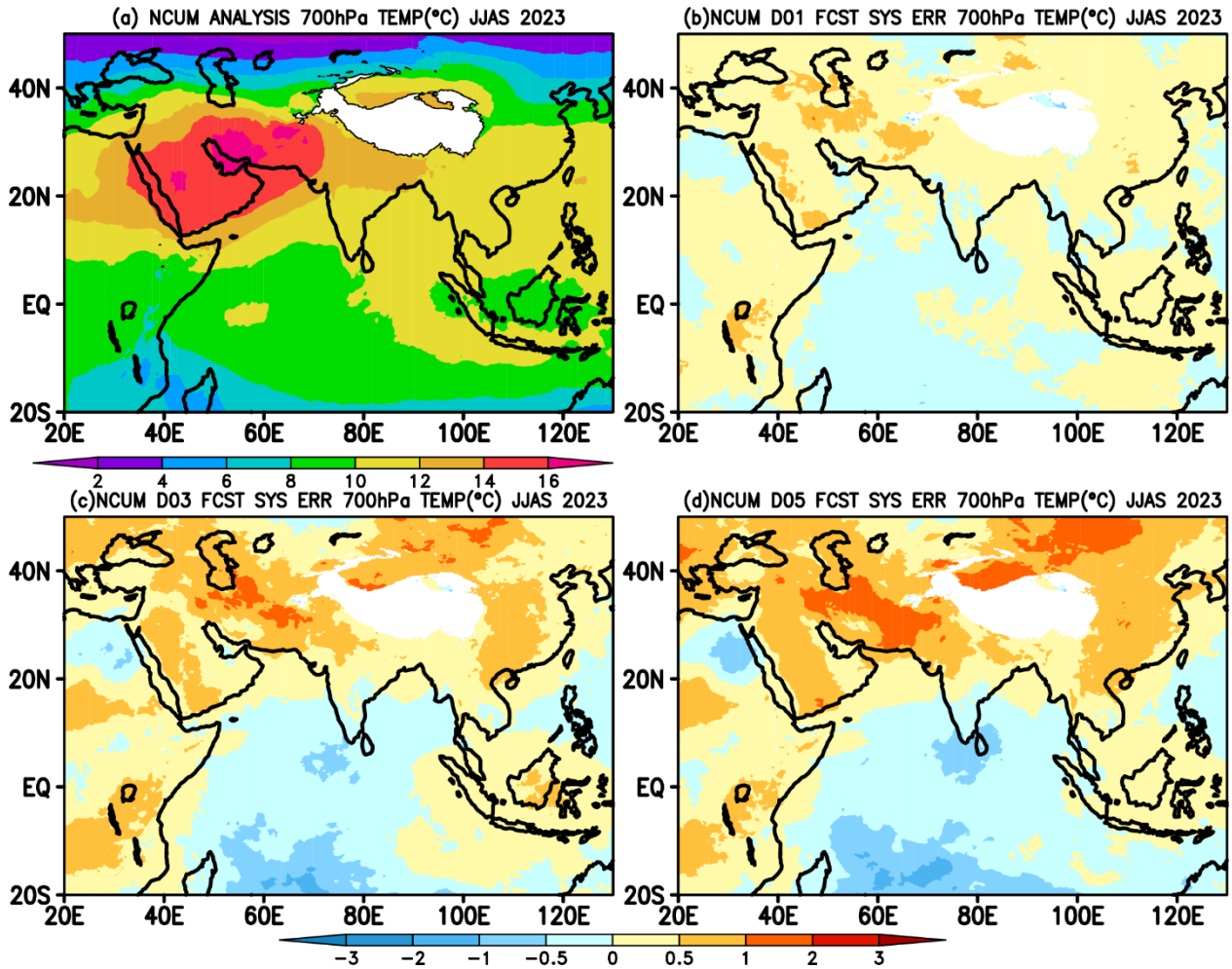
APPENDIX

Figure S1. Mean Temperature and systematic errors (Degree Celsius, ^{0}C) in (b) Day-1, (c) Day-3, and (d) Day-5 forecasts at 700 hPa during JJAS 2023.
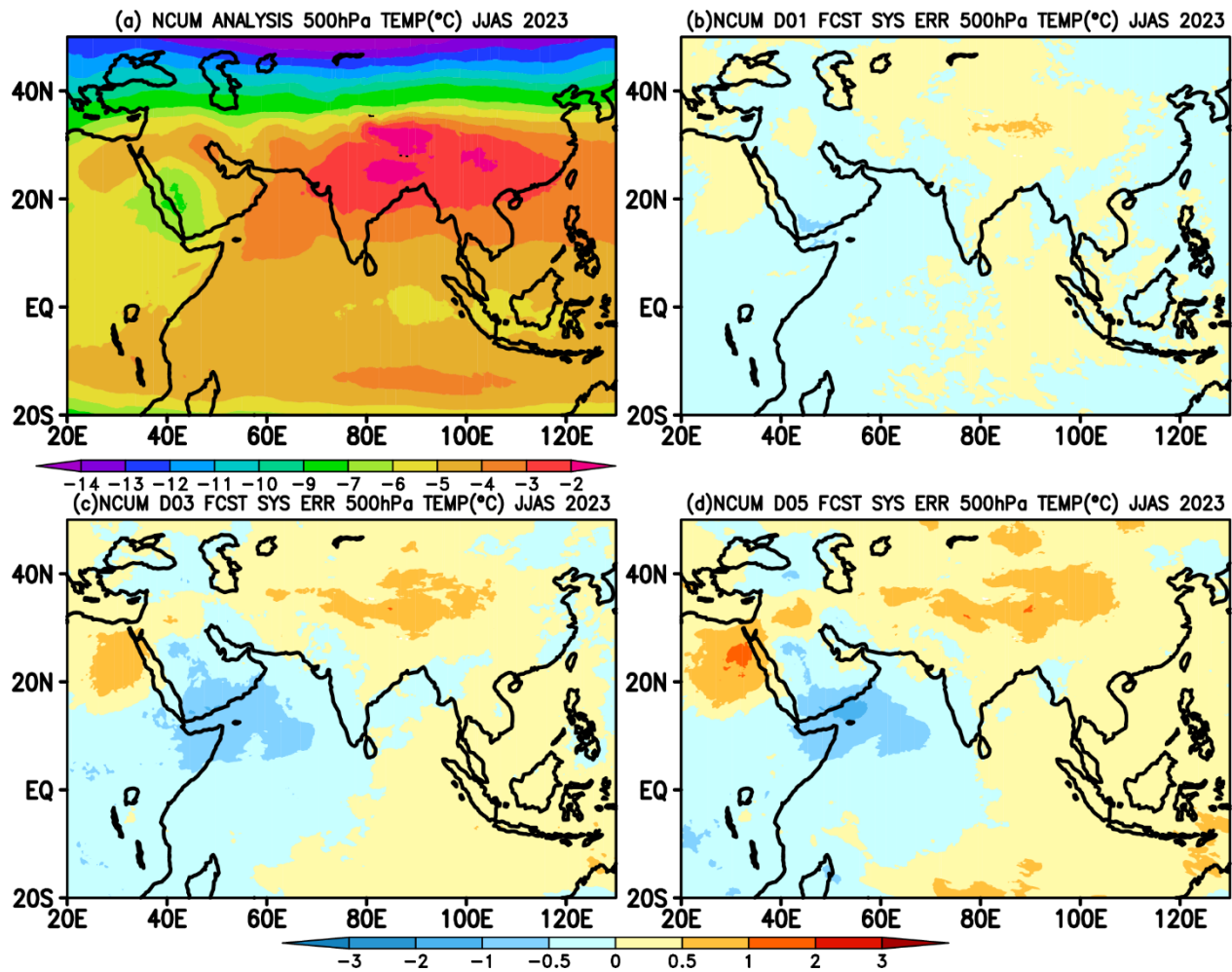
Figure S2. Mean Temperature and systematic errors (Degree Celsius, ^{0}C) in (b) Day-1, (c) Day-3, and (d) Day-5 forecasts at 500 hPa during JJAS 2023.
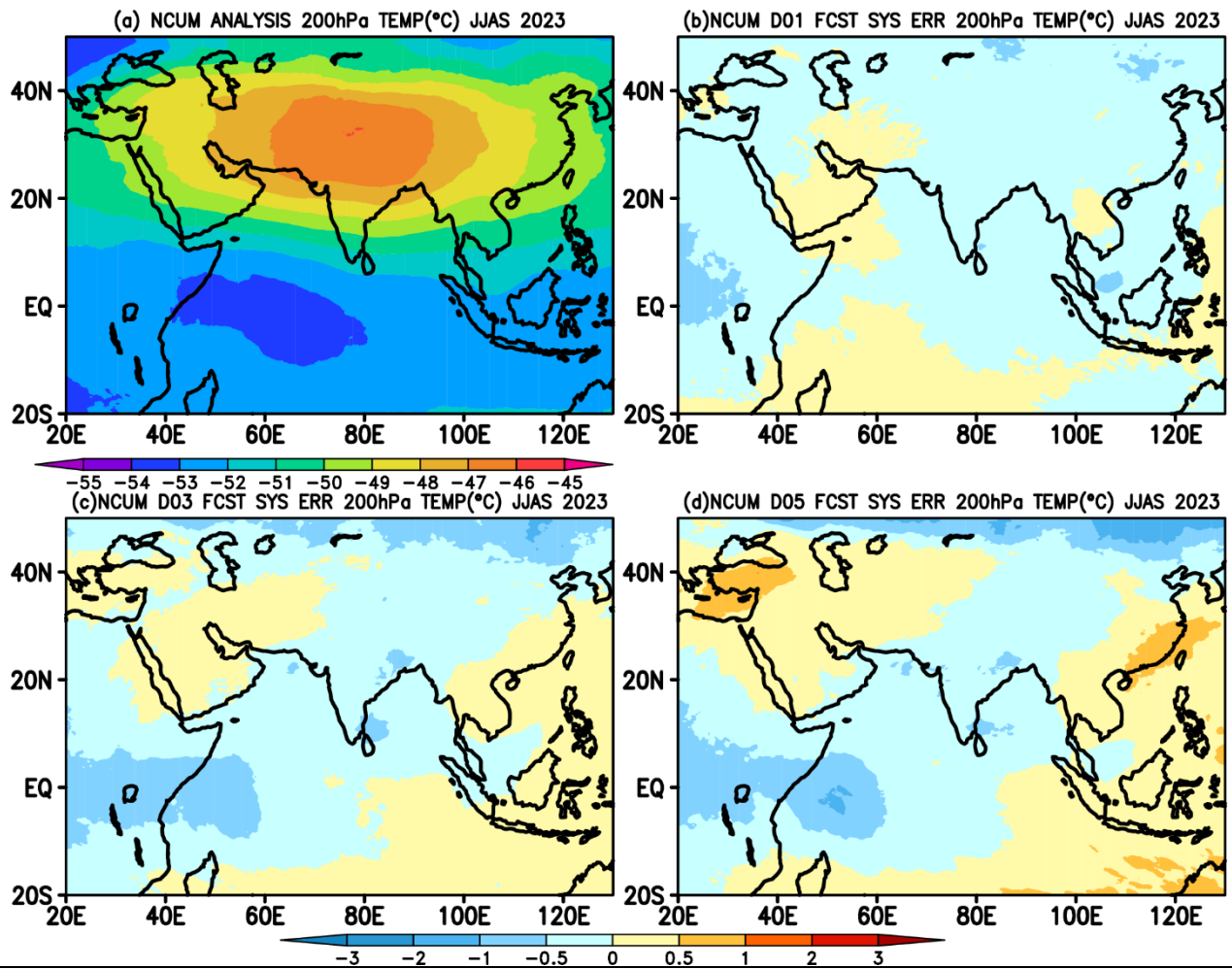
Figure S3. Mean Temperature and systematic errors (Degree Celsius, ⁰C) in (b) Day-1, (c) Day-3, and (d) Day-5 forecasts at 200 hPa during JJAS 2023.
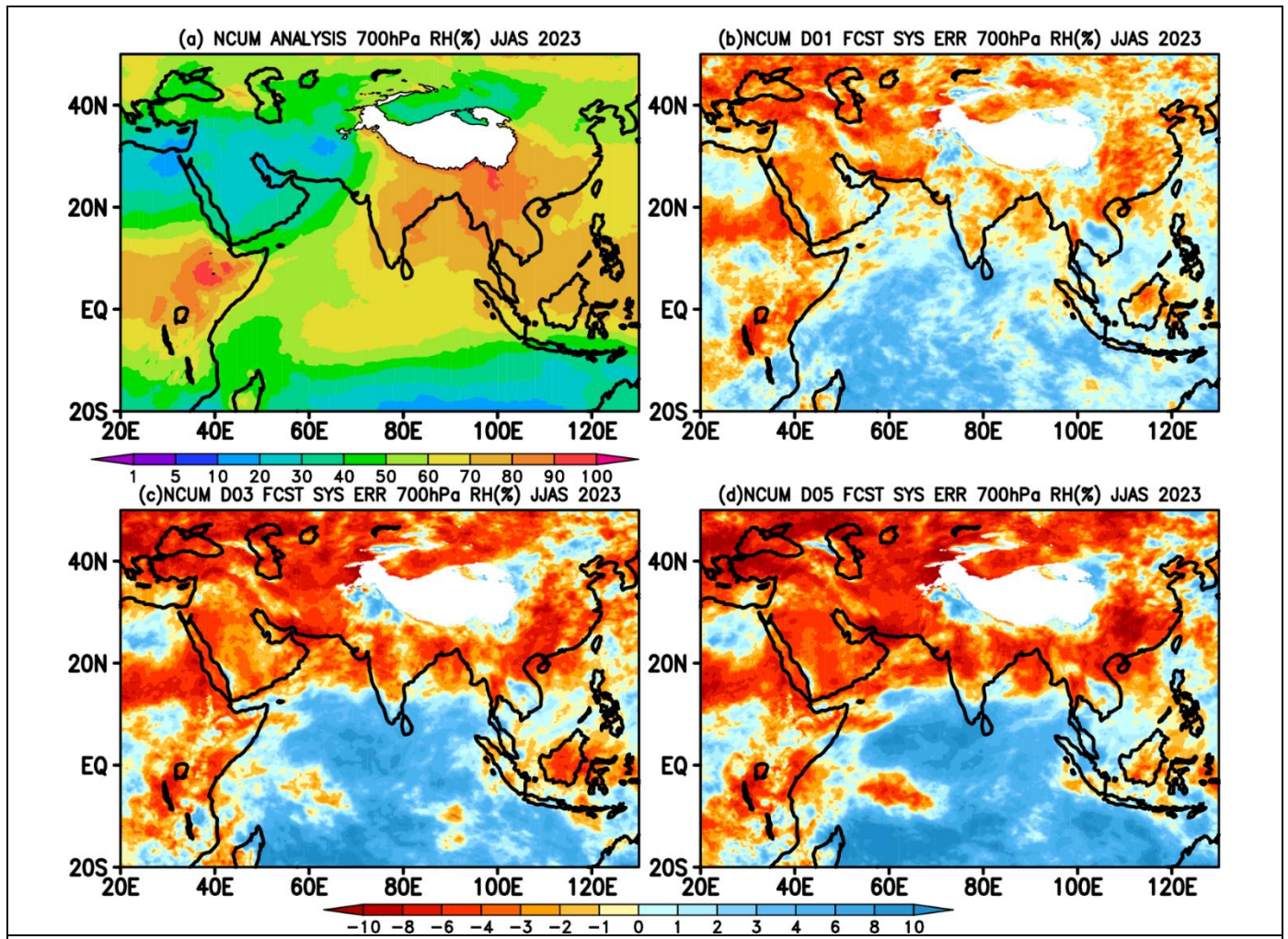
Figure S4. Mean Relative Humidity and systematic errors (%) in (b) Day-1, (c) Day-3, and (d) Day-5 forecasts at 700 hPa during JJAS 2023.
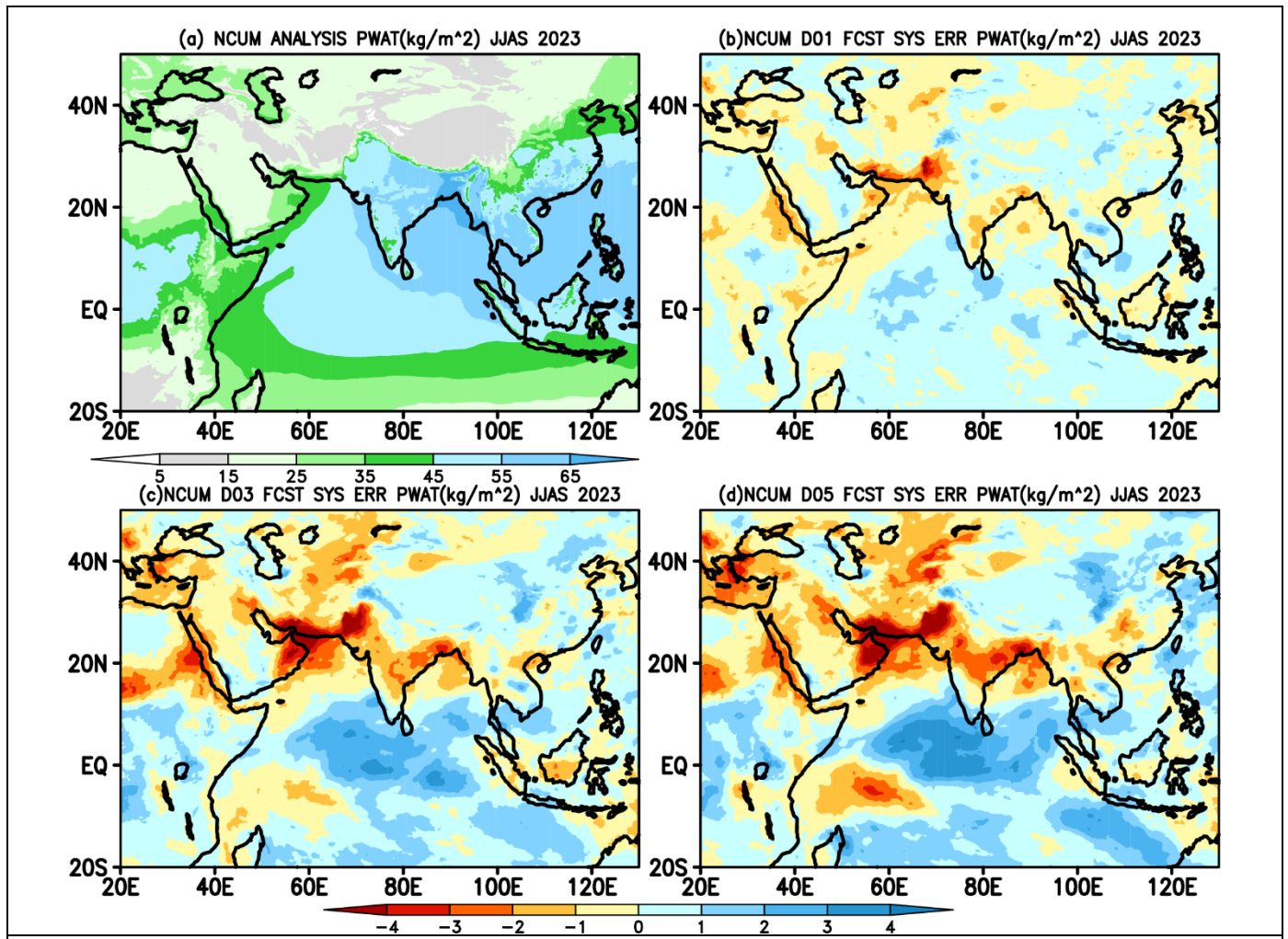
Figure S5. Mean Total Precipitable Water (PWAT) up to model levels and systematic errors (mm) in (b) Day-1, (c) Day-3, and (d) Day-5 forecasts during JJAS 2023.

Categorical Verification of Rainfall Forecasts

The categorical approach of verifying QPF is generally based on the 2 x 2 contingency table which is evaluated for each threshold. We consider an event as a hit (a) when the prediction of an event matches with the observation on a grid point. On the other hand, an event on a grid point is predicted but it is not observed, we denote it as a false alarm (b). A miss (c) occurs when an event is not predicted but it is actually observed. Finally, correct rejection (d) is when an event does not occur and model does not predict. Based on these components of the contingency table, categorical skill scores are computed for different rainfall thresholds.

**Table S1.** Contingency table

		Observed		Total
		Yes	**No**	
Forecast	**Yes**	_Hits_	_False alarms_	_Forecast Yes_
	No	_Miss_	_Correct Negative_	_Forecast No_
Total		_Observed Yes_	_Observed No_	_Total_

**Table S2.** Categorical skill scores.

	Definition	**Formula**
1.	**POD Score or the Hit Rate (H):** POD tries to answer the question, "_What fraction of the observed "yes" events were correctly forecast?_"	$$POD = \frac{hits}{hits + misses}$$ Its value varies from 0 to 1, for perfectly forecasted events POD=1.
2.	**FAR (F)**: _What fraction of the predicted "yes" events actually did not occur?_	$$FAR = \frac{false\ alarms}{hits + falsealarms}$$ Its value varies from 1 to 0, for perfectly forecasted events FAR=0
3.	**CSI:** _How well did the forecast "yes" events correspond to the observed "yes" events?_ The CSI, also known as threat score.	$$CSI = \frac{hits}{hits + misses + falsealarms}$$ Its value varies from 0 to 1, for perfectly forecasted events CSI=1
4.	**BIAS:** _How did the forecast frequency of "yes" events compare to the observed frequency of "yes" events?_	$$BIAS = \frac{hits + false\ alarms}{hits + misses}$$ Its value varies from 0 to ∞, for perfectly forecasted events BIAS=1 _(BIAS>1) =>overforecast events_

		(BIAS<1) =>underforecast events
5.	**ETS:** *How well did the forecast "yes" events correspond to the observed "yes" events (accounting for hits due to chance)?*	$ETS = \dfrac{hits - hits_{random}}{hits + misses + falsealarm - hits_{random}}$ $hits_{random} = \dfrac{(hits + miss)(hits + falsealarms)}{total}$ This score ranges between -1/3 to 1. '0' shows no skill and 1 denotes the perfect skill.
6.	**HK:** *How well did the forecast separate the "yes" events from the "no" events?* The expression is identical to **HK = POD - POFD**, **(HK also known as true skill statistic, Peirce's skill score PSS)**	$HK = \left[\dfrac{hits}{hits + misses}\right] - \left[\dfrac{falsealarms}{falsealarms + correctnegatives}\right]$ The value varies from -1 to 1; 0 indicates no skill and 1 denotes a perfect skill